The interrelations between supermolecular structure, properties and degradability of isotactic poly(1-butene)

Lubomír Beníček

N° d'Ordre : D.U. 1921

UNIVERSITE BLAISE PASCAL

U.F.R. Sciences et Technologies

ECOLE DOCTORALE DES SCIENCES FONDAMENTALES

N° 605

THESE

présentée pour obtenir le grade de

DOCTEUR D'UNIVERSITE

Spécialité : Chimie - Physique

Par **BENÍČEK Lubomír**

Master en chimie et technologie des matériaux

THE INTERRELATIONS BETWEEN SUPERMOLECULAR STRUCTURE, PROPERTIES AND DEGRADABILITY OF ISOTACTIC POLY(1-BUTENE)

Soutenue publiquement le 27 avril 2009 devant la commission d'examen.

Président :	Mme. Sophie COMMEREUC
Examinateurs :	Mme. Berenika HAUSNEROVÁ (rapporteur)
	M. Philippe CASSAGNAU (rapporteur)
	M. Roman ČERMÁK
	M. Michel DUMON
	M. Martin OBADAL
	M. Miroslav RAAB (rapporteur)
	M. Vincent VERNEY

TOMAS BATA UNIVERSITY IN ZLÍN
Faculty of Technology
Department of Polymer Engineering

DOCTORAL THESIS

Lubomír Beníček

THE INTERRELATIONS BETWEEN SUPERMOLECULAR STRUCTURE, PROPERTIES AND DEGRADABILITY OF ISOTACTIC POLY(1-BUTENE)

Programme:	Chemistry and Materials Technology
Course:	Technology of Macromolecular Substances
Co-supervisors:	Dr. Vincent Verney doc. Ing. Martin Obadal, Ph.D.
Consultant:	doc. Ing. Roman Čermák, Ph.D.
Year:	2009

ACKNOWLEDGEMENT

In the first place, I would like to sincerely thank my supervisors Martin OBADAL and Vincent VERNEY for giving me the opportunity of co-supervised Ph.D. study, valuable advices and inspirational suggestions that have helped me to successfully complete this thesis. I also thank Roman ČERMÁK for his help, ideas and discussion during my research as my consultant.

Further, I would like to thank Sophie COMMEREUC, Berenika HAUSNEROVÁ, Philippe CASSAGNAU, Michel DUMON and Miroslav RAAB for being jury members and for their valuable comments.

Special thank belongs:

French government for the financial support (BGF) and Marie-Claire COMTE-ROME from CROUS Clermont-Ferrand.

Faculty of Technology, Tomas Bata University in Zlín and Laboratoire de Photochimie Moleculaire et Macromoleculaire, Université Blaise Pascal for technical and scientific support with experiments.

My colleagues, friends and students who helped me with experiments in the both institutions where I have been studying: Lenka, Solène, Jana, Kristýna, Slavomíra, Martina, Monika, Branislav, Harout, Michal K., Denis, Matthieu, Michal M., Tomáš, Guillaume, Joël CELLIER, Lawrence FREZET and Milan ŽALUDEK.

Last but not least to my fiancée Libuše, parents and family for their great support, patience and love.

RÉSUMÉ

Cette thèse porte sur l'inter relation entre la superstructure moléculaire, les propriétés et la dégradabilité du poly butène isotactique. L'évolution la plus importante est une transformation de phase particulière de la forme cristalline II à la forme cristalline I après cristallisation du polymère à partir de l'état fondu. Cette transformation a été caractérisée par calorimétrie, par diffraction des rayons X aux grands angles et par l'analyse des propriétés mécaniques en fonction des conditions de thermique de recuit. L'effet de la mise en forme sur la superstructure résultante a été mis en évidence sur des échantillons obtenus par injection ou par extrusion en utilisation les propriétés mécaniques en traction. Du fait de la très grande sensibilité du PB-1 vis-à-vis de la photodégradation des effets significatifs sur les propriétés thermiques et sur la transformation de phase ont été observés. Une caractérisation multi-échelle en photodégradation a été réalisée à partir d'analyses calorimétriques, d'analyse en spectroscopie infrarouge, de la diffraction des rayons X et des propriétés mécaniques en traction et ceci tant en photovieillissement en conditions accélérées qu'en conditions d'exposition naturelle.

Mots clés: poly(1-butène) isotactique, transformation de phase, structure, propriétés, photodégradation

ABSTRAKT

Tato dizertační práce je zaměřena na studium vzájemných vztahů mezi nadmolekulární strukturou, vlastnostmi a degradabilitou izotaktického poly(1-butenu) (PB-1). Nejvýznamnější vývoj v PB-1 je jeho zvláštní fázová transformace z formy II do formy I, jenž nastává po krystalizaci z taveniny. Tato fázová transformace je charakterizována pomocí kalorimetrického měření, široko-úhlé rentgenografie a mechanickými zkouškami, kde byly pozorovány změny v závislosti na podmínkách stárnutí. Vliv zpracovatelské technologie – vstřikování a vytlačování - na výslednou nadmolekulární strukturu byl prokázán na základě mechanických zkoušek. Jelikož je PB-1 velmi náchylný k fotodegradaci, významné změny byly zaznamenány v termálních vlastnostech a fázové transformaci. Široce zaměřená charakterizace důsledků fotodegradace byla provedena pomocí kalorimetrických měření, infračervené spektroskopie, reologie, rentgenografie, mikroskopických technik a tahových zkoušek. Rovněž byl posouzen vliv rozdílných degradačních procesů – venkovní stárnutí a zrychlené UV ozařování – které vedly k odlišným výsledkům ovlivňující výsledné makroskopické vlastnosti.

Klíčová slova: izotaktický poly(1-buten), fázová transformace, struktura, vlastnosti, fotodegradace

ABSTRACT

This dissertation work is focused on the interrelations between supermolecular structure, properties and degradability of isotactic poly(1-butene) (PB-1). The most important evolution in PB-1 is a peculiar phase transformation from form II to form I after crystallization from melt. This phase transformation is characterized using calorimetry, wide-angle X-ray scattering and mechanical testing where changes in dependence on annealing conditions in time are observed. The effect of processing on resulting supermolecular structure is proven on injection-molded and extruded specimens using tensile testing. Because of high sensitivity of PB-1 to photodegradation, significant effects on thermal properties and the phase transformation is observed. Multiscale characterization is performed using calorimetric measurements, infra-red spectroscopy, rheology, X-ray scattering, microscopic techniques and tensile testing to describe consequences of photodegradation. As well, the effect of various degradation processes – natural weathering and accelerated UV irradiation lead to different results affecting resulting macroscopic properties.

Keywords: isotactic poly(1-butene), phase transformation, structure, properties, photodegradation

TABLE OF CONTENTS

ACKNOWLEDGEMENT 3

RÉSUMÉ 4

ABSTRACT 5

TABLE OF CONTENTS 6

LIST OF ABBREVATIONS 9

LIST OF FIGURES 11

1 INTRODUCTION 14

2 BIBLIOGRAPHIC STUDY 15

2.1 Isotactic poly(1-butene) 15

2.1.1 History 15

2.1.2 Molecular structure 16

2.1.3 Supermolecular structure 16

2.1.4 Crystallization 17

2.1.5 Polymorphic transformation 18

2.2 Properties of PB-1 23

2.2.1 Mechanical properties 23

2.2.2 Physical properties 24

2.2.3 Processing and application 25

2.3 Photodegradation 27

2.3.1 Radical oxidation 28

2.3.2 Aspects of natural weathering 28

2.3.3 Crystallization of degraded polyolefins 29

3 SUMMARY AND AIMS 31

4 MATERIALS AND EXPERIMENTAL TECHNIQUES 32

4.1 Materials 32

4.2 Sample preparation 32

4.2.1 Compression molding 32

4.2.2 Injection molding 32
4.2.3 Extrusion 33
4.3 Ageing 33
4.3.1 Annealing 33
4.3.2 Natural weathering 33
4.3.3 UV irradiation 33
4.4 Testing and characterization 35
4.4.1 Tensile testing 35
4.4.2 Polarized light microscopy 35
4.4.3 Stereomicroscopy 35
4.4.4 Scanning electron microscopy 35
4.4.5 Wide-angle X-ray scattering 35
4.4.6 Melt rheology 37
4.4.7 Infrared spectroscopy 39
4.4.8 Differential scanning calorimetry 39
5 STUDY OF TRANSFORMATION IN PB-1 41
5.1 DSC study 41
5.2 Evolution of properties of injection-molded PB-1 45
5.2.1 Tensile modulus 45
5.2.2 Tensile yield strength 47
5.2.3 Tensile elongation at break 48
5.2.4 Tensile strength at break 50
5.3 Evolution of structure and properties in PB-1 extrudates 51
5.3.1 WAXS evolution 51
5.3.2 Polarized light microscopy 53
5.3.3 Tensile modulus 54
5.3.4 Tensile elongation at break 56
5.3.5 Tensile strength at break 58
6 MULTISCALE CHARACTERIZATION OF DEGRADATION IN PB-1 61

6.1 Early stages 61
6.1.1 DSC study 61
6.1.2 FTIR characterization 67
6.1.3 Rheology 70
6.2 Prolonged stages 73
6.2.1 DSC study 73
6.2.2 FTIR-ATR characterization 73
6.2.3 Rheology 74
6.2.4 WAXS characterization 77
6.2.5 Stereomicroscopy 78
6.2.6 Scanning Electron Microscopy 78
6.3 Degradation of extruded PB-1 81
6.3.1 Mechanical properties 81
6.3.2 FTIR-ATR characterization 83
6.3.3 WAXS characterization 85
6.3.4 Stereomicroscopy 87
6.3.5 Effect of temperature on crystallinity and form II content 88
7 CONCLUSION AND PERSPECTIVES 90
8 REFERENCES 92
AUTHOR'S PUBLICATIONS 96
CURRICULUM VITAE 98

LIST OF ABBREVATIONS

Å	Angstrom
C-M	Compression-molded
c_x	Relative crystallinity
DSC	Differential scanning calorimetry
FTIR	Fourier Transform Infrared
FTIR-ATR	Fourier Transform Infrared - Attenuated Total Reflectance
G^*	Complex dynamic modulus
G'	Storage modulus
G''	Loss modulus
h	Parameter of the relaxation-time distribution
HDPE	High-density polyethylene
Hg	Mercury
I	Total intensity
I_c	Crystalline part
IR	Infrared
m1, m2	First and second melting corresponding to form I and II
mtr	Melting after transformation is completed
MW	Molecular weight
MWD	Molecular weight distribution
NMR	Nuclear magnetic resonance
NO_x	Nitrogen oxide
PB-1	Isotactic poly(1-butene)
PE	Polyethylene
PLM	Polarized light microscopy
PP	Isotactic polypropylene
R_g	Radius of gyration
SAXS	Small-angle X-ray scattering
SEM	Scanning electron microscopy
$tan\ \delta$	Phase angle
T_c	Crystallization temperature
TEM	Transmission electron microscopy
T_m	Melting temperature
UHMWPE	Ultra-high molecular weight polyethylene
UV	Ultra-violet
WAXS	Wide-angle X-ray scattering
Δl	Elongation
η^*	Complex viscosity
η', η''	Real and imaginary viscosity components

η_0	Zero shear viscosity
λ_0	Average relaxation time
ω	Frequency

LIST OF FIGURES

Fig. 1 Chemical formula of monomer and PB-1 polymer 16
Fig. 2 Interconversion between various physical forms of PB-1. (For simplicity, only an amyl acetate solution is considered in this figure) [32] 19
Fig. 3 Dependence of phase transformation of form II to form I on ambient temperature and pressure [34]. 19
Fig. 4 Tensile behavior of PB-1 vs. other polyolefins [34] 24
Fig. 5 Scheme of standard mechanism of the oxidation in polymer chain [62] 28
Fig. 6 Scheme of a SEPAP 12-24 34
Fig. 7 Spectra of lamps vapor Hg medium pressure used in a Sepap 12-24 34
Fig. 8 Wide-angle X-ray scattering patterns at different times [26] 37
Fig. 9 Deconvolution of the DSC curve obtained by PEAK-FIT V4 [105] 40
Fig. 10 Evolution of form I content in DP 0401M for various annealing temperatures 42
Fig. 11 Evolution of form I content in PB 0300M for various annealing temperatures 42
Fig. 12 Evolution of form I content in PB 8640M for various annealing temperatures 43
Fig. 13 Evolution of form I content in the whole temperature range for all materials in selected annealing days 44
Fig. 14 Evolution of tensile modulus in injection-molded PB 0300M 46
Fig. 15 Evolution of tensile modulus in injection-molded DP 0401M 46
Fig. 16 Evolution of tensile modulus in injection-molded PB 8640M 47
Fig. 17 Evolution of tensile strength at yield in injection-molded DP 0401M 47
Fig. 18 Evolution of tensile elongation at break in injection-molded PB 0300M 48
Fig. 19 Evolution of tensile elongation at break in injection-molded PB 8640M 49
Fig. 20 Evolution of tensile strength at break in injection-molded PB 0300M 50
Fig. 21 Evolution of tensile strength at break in injection-molded PB 8640M 50
Fig. 22 WAXS evolution of the form I content in extruded PB 0300M for various annealing temperatures upon time 52
Fig. 23 Images of morphology in extruded PB-1(bottom is border of specimen) 53
Fig. 24 Evolution of tensile modulus in extruded PB 0300M 55
Fig. 25 Evolution of tensile modulus in extruded DP 0401M 55
Fig. 26 Evolution of tensile modulus in extruded PB 8640M 56
Fig. 27 Evolution of tensile elongation at break in extruded PB 0300M 57
Fig. 28 Evolution of tensile elongation at break in extruded DP 0401M 57
Fig. 29 Evolution of tensile elongation at break in extruded PB 8640M 58
Fig. 30 Evolution of tensile strength at break in extruded PB 0300M 59
Fig. 31 Evolution of tensile strength at break in extruded DP 0401M 59
Fig. 32 Evolution of tensile strength at break in extruded PB 8640M 60

Fig. 33 Melting behavior of PB 0300M and DP 0401M (m1 – first melting, m2 – second melting, mtr – melting after transformation is completed)..... 62
Fig. 34 Crystallization behavior of PB 0300M and DP 0401M 62
Fig. 35 Melting and crystallization behavior of DP 0401M exposed to natural weathering, (m1 – first melting, m2 – second melting, mtr – melting after transformation is completed)..... 63
Fig. 36 Evolution of form I content during transformation of degraded specimens for various irradiation times in DP 0401M..... 64
Fig. 37 Evolution of ratio of form I to II during transformation of degraded specimens for various irradiation times in DP 0401M..... 65
Fig. 38 Evolution of form I content during transformation of degraded specimens for various irradiation times in PB 0300M..... 65
Fig. 39 Evolution of ratio of form I to II during transformation of degraded specimens for various irradiation times in PB 0300M..... 66
Fig. 40 Evolution of form I content during transformation of degraded specimens for various exposition times in DP 0401M..... 66
Fig. 41 Evolution of ratio of form I to II during transformation of degraded specimens for various exposition times in DP 0401M specimens..... 67
Fig. 42 FTIR spectra of DP 0401M - evolution in carbonyl area during UV irradition..... 68
Fig. 43 FTIR spectra of PB 0300M - evolution in carbonyl area during UV irradiation..... 68
Fig. 44 FTIR spectra of DP 0401M - evolution in carbonyl area during natural exposition..... 69
Fig. 45 Comparison of absorbancies at 1712 cm^{-1} in UV irradiated and naturally exposed specimens..... 70
Fig. 46 Cole-Cole plot of DP 0401M up to 10 hours of UV irradiation..... 71
Fig. 47 Cole-Cole plot of PB 0300M up to 10 hours of UV irradiation..... 71
Fig. 48 Evolution of zero shear viscosity and distribution parameter during UV irradiation..... 72
Fig. 49 Melting and crystallization behavior of PB 0401M (m1 – first melting, m2 – second melting, mtr – melting after transformation is completed)..... 73
Fig. 50 FTIR-ATR spectra of DP 0401M - evolution of carbonyl area during UV irradiation..... 74
Fig. 51 Cole-Cole plot of DP 0401M up to 20 hours of UV irradiation..... 75
Fig. 52 Cole-Cole plot of PB 0300M up to 20 hours of UV irradiation..... 75
Fig. 53 Evolution of zero shear viscosity and distribution parameter during UV irradiation in DP 0401M... 76
Fig. 54 Evolution of zero shear viscosity and distribution parameter during UV irradiation in PB 0300M... 76
Fig. 55 Evolution of crystallinity and form II content in UV irradiated specimens DP 0401M..... 77
Fig. 56 Evolution of crystallinity and form II content in naturally exposed specimens DP 0401M..... 77
Fig. 57 Images of surface degradation in DP 0401M in various UV irradiation times..... 78
Fig. 58 SEM images of surface degradation in the materials for various UV irradiation times..... 79
Fig. 59 SEM images of surface degradation in the DP 0401 naturally degraded at various exposition times 80
Fig. 60 Evolution of tensile modulus in UV irradiated and naturally exposed specimens..... 81

Fig. 61 Evolution of tensile stress at break in UV irradiated and naturally exposed specimens 82
Fig. 62 Evolution of tensile elongation at break in UV irradiated and naturally exposed specimens 82
Fig. 63 FTIR-ATR spectra of UV irradiated specimens..... 84
Fig. 64 FTIR-ATR spectra of naturally exposed specimens 84
Fig. 65 Comparison of absorbancies at 1712 cm^{-1} in UV irradiated and naturally exposed specimens..... 85
Fig. 66 Evolution of crystallinity and form II content in UV irradiated specimens 86
Fig. 67 Evolution of crystallinity and form II content in naturally exposed specimens..... 86
Fig. 68 Images of extruded tapes DP 0401M in various UV irradiation times 87
Fig. 69 Evolution of crystallinity in annealed and degraded specimens 88
Fig. 70 Evolution of form II content in annealed and degraded specimens 89

1 INTRODUCTION

This Ph.D. thesis (these en co-tutelle - co-supervised dissertation) has arisen from previous cooperation between Department of Polymer Engineering, Faculty of technology, Tomas Bata University in Zlín and Laboratoire de Photochimie Moleculaire et Macromoleculaire, Université Blaise Pascal, Clermont-Ferrand. The French government (Bourse de Gouvernement Francais) financed 18 months long study in France after successful presentation of the proposed project. The realization was performed during last 3 years with alternation of 6 months in France and 6 months in Czech Republic.

Studies related to the phase transformation of isotactic poly(1-butene) (PB-1) possesses, in general, rather high practical importance, as this phenomenon directly influences all material (product) properties; surprisingly, there are virtually no articles screening overall consequences arising from and after processing and during lifetime. Actually, these difficult interrelations are, in fact, a principal reason, why PB-1 has not found wide spectrum of applications yet, although its properties are favorably placed between isotactic polypropylene (PP) and high-density polyethylene (HDPE) and in some of them, even it exceeds their properties, e.g. creep behavior. Many articles have been devoted to explain a mechanism of the phase transformation, however these do not fully answer industrial questions how much time it takes until phase transformation is completed and at which temperature the processed products should be stored to obtain the fastest transformation rate. Both questions are closely connected with economical aspects of PB-1 production. A PB-1 degradability has not been practically studied at all, in term of assessment of durability the commercially produced PB-1. In addition, the question of subsequent recycling is nowadays frequently discussed; the properties of recycled PB-1 are practically unknown, neither the effect of oxidation on the phase transformation in such degraded material.

Thus, the knowledge of the interrelations between the supermolecular structure and the properties is therefore an important prerequisite enabling an estimation of the applicability of polymer materials. For this reason and mentioned questions, thesis is basically divided into two main parts.

The first part is concerned to the phase transformation of PB-1 itself; initially, using differential scanning calorimetry the transformation behavior is investigated in respect to different annealing condition. Afterward, the phase evolution is studied in both injection-molded and extruded PB-1 specimens using tensile testing with supplementary structural analysis being done with the help of X-ray scattering and microscopy.

The second part deals with a study of degradability of compression molded and extruded specimens under natural and accelerated UV conditions. Calorimetric characterization is performed to determine thermal properties and subsequently to observe the effect of degradation on phase transformation behavior. The particular attention is paid to a rheological characterization, which highly is sensitive to detect early stages of degradation. The property evolution on macroscopic scale of degraded specimens predicting its lifetime is observed through tensile behavior. The changes on supermolecular structural level are again screened using X-ray scattering, microscopy and infrared spectroscopy.

2 BIBLIOGRAPHIC STUDY

2.1 Isotactic poly(1-butene)

2.1.1 History

Isotactic poly(1-butene) (PB-1) was first synthesized in 1954, one year after polypropylene. It took another 10 years until Chemische Werke HÜLS, Germany, started the first industrial production in 1964. Vestolen BT was introduced to the market [1,2].

Independently, Mobil Oil in the USA developed their own PB-1 process technology and built a small industrial plant in Taft, Louisiana, in 1968. In early 70's the plant was taken over and operated by Witco Chemical Corporation.

In 1973 HÜLS withdrew Vestolen BT from the market after some manufacturing issues in their polymerization plant.

At the end of 1977 Shell Chemicals USA, a subsidiary of Shell Oil Company, acquired the PB-1 business from Witco, including the Taft plant. Shell then started a major investment program to improve the product quality and to increase the production capacity.

In 1988, the management of the PB-1 portfolio was put into the hands of Shell's subsidiary Montell Polyolefins. Exactly two years later, in October 2000, Montell Polyolefins merged with Targor GmbH and Elenac GmbH to form Basell Polyolefins.

In December 2000 Basell's management board approved an investment to construct a new plant in Europe. It utilizes a new process technology, which has been developed by Basell's Research and Development Centre in Ferrara, Italy. The new plant was constructed in Moerdijk, The Netherlands in 2003 [3]. In December 2007, Basell and Lyondell Chemical Company completed their merger to create LyondellBasell – one of the world's largest polymers, chemicals and fuels companies.

Apart from LyondellBasell, Mitsui Chemicals also manufacture PB-1 on their multi-purpose plants in Japan.

2.1.2 Molecular structure

There are three possibilities of stereochemical arrangement of the polymeric chains in poly(1-butene): syndiotactic, isotactic and atactic. While PB-1 was successfully synthesized and extensively studied in the mid-1950s, the synthesis of syndiotactic poly(1-butene) was just achieved by the recent discovery of the homogeneous metallocene catalytic systems [4].

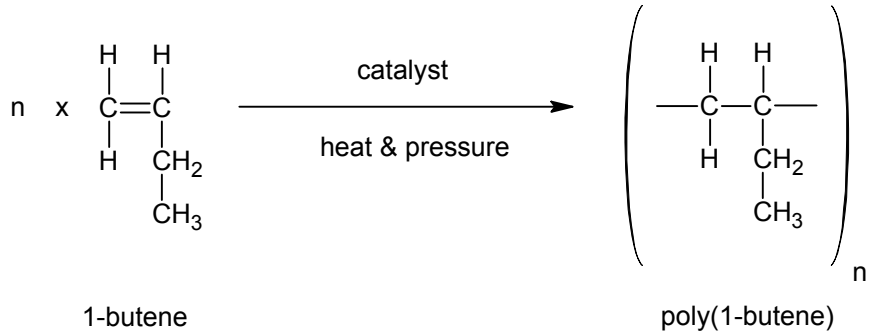

Fig. 1 Chemical formula of monomer and PB-1 polymer

The stereochemical configuration or "relative handedness" of successive monomer units in polyolefins such as PB-1 can strongly affect the physical and mechanical properties of the polymers. The stereo-specific Ziegler-Natta catalyst system is employed and the polymerization conditions are used to control polymer stereoregularity. The tacticity of PB-1 is strongly dependent on the catalyst system used, polymerization temperature, and reaction diluents [5]. Several methods can be used to quantify the isotacticity of PB-1. These methods include selective solvent extraction, infrared spectroscopy, scattering, NMR spectroscopy [4,6].

2.1.3 Supermolecular structure

For over 50 years it has been known that crystalline PB-1 occurs in multiple supermolecular forms. As all stereoregular polyolefins, PB-1 exhibits also polymorphic crystallization behavior. Five different crystalline forms have been recently reported in the literature, which are referred to as I, II, III, I', and II' [7].

In 1955, Natta et al. [8,9] reported the first two forms, with one of these being sufficiently unstable that it converted rapidly to the other, at pressures of around 10 MPa. The most common of these, called form I, was extensively studied in 1960. The crystal structure of form II was determined 3 years later, in 1963. Cojazzi [10] reported a form III of PB-1, obtained by evaporation from solution, in 1976.

Form II possesses 11/3 helical conformation with a tetragonal unit cell when crystallizing from the melt [11], with identity period of 6.8 Å [12]. Form II is unstable and transforms into a stable 3/1 helix conformation known as form I with twinned hexagonal [8] (rhombohedral) unit cells at room temperature and atmospheric pressure [8], with identity period of 6.5 Å [12]. The form I is being also assigned as trigonal form by some authors [13].

Orthorombic form III with 4/1 helical conformation has been observed in films of PB-1 precipitated from certain solvents [38].

The appearance of untwinned hexagonal form I' and form II' is related to crystallization under pressure [14] or from solution in case of form I' [15,16].

The first effort to study the kinetics of the crystallization and subsequent phase transformationhas been offered by Boor and Mitchell [17].

2.1.4 Crystallization

Cooke et al. studied using WAXS, SAXS and DSC the changes in the Avrami exponent at different crystallization temperatures, which are attributed to a change in nucleation mechanism [18].

The effect of molecular and processing parameters on shear-induced crystallization has been preliminary studied by Baert et al. [19]. They expect that the growth rate at high T_c is determined by the formation of stable nuclei and not so much by diffusion of polymer chains as in the case at low T_c, which results from Lauritzen-Hoffman polymer crystallization theory [20]. They also reported occurrence of the two different crystalline structures – besides expected spherulites, a square-like morphologies called hedrites being earlier reported [21-23]. Fu et al. [23] explained this effect as a change in the crystallization mechanism from folded-chain to chain-extended crystallization taking when the crystal thickness gets larger than the radius of gyration R_g of the chains.

The morphology of melt-crystallized PB-1 depends remarkably on the temperature of crystallization. When crystallizing the iPB-1 at temperatures lower than 60 °C, spherulitic structures were observed. Flat-on lathlike crystals could be formed at temperatures higher than 90 °C. In the temperature range from 60 to 90 °C, the spherulitic and flat-on lathlike structures coexist in the same sample [24].

The application of SCORIM (shear controlled orientation in injection molding) in PB-1 was studied by Kalay et al. [4]; a shish-kebab morphology was formed by a SCORIM injection molding, improved mechanical properties were observed.

The correlation between the gel time (measured from the change in tg δ) and quiescent/quasi-quiescent crystallization onset time of PB-1 using rheological measurement was studied by Hadinata et al. [25].

2.1.5 Polymorphic transformation

The most important phenomenon is following peculiar transformation - upon solidification from the melt PB-1 crystallizes into form II which is kinetically favored. In this stage iPB-1 is a rather soft, mechanically weak material. Over several days the material hardens by transforming into form I, which is thermodynamically favored. This transformation results in the desirable properties of the material [12,26,27]. The melting point increases from 120 to 135 °C.

The kinetics of this phase transformation is known to be influenced by strain [28], pressure [29], and temperature [27] (see Fig. 3). Actually, this rather slow kinetics is the principal reason why the commercial development of PB-1 has been much delayed.

Nakafuku and Miyaki [29] studied the effect of pressure on the crystallization behavior of PB-1 and reported that its melt crystallization under high pressure produces stable form I', which shows the same X-ray diffraction pattern as form I but has a much lower melting temperature (96 versus l30 °C) at atmospheric pressure. Above 200 MPa, form I' and form II' are crystallized from the melt. Form II' shows the same X-ray diffraction pattern as form II, but a lower melting temperature than form II. Form II' is metastable at atmospheric pressure and transforms to form I' on standing at room temperature [4].

Maring et al. [6,30] extensively studied a dynamic in the crystalline polymorphic forms I, II and III using NMR. Later, Miyoshi et al. [31] elucidated that side-chain conformation in form II is disordered as well as in amorphous sample, and the side-chain mobility in form II is higher than that in the amorphous sample. Furthermore, the distributed main-chain conformations in form II are partially ordered with reduction of the side-chain mobility. They suggested that the side-chain dynamics influences the main-chain conformation in form II.

The samples as-polymerized with the Ziegler-type catalysts contain form I' and form III. Melt crystallization usually leads to the formation of form II. However, when PB-1 is melt-crystallized under high hydrostatic pressure (>100 MPa), by a special meltstretching technique or onto specific substrates for epitaxial growth, formation of form I' has been reported. The formation of form III has also been reported when PB-1 is melt-crystallized with a specific nucleating agent. In the case of crystallization from a dilute amyl acetate solution, all three forms can be obtained by controlling dissolution and crystallization temperatures. When form I' and III were formed directly from the melt or from the amyl acetate solution, they transform into form II by annealing at 90 ~ 100 °C (probably through a melting-recrystallization process) [32]. The crystallization and morphology of the form III has been studied by Lotz and Thierry [33].

The interconversion between various physical forms of PB-1 is schematically shown in Fig. 2 [32].

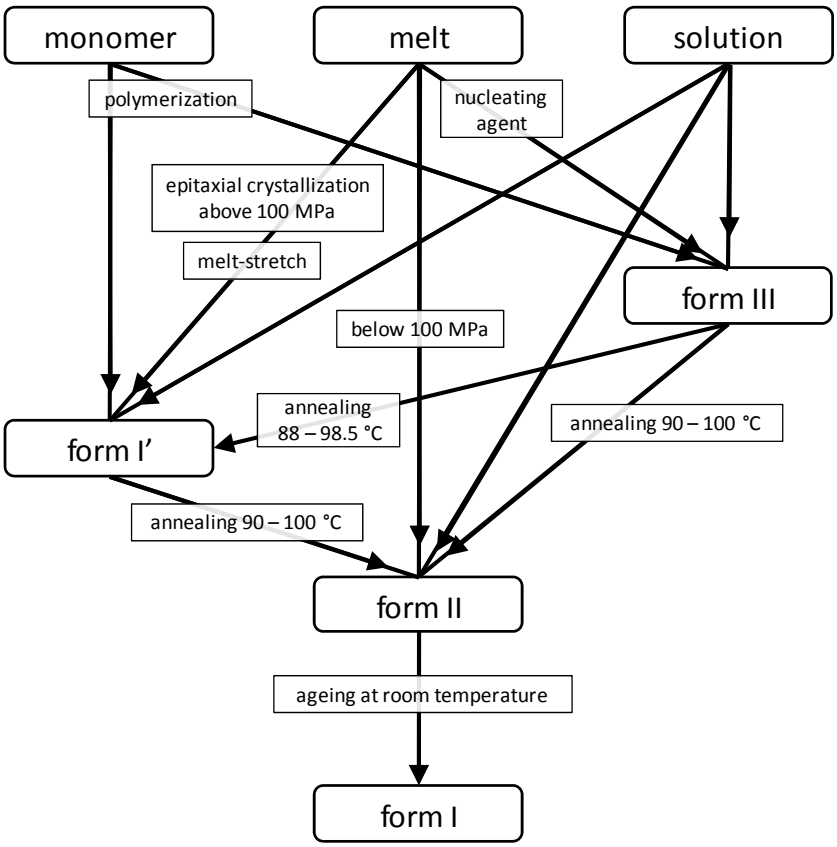

Fig. 2 Interconversion between various physical forms of PB-1. (For simplicity, only an amyl acetate solution is considered in this figure) [32]

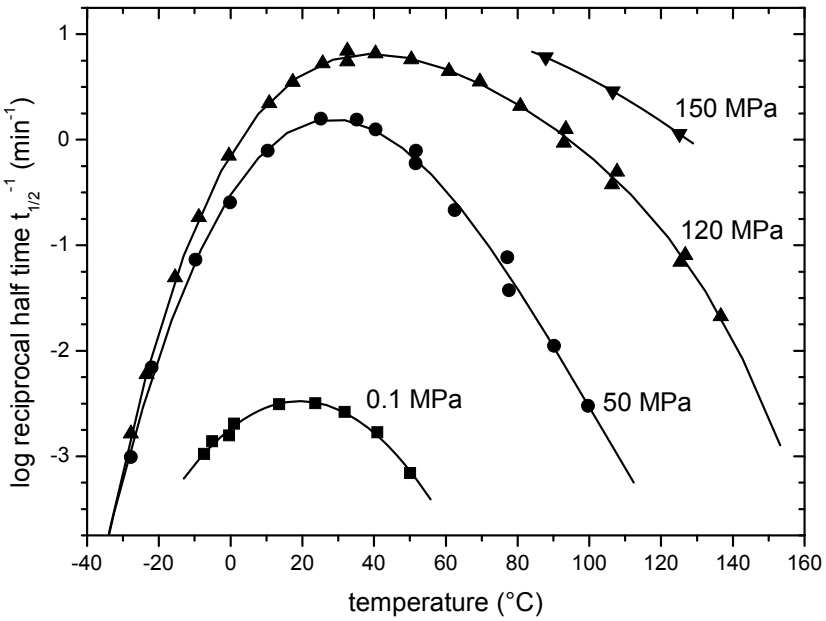

Fig. 3 Dependence of phase transformation of form II to form I on ambient temperature and pressure [34]

It is interesting that form II gradually transforms into form I during annealing at room temperature. In the case of solution grown single crystals, the morphological change induced by this transformation is not observed except for formation of small cracks. The form I that was obtained by the transformation from form II is the most stable and does not change into form II even when the sample is annealed again. In this context, the form I which is formed directly and can transform into form II by annealing is denoted as form I'. Because form I' showed broader crystalline reflection peaks in the X-ray spectrum than form I, form I' has been regarded to be an imperfect form I with many defects. It is still unclear, in terms of the molecular movements, how form II transforms into form I without changing the original shape [32].

In the early work by Miller and Holland [35], the formation of form I crystals twinning along the diagonals of the original squareshaped single crystal of form II was proposed; it was assumed that each quadrant of the square is an "untwinned" form I and adjacent quadrants are rotated by 90° with respect to each other. However, the twinning may not be essential for the transformation.

Fujiwara [36] investigated the transformation of oriented form II specimens and found that the "untwinned" form I appears by applying shear stress; the orientation of form I changed according to the relative direction of the stress. He proposed a nucleation mechanism for the transformation.

Kopp et al. [12] investigated the form II single crystals grown from an octanol solution by transmission electron microscopy (TEM), and their observation was explained by the molecular mechanism proposed by Fujiwara [36]. Tosaka et al. [32] recognized that, the transformation of PB-1 from form II to form I is initiated by stress, the nucleation of form I may occur as was proposed by Fujiwara [36]. However, another type of nucleation mechanism, which creates the "twinned" form I seems to exist. Once the form I domain is nucleated, it may grow by reeling in the molecular chains from the surrounding form II domains, creating new stems for form I. The traction force to reel in the molecules may sometimes rotate the form I domain itself. After the nucleation, the form I domain may be able to grow even when there is misalignment in the relative orientation with the surrounding form II domain. There is no specific crystallographic direction along which the form I domain tends to grow, and accordingly, the shape of the form I domain is irregular [32].

Marigo et al. [26] studied phase transformation II to I by WAXS and SAXS and suppose that a twofold mechanism of transformation could take place in PB-1. The transition nucleation seems to be localized on lamellar distortion points, and the transition itself involves the rearrangement of lamellae and of lamellar stacks. Moreover, a further crystallization of the amorphous phase into form I, seems to take place, with the appearance of new thin lamellae inside lamellar stacks.

Kaszonyiova et al. [37] found that organic and inorganic nucleating agents commonly used for polypropylene did not influence the polymorphism, but only crystallization rate.

It is reported that phase transformation is not accompanied by changes in macroscopic morphology and the overall crystallinity [38]: at most, an increase of the degree of crystallinity of about 5 % for samples quenched from melt.

While earlier studies of electron microscopy suggested that the phase transformation might produce fragmentation of lamellae into small blocks separated cracks [39], recent highresolution transmission electron microscopy studies could not provide an evidence of such cracks in transformed solution grown lamellae [32].

Several articles dealt with direct crystallization of the form I from the melt in solutions [12,13,40-42], however these attempts lead to single crystal without any perspective of industrial utilization.

Azzurri et al. [43,44] studied phase transformation by measurement of microindentation hardness and calorimetry. They observed that the form I has notably higher hardness than the from II. A good agreement was found between the degree of transformation evaluated from microhardness data and the calorimetry measurements. It is suggested, also by Gohil et al. [45] that the transformation rate does not depend on molecular mass (studied on PB-1 homopolymer supplied by Basell). High crystallization temperatures increase the transformation rate. The increase in the rate of the process with decreasing fraction of amorphous material is tentatively explained on the basis of the role by taut molecules at the crystal – amorphous interphase eventually favoring the helix extension needed for the phase transformation.

On the contrary, former study of Chau et al. [46] claimed that the transformation rate is lower in the high molecular weight sample and taut tie molecules cannot be a predominant factor which determines the transformation rate.

Earlier study of Luongo and Salovey [47] discovered from their infrared spectroscopic study that the rate of the phase transformation depends on the thickness of the compression molded films, decreasing with increasing thickness.

Choi and White [48] observed that in thin melt spun fibers, transformation rate II – I increases with the level of polymer chain orientation developed during melt spinning. In case of thick rods, the transformation rate is faster in the core section and slow at the outer surface. It suggested to be due to the development of quench stresses.

On the other hand, the effect of comonomeric units randomly distributed along the chain has been less studied by Foglia [49], Turner-Jones [50] - investigation of copolymers of 1-butene with various α-olefins. They observed that copolymerization of PB-1with α-olefins with less than 5 carbon atoms increases the transformation rate while long linear α-olefins or branched co-units speed up the rate of the process. Turner-Jones [50] explained these results by considering that the insertion of co-units having a small cross-sectional area favors the 3_1 helical conformation and therefore increases the transformation rate. On the

contrary, long linear co-units, with more than 5 carbons, or branched comonomers, stabilize the 11_3 helix due to steric factors and hinder the II - I transformation. Recently, Azzurri et al. [51] reinvestigated the phase transformation in a series of PB-1 copolymers containing randomly distributed ethylene units. It was observed that, similar to the homopolymers, the rate of the transformation does not depend on the average length of constituent chains. On the other hand, a small amount of this type of co-unit is sufficient to strongly accelerate the transformation to the extent that, at room temperature, only a few hours is sufficient to complete the process, while in case of the homopolymers it takes several days.

It was found, in several studies that the presence of nanofillers in PB-1 matrices such as layered silicates, nanotubes, nanoparticles, modified clays increases the transformation rate [52-57]. Wanjale and Jog [52] suggested from their study on PB-1 with carbon nanotubes that it is attributed to the decrease in the amorphous content and to the enhanced nucleation of form I due to disordered crystallite morphology.

2.2 Properties of PB-1

Isotactic poly(1-butene) can be regarded as a polymer having a number of attractive properties that distinguish it from the most common polyolefins like isotactic polypropylene or polyethylene. PB-1 is a semi-crystalline polymer with high isotacticity and consequently high crystallinity. Generally, the crystalline part determines a number of intrinsic characteristics of the polymer. It exhibits advantages over the other polyolefins in toughness, tear strength, flexibility, creep, stress cracking resistance, impact resistance and abrasion resistance. The crystalline layers in PB-1 are connected by entangled tie-molecules. These tie-molecules reside in the amorphous part. Because of the high molecular mass a large number of tie-molecules is generated and the relatively long C_2H_5 side groups prevent extensive slipping of entanglement chains. These two factors make the bonds between adjacent crystallites very stable. The crystalline lamellae form spherical superstructures, consequently, a strong 3-dimensional network of entangled crystallites is formed [34].

2.2.1 Mechanical properties

The Tab. 1 shows the mechanical properties of PB-1. The values shown are typical mid-range figures and should not be considered as a specification – in fact, several different grades of PB-1 are produced with properties tailored to satisfy different application requirements [47].

Tab. 1 Mechanical properties of PB-1 [34]

Material Properties	Method	Unit	PB-1 4237
Tensile strength at yield	ISO R 527	MPa	20
Tensile strength at break	ISO R 527	MPa	35
Elongation at break	ISO R 527	%	300
Flexural Elastic Modulus	ISO 178	MPa	450
Notched Impact Strength at 20 °C	ISO 180	$kJ.m^{-2}$	20
Notched Impact Strength at 0 °C	ISO 180	$kJ.m^{-2}$	7

The peculiar tensile behavior of PB-1 is based mainly on the chain entanglements mentioned above. PB-1 does not show the typical necking behavior; instead, it tends to support the load while it continues to stretch. This is sometimes referred to as “ductile with work-hardening”. Depending on the preparation of the test specimen and the conditions of measurement, PB-1 may exhibit a very little yielding in stress-strain behavior (see Fig. 4).

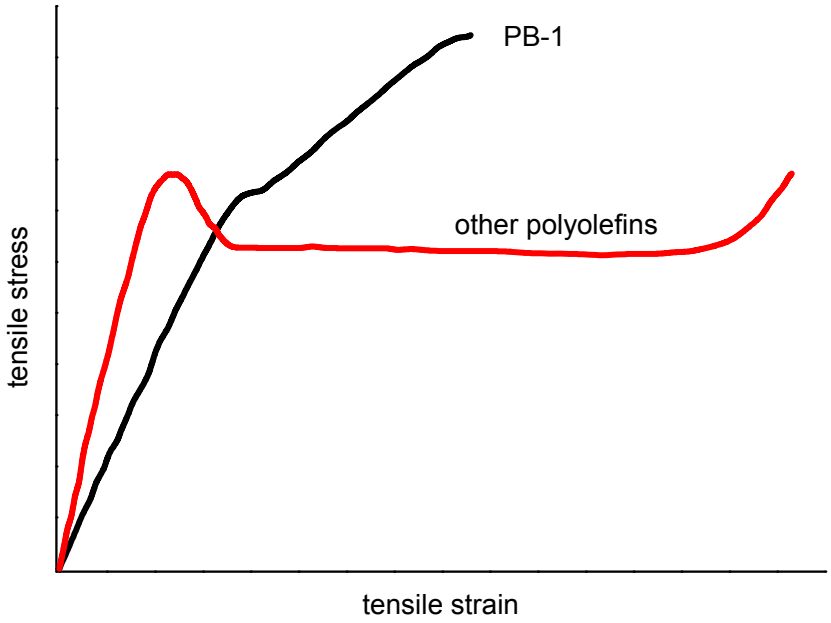

Fig. 4 Tensile behavior of PB-1 vs. other polyolefins [34]

PB-1 has excellent impact toughness. The IZOD notched impact strength (ISO 180) of PB-1 is classified "no break" at room temperature. The material retains its flexibility even at temperatures below freezing point, which strongly facilitates installation during cold seasons. The glass transition temperature determining the ductile/brittle transition of PB-1 lies at approx. –16 °C [34].

2.2.2 Physical properties

Density and melting point of various crystallographic forms of PB-1 shows Tab. 2.

Tab. 2 Density and melting point of PB-1

Material	density $g.cm^{-3}$	T_m °C	ref
PB-1 amorphous	0.868		[58]
PB-1 form I	0.95 ~ 0.96	126 ~ 139	[59]
	0.95	125	[58]
PB-1 form II	0.819 ~ 0.902	120 ~ 130	[59]
	0.907		[58]
PB-1 form III	0.897 ~ 0.906	106 ~ 110	[59]

Isotactic poly(1-butene) has an excellent wet abrasion resistance, when tested in sand/slurry type conditions. It performs as well as UHMW-PE which is well known for its outstanding abrasion and wear resistance [34].

Thermal degradation of PB-1 results in decrease of molecular weight, melting temperature and glass transition temperature [60].

2.2.3 Processing and application

However, even after more than 50 years from its discovery, and despite its potentials, PB-1 is still a relatively new resin (particularly in respect to its application range) that is being produced in limited quantities and has not yet found a large commercial success as compared to the other polyolefins. This is likely due to both the relatively high monomer cost, possibly coupled with difficulties in polymerization technology, and the peculiar crystallization behavior of the polymer [26].

Several possibilities of the polymer processing are reported [10]. PB-1 can be injection-molded, blow molded, cast or blown into sheets and films, and extruded for wires coating [61]. The processing behavior of PB-1 is somewhat intermediate between the behavior of HDPE and PP. Processing temperatures are in the range 160 ~ 240 °C. Both die swell and cooling shrinkage are greater than for PE. The crystalline material formed initially on cooling from melt is rather weak and must be handled with care on the haul of equipment. As mentioned above the polymer must be aged for about a week in order to allow the more stable crystalline form to develop [1].

Today, PB-1 is being discovered as a key to unlock opportunities in applications such as packaging, construction, fibers and fabrics, compounds, adhesives, and coatings, just to name a few [3].

The main interest in PB-1 is in its use as a piping material, where the ability to use a lower wall thickness for a given pressure requirement than necessary with other polyolefins, together with low density, can lead in some cases to economic use. The principal application is for small-bore cold and hot water piping (up to 95 °C) for domestic plumbing [1]. In Europe and Asia, PB-1 has been developed over the past 30 years to be arguably the technically preferred material. Pipe system manufacturers state that piping systems made from PB-1 offer easy, fast installation with a reduced number of joints and connectors compared to much stiffer conventional plumbing materials. In service, they note that the piping does not corrode or fur up in hard water areas, it does not split at sub-zero temperatures and is quieter in use as it does not suffer from "water hammer". It is used both in the construction of new buildings and the renovation of older properties. A major UK housebuilder uses exclusively PB-1 piping systems. LyondellBasell's PB-1 is not being sold for pipe applications intended for use in North America [2].

Further important application area for PB-1 is seal-peel or easy-open packaging. Typical examples include carton liners (e.g. cereal packaging) and packs for pre-packed delicatessen products like cold meats, cheeses and smoked salmon. PB-1 offers the ability to customize sealing temperatures and seal strength whilst giving consistent, reliable processing and sealing performance on existing equipment, and built-in tamper-evidence. PB-1 can also be used in film modification to increase flexibility and softness without sacrificing clarity. In a similar vein, PB-1 is used to modify polypropylene fibers to enhance softness, flexibility and to provide a unique feel [2].

PB-1 is also used commercially in films that require creep resistance such as insulation compression packaging. It can also be used as a layer or overall film for hot filled heavy duty packaging, tapes for bundling and holding loads at elevated temperature such as bale wrap, specialty sheet applications such as anti-erosion geo-grids and netting and cable ties [2].

PB-1 features in hot melt adhesives, where its unique crystallization behavior reduces the melting point and extends the "open time" of the adhesive to as much as 30 minutes, to enable time for repositioning of components prior to setting. It is widely used as a component in hot melt adhesives for non-woven fiber webs [2].

PB-1 is also typically used in applications that see continuous load at moderate to high temperatures. It is used in electric domestic heaters in North America, where it is blow molded into large 15 ~ 20 kg tanks. Other logical extensions may include fire extinguishers, residential and swimming pool water filter housings, pressurized pneumatic holding tanks, hoses, compressed gas cylinders and aerosol dispensers, to name just a few. There is also considerable interest in the potential of PB-1 to be used as a component in synthetic wine corks [2].

PB-1 is also employed in compounded polymer products to provide unique benefits. It accepts extremely high filler loadings (>70 %), which combined with its low melting point, enables it to be used in halogen-free flame retardant composites or as a masterbatch carrier for difficult-to-disperse or temperature-sensitive pigments [2].

2.3 Photodegradation

Photodegradation (chain scission and/or crosslinking) occurs by the activation of the polymer macromolecule provided by absorption of a photon of light by the polymer. In the case of photoinitiated degradation light is absorbed by photoinitiators, which are photocleaved into free radicals, which further initiate degradation (in non-photochemical processes) of the polymer macromolecules. In photo-thermal degradation both photodegradation and thermal degradation processes occur simultaneously and one of these can accelerate another. Photoageing is usually initiated by solar UV radiation, air and pollutants, whereas water, organic solvents, temperature and mechanical stresses enhance these processes [62].

In spite of extensive studies of photodegradation of polymers, there are many unsolved problems. Many publishers results are even contradictory and it is difficult to compare them, as the results are frequently obtained on different samples of the same polymer and under different experimental conditions. Many proposed mechanisms are still not experimentally proven [62].

Neat PB-1 because of contains only C-C and C-H bonds and is not, therefore, expected to absorb light at wavelengths longer than 200 nm. The fact that photodegradation of polymers occurs even with light >300 nm indicates that some kind of chromophoric groups must be present in these polymers. The chromophores in commercial PB-1 are developed during polymerization and thermal processing.

During polymer photodegradation two types of processes occur: (i) primary photochemical reactions due to the absorbed radiation, resulting in the formation of free radicals or non-radicals rearrangement; (ii) secondary reactions in which radicals formed initiate a number of reactions which are independent of the light [62].

As generally accepted, degradation reactions of semicrystalline polymers proceed predominantly in amorphous regions. Nevertheless, physical factors, such as the size, arrangement and distribution of crystalline regions, affect the degradation process as well. Photodegradation kinetics in polymer systems depends on oxygen permeability through the material [63]. The rate of oxidation drops with decreasing oxygen diffusion, following the increase of crystallinity and molecular orientation [64,65].

On the other hand, the crystallinity and the molecular orientation determine the mobility of the radicals and therefore reduce the rate of termination, allowing an increase in the propagation of chemical reactions leading to molecule scission, and this effect is opposite to that caused by reduced oxygen mobility. Which of these two effects will predominate depends on the oxidation conditions, including the type of degradation, temperature and oxygen concentration [65].

2.3.1 Radical oxidation

Hydroperoxides are well known to be crucial products of the free radical oxidation of most polymers [66]. The mechanism of radical oxidation in poly(1-butene) is still unknown, nevertheless, the similar mechanism as in the case of polypropylene is suggested, where resulting hydroperoxides are predominantly tertiary (~ 90 %), the remainder being essentially secondary ones [67], on the contrary in polyethylene only secondary hydroperoxides are present [68]. The general mechanism is shown in Fig. 5. These hydroperoxides groups are the key products for understanding the mechanism as well as for gaining better insight into the function of stabilizers [69]. Ouldmetidji et al. [70] found that peroxides in macromolecular media can be detected using DSC which is more precise than classical titration of peroxides. Unfortunately, in case of PB-1, its melting temperature is close to peroxide decomposition temperature, thus a modulated DSC is required to detect the peroxide groups in PB-1.

initiation	$PH \xrightarrow{\Delta,\ h\upsilon} P\cdot$	
chain propagation	$P\cdot + O_2 \longrightarrow POO\cdot$ $POO\cdot + PH + O_2 \longrightarrow POOH + P\cdot$	
chain branching	$POOH \xrightarrow{\Delta,\ h\upsilon} PO\cdot + \cdot OH$ $2\ POOH \xrightarrow{\Delta,\ h\upsilon} PO\cdot + H_2O + POO\cdot$ $PO\cdot \longrightarrow chain\ scission\ reaction$	
termination	$P\cdot + P\cdot \longrightarrow products$ $P\cdot + POO\cdot \longrightarrow products$ $POO\cdot + POO\cdot \longrightarrow products + O_2$	$crosslinking\ reactions\ to\ non-radical\ products$

Fig. 5 Scheme of standard mechanism of the oxidation in polymer chain [62]

2.3.2 Aspects of natural weathering

Natural weathering offers reliable data on durability of stabilized polymers in a particular area of application [71]. Nevertheless, this technique has some disadvantages. It is difficult to compare results obtained in different geographical regions even when the materials are stressed by similar intensity of solar radiation, however at different temperatures and atmospheric pollution [72].

Indeed, the weather as a whole is unpredictable and itself not a reproducible factor in short-term as well as long-term periods. This is an unfavorable basis for attempts to predict long-term lifetime of polymers affected by weathering. Basic data on weather components reflected in polymer weathering are briefly mentioned here: solar radiation, oxygen and casual oxidizing and acid atmospheric pollutants are principal atmospheric detergents responsible together with environmental temperature and humidity for the reduced durability of outdoor exposed stabilized polymers. Microorganisms add to the failure. Various detergents act in concerted processes and their effects are mostly complementary or even synergistic [73].

UV radiation of 295 ~ 400 nm characteristic of a continuous spectrum and constituting about 1 ~ 5 % of the total solar radiation is a dangerous component initiating most outdoor processes by photolysis of polymer or additive covalent bonds, photolysis of hydroperoxides and excitation of chromophores [62,74]. It follows that an increase in intensity of UV radiation or involvement of more energetic UV-B radiation below 295 nm in artificial radiation sources accelerates photoprocesses, but may at the same time cause differences in degradation mechanisms and stabilizer durability. Visible light (400 ~ 760 nm) forms 39 ~ 53 % of the terrestrial solar radiation and increases photodegradation by sensitization of visible light-absorbing chromophores or additives. Besides UV radiation, some level of visible light emitted by artificial sources in accelerated tests is recommended. Infrared radiation (760 ~ 2500 nm, 42 ~ 60 % of the solar radiation) triggers thermal effects, particularly in dark pigmented polymers [74]. Infrared radiation is a source of differences measured between environmental temperature and surface temperature of the irradiated polymer. Formally, an exact simulation of the ‘‘standard’’ solar radiation distribution in well-designed accelerated tests is possible. However, under natural conditions, sunlight emissions vary in spectral energy distribution and intensity [71]. Even on using optimized artificial radiation sources (e.g., filtered xenon arcs) an exact simulation of natural exposure is hindered. Nevertheless, application of devices with artificial sources makes possible a comparison of results between various laboratories [73].

Besides oxygen, the common oxidizing component, the Earth’s atmosphere contains traces of pollutants arising from biogenic or anthropogenic emissions. Ozone and nitrogen oxides (NO_x) are oxidizing and reducing pollutants co-acting with solar radiation. Their atmospheric photochemistry as well as details of their effects on rubbers is well understood [75,76]. Interactions with plastics or stabilizers in particular are not fully explained. They can be generally categorized as phototriggering impurities [74]. Moreover, NO_x are responsible for photo-assisted depletion of phenolic antioxidants (in gas fading) [77].

The effect of pressurized chlorinated water in PB-1 pipes was studied by Lundback et al. [78]. It was observed that antioxidant concentration is independent of chlorine concentration and the lifetime shortening was approx. by a factor 10 with respect to that obtained in pure water.

PB-1 is sensitive to oxidizing acids, aromatic and chlorinated hydrocarbons. The polymer is very sensitive to environmental stress cracking [2].

2.3.3 Crystallization of degraded polyolefins

The crystallization of polymers depends on many factors including the shape and stereoregularity of the repeat unit, the presence of branches and crosslinks, and the molecular chain length in the linear segments. In polypropylene, the repeat unit is small and can easily be assembled into crystal form. When polypropylene is subjected to photo-oxidation several changes occur that influence the crystallinity and the crystallizability of the material [65,79]. Caig et al. [79] studied oxidation that occurs at or near to ambient

temperature, when the polymer is in solid form, well below the crystallization temperature. The changes occur predominantly in the non-crystalline phase because oxygen can diffuse through such regions relatively freely but is almost excluded from the crystalline regions. The principal changes are (i) chain scission; (ii) crosslinking; and (iii) the formation of molecular defects such as carbonyl groups. Chain scission releases chain segments that were previously entangled and allows them to crystallize. If enough material of this kind becomes available to crystallize, new crystals could form but it is more likely that these segments will attach to the growth faces of pre-existing crystals nearby. This will increase crystallinity and is a form of secondary crystallization often known as "chemi-crystallization" [64,80,81]. Crosslinks inhibit further crystallization of the chain segments that are connected by them. Molecular defects such as carbonyl groups, which are formed, do not fit into the crystal lattice and the parts of the molecular segments containing them will not be able to take part in secondary crystallization [79].

Chemi-crystallization is caused by a variety of molecular degradation processes and has been detected in many polymers [82-86]. If, as expected, oxidation within the crystal phase is relatively rare, the network effect of photo-oxidation will be an increase in crystallinity and the formation of material in the amorphous phase that becomes increasingly unable to crystallize even if scission events or elevated temperature mobilize the chain segments. Thus, it is expected that, after a certain exposure, the rate of chemi-crystallization will decay to zero. Chemi-crystallization is an important phenomenon because the density of the crystals is higher than that of the amorphous material and shrinkage occurs. Under UV irradiation, the scission (and hence secondary crystallization and, in turn, shrinkage) tends to vary very sharply with distance from the exposed surface [87,88] and this leads to the development of tensile residual stresses near the surface [89,90]. The residual stresses and also freezed stresses arising from a processing [91] can lead to cracking of the material that has already been embrittled by the molecular degradation, through the loss of entanglements and the consequent loss of mechanical integrity provided by the molecular network, and through the reduced flexibility that results from increased crystallinity and crosslinking that may be present additionally [87,88]. Serious deterioration of engineering properties may therefore occur. If the cracks are not very deep and do not lead to total failure, the appearance may become unacceptable because of fine surface cracks that spoil the glossy appearance, etc. Residual stresses lead to distortion if they are not balanced across the molding section.

When photo-oxidized material is melted and cooled down again, the crystallinity of the newly solidified material will depend not only on the polymer and the cooling conditions but also on the molecular changes that occurred during photo-oxidation. The shorter chains produced by scission events (which are still regular) will crystallize more readily whereas crosslinks and molecular defects will not be able to crystallize and will be rejected from the newly formed crystals. Thus, there are two opposing effects, one that promotes greater crystallizability and the other inhibiting crystallization [79].

3 SUMMARY AND AIMS

Isotactic polybutene-1 is a polymorphic material similar to isotactic polypropylene, however its peculiar transformation behavior is a main factor inhibiting its use as compared the other polyolefins, namely polyethylene and polypropylene. As written above in Chapter 2, PB-1 crystallizes from melt to kinetically favored form II and according to annealing conditions it recrystallizes to thermodynamically stable form I. The transformation behavior of technologically processed materials has not practically been studied yet and the degradation behavior of PB-1 is unknown as well. The lack of knowledge can be considered as one of the reasons explaining rather low practical use of PB-1.

Therefore, this thesis is concentrated on study of transformation behavior in processed PB-1 under various thermodynamic conditions and changes in structure and properties are observed; the degradation behavior of naturally weathered and accelerated UV irradiation.

The main aims of this thesis are according to present knowledge following:

1. Phase transformation in PB-1 upon various thermodynamic conditions.
2. Evolution of structure and properties of injection-molded and extruded PB-1.
3. The effect of photodegradation on the evolution of structure and properties in PB-1.

4 MATERIALS AND EXPERIMENTAL TECHNIQUES

4.1 Materials

In this work, three commercially-available grades of isotactic poly(1-butene) produced by Basell Polyolefins, Louvain la Neuve, Belgium were used. The basic properties of PB-1 grades are described in table Tab. 3.

Tab. 3 Used materials of PB-1 [92]

Material grade – method	PB 8640M	DP 0401M	PB 0300M
Characteristics	Random copolymer of butane-1 and ethylene	Semi-crystalline homopolymer	Semi-crystalline homopolymer
Density ($g.cm^{-3}$) - ISO 1183	0.906	0.915	0.915
Melt flow index - ISO 1133 (190 °C / 2.16 kg)	1 g/10 min	15 g/10 min	4 g/10 min
Flexural modulus - ISO 178	250 MPa	450 MPa	450 MPa
Tensile strength at yield ISO 8986-2		22 MPa	19.5 MPa
Tensile strength at break ISO 8986-2	30 MPa	29 MPa	35 MPa
Tensile elongation at break ISO 8986-2	300 %	300 %	300 %
Melting temperature m1 DSC	113 °C	126 °C	127 °C
Melting temperature m2 DSC	97 °C	114 °C	116 °C

Mechanical properties were measured on specimens conditioned for 10 days at 20 °C

4.2 Sample preparation

4.2.1 Compression molding

Sheets with thickness of 0.3 and 1.0 mm were prepared by compression molding at temperature of 190 °C, compression time of 5 minutes and subsequent cooling to 20 °C for 5 minutes.

4.2.2 Injection molding

A DEMAG NC 4 injection molding machine was employed for production of tensile testing specimens according to standard ISO 527 (tensile dumbbell test bars with a gauge length of 80 mm, width of 10 mm and thickness of 4 mm). The main processing parameters were following for all material grades: Temperatures in the barrel: 50, 170, 190, 200 and 210 °C (feed, transition, metering and nozzle); injection pressure 75 MPa with injection speed 50 mm/s; holding pressure 50 MPa with time 25 s; cooling time 40 s; mold temperature 50 °C.

4.2.3 Extrusion

The materials were extruded using a Brabender extruder with temperature setting 140 °C, 145 °C, 150 °C (barrel) and 150 °C (head) . A rotation speed was 20 rpm. The extruded tape had approx. 20 mm width and thickness approx. 2 mm. Then, the tapes were cut off to the pieces with length 160 mm.

4.3 Ageing

4.3.1 Annealing

The prepared specimens were immediately after processing annealed at various temperatures: -22, +5, +22, +40 and +60 °C at atmospheric pressure for various times. The temperatures were chosen with respect to utilization of PB-1, which can be used for tanks, hose, tubing, molded parts, films, etc. at various temperatures. The chosen temperature of -22 °C is generally temperature in freezer; +5 °C refrigerator, cold water; +22 °C room temperature; +40 °C hot weather temperature, water; +60 °C hot water, heating.

4.3.2 Natural weathering

Natural weathering was performed in Nivnice, Czech Republic, altitude of 250 meters, geographical position 48°58′42″N and 17°38′47″E. Specimens were exposed in south direction under the exposition angle of 45°, between May 7 and July 13, 2008, i.e. 0 ~ 63 days in case of sheets 0.3 mm thick and during June 6 to September 17 2008 i.e. 0 ~ 103 days in case of dog-bone specimens.

The meteorological data are in the table 4.

Tab. 4 meteorological data [93]

Month	rain-fall (mm)	ØT (°C)	clearness day	cloudiness day	thunderstorm	summer day	tropic day
May	82.2	15.2	9	4	6	12	1
June	78.8	19.8	10	1	17	14	10
July	104.7	19.7	10	14	8	12	10
August	95.3	18.9	14	1	12	18	7
September	62.3	13.7	9	9	1	9	3

Explanation: ØT - average temperature (calculated by three temperatures at 7, 14 and 21 hours; evening observation is calculated twice and divided by 4); clearness day – max 20 % of covered sky; cloudiness day – cloudy 80 – 100 %; summer day – part of day >25 °C; tropic day – part of day >30 °C

4.3.3 UV irradiation

For accelerated UV irradiation, a SEPAP 12/24 MPC type of commercial device was employed at temperature of 60 °C, UV irradiation wavelength $\lambda > 300$ nm and the sampling was performed in various ageing times.

Each quarter angle of rotating carousel with specimens is covered by one lamp vapor mercury "medium pressure" (MAZDA 400W) (Fig. 6), en emission of spectra of which is polychromatic. The wavelength shorter than 300 nm is filtered by Pyrex glass cover adjustment of lamps where its emission of spectra is superposed to the sun spectra (Fig. 7). The carousel with specimens rotates with speed 4 rotations per minute to assure the homogenization of the luminous flux by specimens. Distance between the specimen and the lamp is 20 cm. The temperature on the surface of the specimens is controlled by a platinum sonde (Pt 100) which is in contact with PE film fixed on carousel. Temperature regulation is assured by a ventilator; the temperature was fixed to 60 °C.

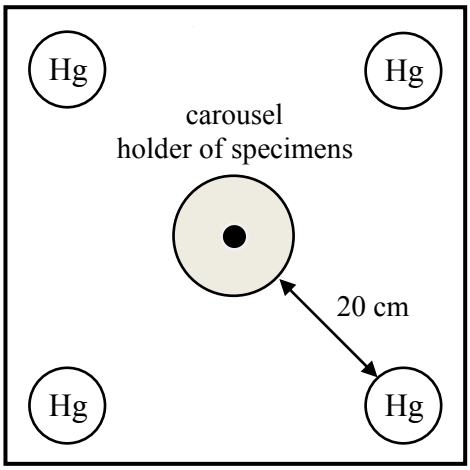

Fig. 6 Scheme of a SEPAP 12-24

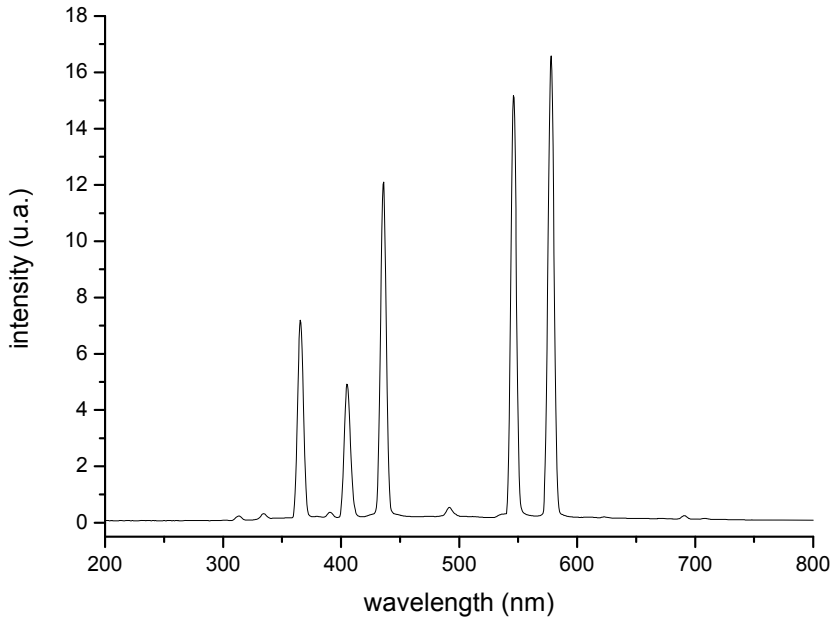

Fig. 7 Spectra of lamps vapor Hg medium pressure used in a Sepap 12-24

4.4 Testing and characterization

4.4.1 Tensile testing

Tensile testing was performed using an INSTRON 8871 apparatus at room temperature. The specimens with a gauge length of 80 mm were deformed to a maximum elongation Δl = 100 mm. The rate of extension was 100 mm/min.; tensile modulus, yield stress and extension at break were calculated by a Bluehill software, which is a part of the tensile testing apparatus for its operating and evaluation of the results. Five specimens were tested and average values are reported.

In addition, a Zwick 145665 multipurpose tester was used for the tensile testing of extruded tapes with a gauge length of 80 mm (specimen dimensions - width x thickness x length – 20 x 2 x 110 mm) and dog bone-shaped specimens (ISO 527-3 type 5A) cut out from the tapes with a gauge length of 30 mm. The specimens were strained at room temperature up to break at a test speed of 50 and 100 mm/min. From the stress–strain traces, yield stress, yield strain, stress at break and strain at break were derived. Besides, the elastic modulus was evaluated using a Zwick external extensometer (gauge length of 20mm) at a test speed of 1mm/min. Five specimens were tested and average values are reported.

4.4.2 Polarized light microscopy

The spherulitic morphology of the specimens was observed using a Zeiss NU light microscope equipped with a polarizer. For this purpose, thin slices with thickness approximately of 40 μm were cut out using a Leica rotational microtome. The observed morphologies were taken by Sony DSC F717 camera.

4.4.3 Stereomicroscopy

The surfaces of the degraded materials were surveyed by Stereo microscope ZEISS Stemi 2000-C equipped by Sony DSC F717 camera.

4.4.4 Scanning electron microscopy

Scanning electron microscopy (SEM) is useful method for most types of surface morphology examination. In this work, it was used for analyzing of degraded surfaces.

The surface of the specimens were coated with a thin gold/palladium (SC7620 Mini Sputter Coater) film and examined in a scanning electron microscope Vega\\LMU (Tescan, Czech Republic).

4.4.5 Wide-angle X-ray scattering

Wide-angle X-ray scattering (WAXS) is the traditional method of crystallographic structure determination, the standard technique and analysis procedure, which can be used in the study of crystalline polymers. WAXS measurements were used to determine the degree of crystallinity and polymorphic composition of the prepared specimens.

For scattering in the transmission mode, diffraction angle with interval 2θ = 7 ~ 25°, the measuring step of 0.05° and holding time of 5 s were used. A URD6 diffractometer CuKα radiation monochromatized with a Ni filter (λ = 0.154 nm) was employed for measuring of PB-1 extrudates in reflection mode. Whole extrudates (only cut in length) were used as specimens for scattering.

For scattering in the reflection mode, a Philips Xpert was employed with interval 2θ = 5 ~ 30°, measuring step of 0.05° and holding time of 0.5 s, CuKα radiation monochromatized with a Ni filter (λ = 0.154 nm). The degraded sheets with thickness of 1 mm and the degraded extrudates were scattered by this device.

The reflections relative to the tetragonal form of PB-1 are basically three main peaks at 11.9, 16.9 and 18.48 2θ, corresponding to the (200), (220) and (301) planes. The hexagonal phase I is characterized by four diffraction peaks at 9.9, 17.3, 20.2 and 20.58 2θ, originated by the (110), (300), (220) and (211) planes, respectively [20]. It may be noted that, as a consequence of the phase transition, with increasing time the intensity of the peaks typical of the hexagonal phase I (i.e.(110) at 9.98 2θ) increases, whereas the intensity of peaks related to the tetragonal phase II (i.e. (200) at 11.98 2θ) decreases (see Fig. 8).

A PEAKFIT v4 was used for the evaluation of crystalline part in the specimens. It is suggested to follow the disappearing of the peak at 11.8° 2θ (reflection plane 200) the form II rather than increase the peak at 9.9° 2θ (reflection plane 110) of the form I because, together with the phase transformation, a post crystallization phenomenon takes place during which part of the amorphous polymer crystallizes into the form I [26]. However, in this work, it was not possible to measure the identical specimen but a series of specimens prepared under controlled conditions. It was decided to follow evolution of the both peaks of forms I and II (at 9.9° and 10.8° 2θ) and calculate the ratio of heights both peaks and content of the form I from the total sum of both heights. The same approach has been used in several works by Azzuri et al. [51], Samon et al. [94] and Natta et al. [8]. The similar approach was used in work of Kaszonyiova et al. [37] or in case of isotactic polypropylene, which is also a polymorphic material [95,96].

Relative crystallinity c_x was calculated according to the equation (1) as a ratio of integral intensity diffracted in certain measuring direction by crystalline part I_c and a total intensity I:

$$c_x = (I_c/I) \cdot 100\ \% \qquad (1)$$

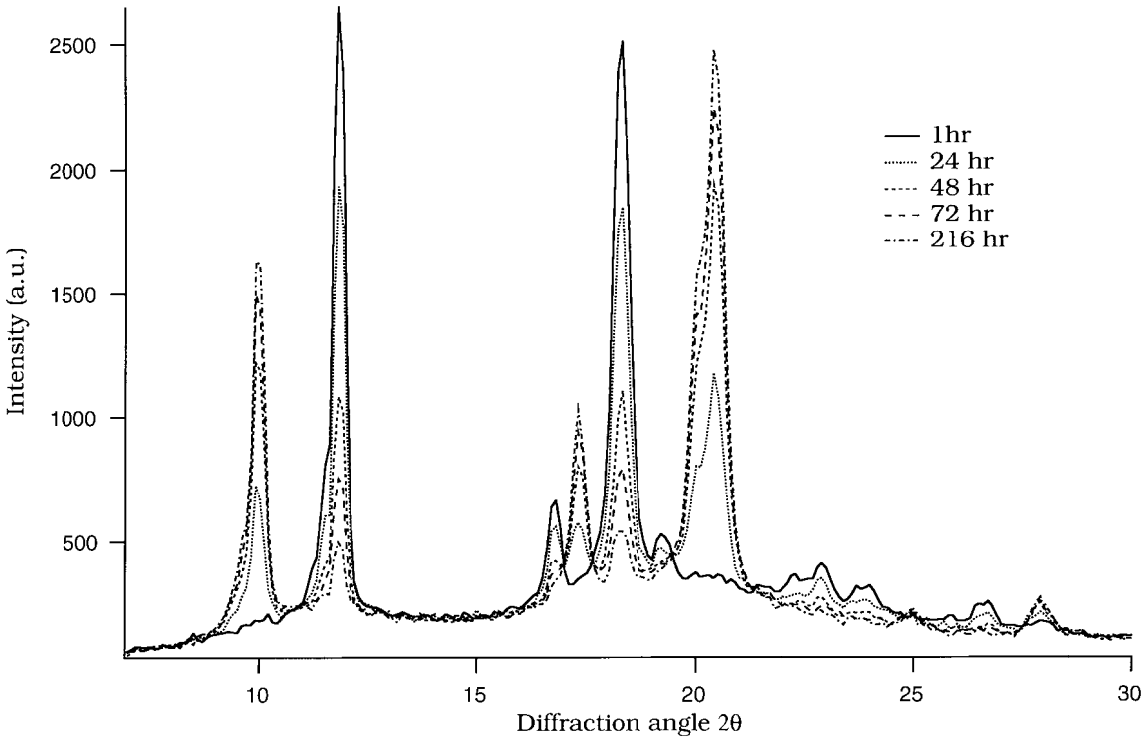

Fig. 8 Wide-angle X-ray scattering patterns at different times [26]

4.4.6 Melt rheology

It is well known that melt viscoelasticity measurements can provide information about molecular parameters through structure relationships. Hence, the evolution of rheological properties directly reflects the changes of such molecular parameters as molecular weight (MW), and molecular weight distribution (MWD). Through photo-ageing, these changes can be correlated to chain scission and/or recombinations which involve cross-linking in case of elastomers [76].

Basic melt viscoelasticity [97]:

Most polymeric materials exhibit a viscoelastic behavior. Viscoelastic properties are investigated using rheological experiments such as dynamic mechanical testing, which offers a convenient way to assess time dependence of mechanical properties of polymers.

No single parameter can be used to characterize the stress-strain relationship in viscoelastic material. The complex dynamic modulus (G^*) is resolved into two components using complex notation:

$$G^* = {}^{\sigma^*}/_{\varepsilon^*} = G' + \mathrm{i}G'' \qquad (2)$$

The real part of the complex modulus (*G'*) describes stress-strain relationships that are in phase. *G'* is called the storage modulus (or elastic modulus). The imaginary component (*G"*) characterizes the out-of-phase component and is named the loss modulus (or viscous modulus). Dynamic viscosity (η^*) is related to the complex modulus by

$$\eta^* = \sigma/(\mathrm{d}\varepsilon^*/\mathrm{d}t) = G^*/(\mathrm{i}\omega) = \eta' - \mathrm{i}\eta'' \quad (3)$$

with $\eta' = G''/\omega$ and $\eta'' = G'/\omega$. Then, the real component of the complex viscosity (η') describes the viscous dissipation in the specimen, while the imaginary component (η'') represents the stored elastic energy. Furthermore, the tangent of the phase angle (tan δ) describes the balance between the viscous and elastic behaviors in a polymer melt:

$$\tan\delta = G''/G' = \eta'/\eta'' \quad (4)$$

It is well known that the evolution of the rheological material properties directly reflects changes in molecular parameters. The linear viscoelastic properties in dynamic experiments are sensitive both to the chain scission and to the three-dimensional network formation. Thus, melt rheology provides a convenient tool to view the particular behavior due to the competition of chain scissions and recombination reactions occurring through ageing.

It is also well known that the zero shear viscosity η_0 depends on the molecular weight and obeys a power law [98,99]:

$$\eta_0 \propto M_w^{\alpha} \quad (5)$$

with the widely quoted viscosity exponent $\alpha = 3.4$.

The zero shear viscosity η_0 can be obtained from the complex viscosity $\eta^*(\omega)$:

$$\eta^* = G^*(\omega)/(\mathrm{i}\omega) = \eta' - \mathrm{i}\eta'' \quad (6)$$

and

$$|\eta^*|_{\omega\to 0} = |\eta'|_{\omega\to 0} = \eta_0 \quad (7)$$

An empirical rheological model used to fit dynamic data is the Cole-Cole distribution expressed by [100-104]:

$$\eta^*(\omega) = \frac{\eta_0}{[1+(\mathrm{i}\omega\lambda_0)^{1-h}]} \quad (8)$$

where λ_0 is the average relaxation time and h is a parameter of the relaxation-time distribution.

In the complex plane this model predicts the variation of the viscosity components (η' versus η'') to be an arc of circle. From this representation it is easy to determine the parameters of the distribution: η_0 is

obtained through the extrapolation of the arc of the circle on the real axis and the distribution parameter h through the measurement of the angle $\Phi = h\Pi/2$ between the real axis and the radius going from the origin of the axis to the centre of the arc of the circle.

Molecular changes were characterized by melt viscoelasticity experiments in oscillatory shear mode using a TA ARES mechanical spectrometer, equipped with parallel plate geometry with diameter of 8 mm and 25 mm and the gap between the plates was 1 mm. The experiments were carried out at temperatures of 120, 140 and 160 °C.

IRIS 2006 (Innovative Rheological Interface Software) was used to create master curves by the automatic time-temperature superposition at temperature of 140 °C.

4.4.7 Infrared spectroscopy

For the purpose of identification the chemical changes of PB-1 through UV irradiation, several devices were employed.

A Nicolet Impact 760 spectrometer in FTIR transmission mode, with nominal resolution of 4 cm^{-1} and 32 acquisitions was employed.

A Nicolet 380 FT-IR spectrometer equipped with SPECAC ATR Diamand-Germanium crystal, with nominal resolution of 4 cm^{-1} and 32 acquisitions, was employed for surface analysis of degraded specimens.

Omnic software was used for collection of all spectra.

4.4.8 Differential scanning calorimetry

Melting, remelting and crystallization behaviors of UV irradiated specimens were studied using a power-compensated differential scanning calorimeter (DSC - Pyris1, The Perkin-Elmer Co., USA). Nitrogen as a purge gas, was used and constantly passed (20 ml/s) through the heat sink and over the cells. Temperature calibration was performed using indium as a standard. Approx. 5 mg of irradiated material was loaded into standard aluminum pans. Observations were performed at a rate of ±10 °C/min in interval from 40 to 170 °C. To observe melting temperature of the form II, which is present after melting and transforms in time into form I, second subsequent melting and crystallization was performed. The specimens were kept at room temperature at 23 °C and the phase transformation followed.

It is generally known that differences in melting temperatures of the forms I and II are about of 10 ~ 15 °C. Thus melting curves obtained from DSC exhibit partial superposition. Only one melting peak of the form I or II on the melting curve is detected immediately after crystallization or when polymorphic transformation terminates respectively.

In this respect, the melting curves must be deconvoluted to reliably evaluate the transformation. Therefore, we particularly followed the approach of Alfonso et al. [105].

It is supposed that overall degree of crystallinity does not change during transformation [38,43,105]. Unfortunately, there are no exact values of melting enthalpy of forms I and II.

Thus, we integrated the areas of the peaks of the forms I and II deconvoluted via a PEAK-FIT V4 software using a Gaussian function. Then, areas and heights of individual melting peaks were obtained. It was found that ratios of the deconvoluted peaks areas are equaled to the heights of the melting peaks. The contents of the increasing form I in time were calculated as the ratio height of peak form I and sum of heights of both peaks. Also the ratios of the forms I and II were calculated, however in time 0 and after transformation is completed the ratios are zero or infinitive.

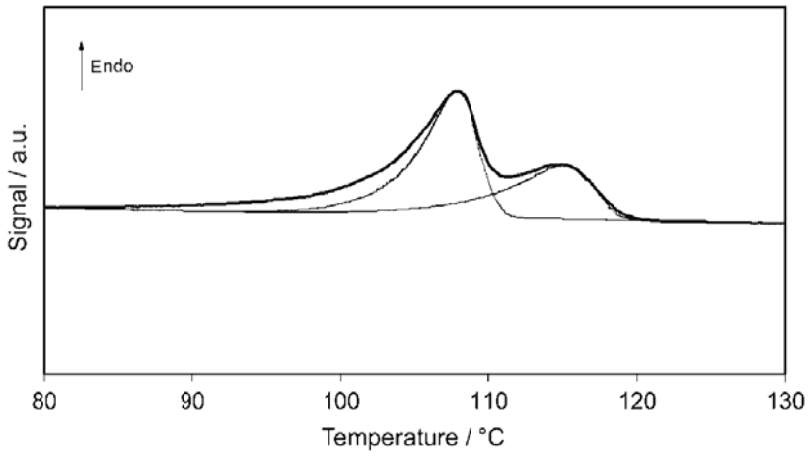

Fig. 9 Deconvolution of the DSC curve obtained by PEAK-FIT V4 [105]

5 STUDY OF TRANSFORMATION IN PB-1

Due to of manufacturing PB-1 parts from its melt, the resulting properties are affected by the phase transformation. Therefore, the understanding of the transformation is desirable in connection with polymer applications. The purpose of this study was to characterize influence of the temperature on phase transformation and evolution of mechanical properties in injection-molded and extruded PB-1 specimens.

5.1 DSC study

The phase transformation behavior was in the first step observed by DSC experiments. The crystallization temperatures of the used materials, done on compression-molded specimens, during non-isothermal crystallization at cooling rate of 10 °C/min are following: DP 0401M = 78 °C; PB 0300M = 84 °C; PB 8640M = 51 °C.

In the following Figs 10-12 the temperature dependent evolution of form I content in all three materials can be seen. The evolutions in selected days for all three materials in whole temperature range are illustrated in Fig. 13.

What can be seen in all materials is that fastest phase transformation occurs at temperatures of +5 and +22 °C. At temperature of +40 °C, a slower transformation is observed in PB 0300M and PB 8640. It was already found that addition of ethylene copolymer to PB-1 increases phase transformation rate; this fact is confirmed in case of ethylene copolymer PB 8640M at temperature of -22 °C. This can be actually related to a decrease of glass transition temperature by the ethylene addition which can still keep the molecular mobility in the system. The reason, why the fastest transformation rate is not observed at higher temperatures (+40 and +60 °C) can be explained by an influence of annealing at temperature above the crystallization temperature, which is in case of PB 8640M 51 °C, while in case of homopolymers (PB 0300M and DP 0401M) it lies above annealing temperatures. Probably post-crystallization occurs at this temperature of 60 °C in PB 8640M, which can cause a competition the original crystallite perfection and the phase transformation and thus, it is slowed down.

In case of both homopolymers at temperatures of -22 and 60 °C similar behavior can be seen with the difference in the reached amount of the form I content which is in PB 0300M higher approx. about 10 % compared to DP 0401M. This can be caused by different MW, which is higher in PB 0300M than in DP 0401M.

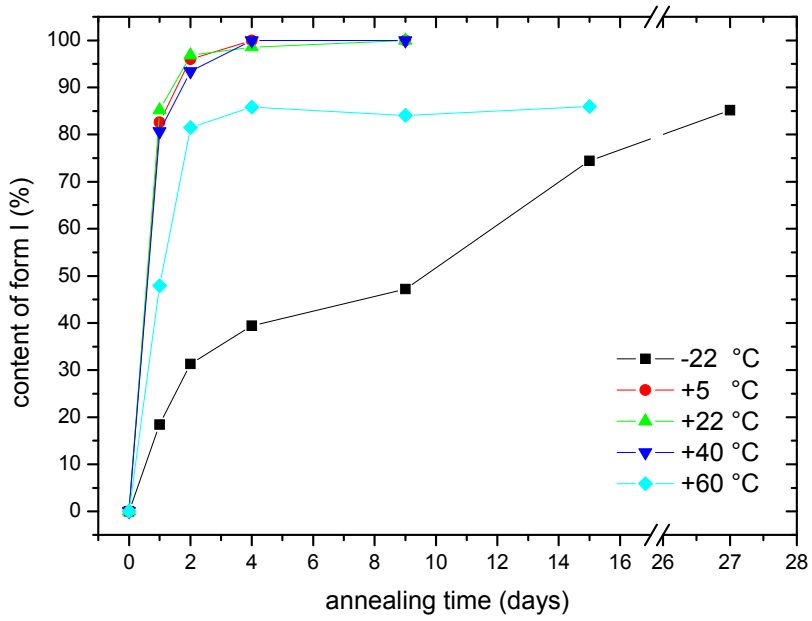

Fig. 10 Evolution of form I content in DP 0401M for various annealing temperatures

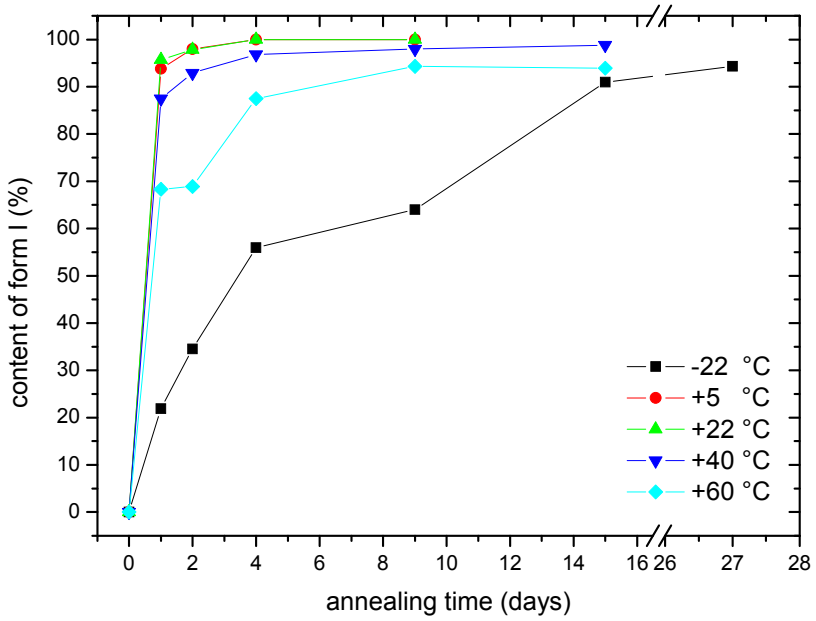

Fig. 11 Evolution of form I content in PB 0300M for various annealing temperatures

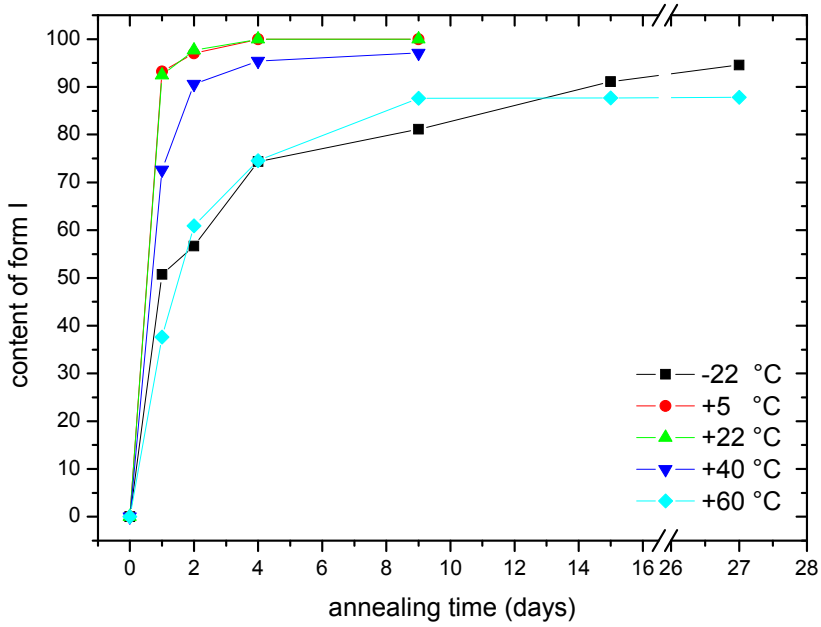

Fig. 12 Evolution of form I content in PB 8640M for various annealing temperatures

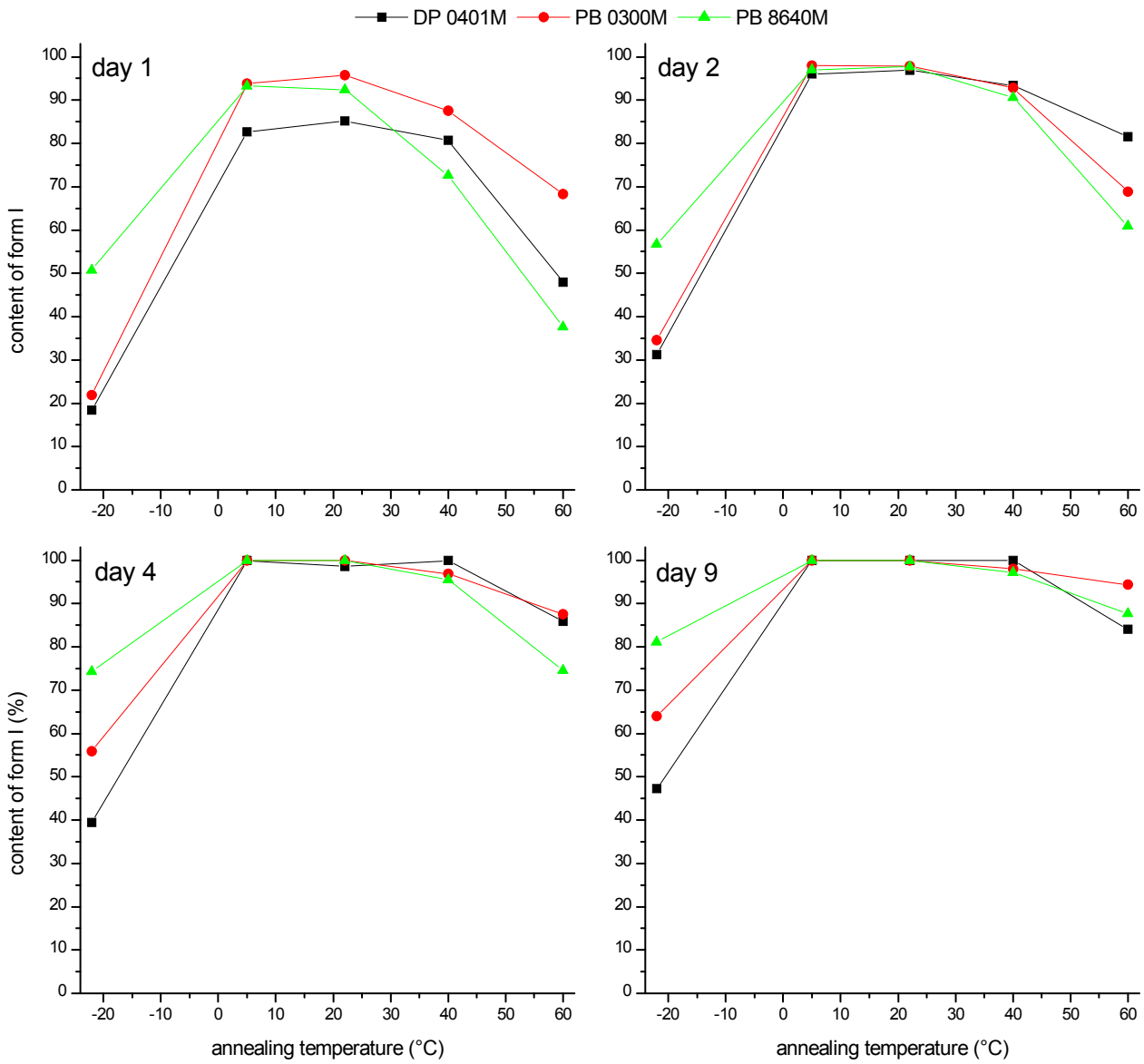

Fig. 13 Evolution of form I content in the whole temperature range for all materials in selected annealing days

5.2 Evolution of properties of injection-molded PB-1

5.2.1 Tensile modulus

Results of tensile testing (elastic modulus) for all materials are illustrated in Figs 14-16. The non-monotonic evolution of tensile modulus in dependence on annealing temperature is obvious.

In all materials, the fastest evolution of tensile modulus is evident at temperature of +5 and +22 °C, followed by a bit slower evolution at temperature of +40 °C. This is in agreement with previous Chapter 5.1, and below or above +5 ~ +22 °C it slows down. The slowest evolution was observed in the specimens annealed at temperature of +60 °C and -22 °C with distinct differences.

The differences between homopolymers (Figs 14 and 15) and PB 8640M (Fig. 16) can be seen, even between two homopolymers.

PB-1 ethylene copolymer PB 8640M exhibits faster evolution at temperatures -22 and +60 °C compared to homopolymers, which is in agreement with previous findings. Also, as for the other temperatures it shows notable higher increase in elastic moduli in the first two annealing days compared to homopolymers, nevertheless the further evolution is slow and the maximum tensile modulus are reached after 14 annealing days, particularly at temperature of +60 °C.

Apparent differences were observed in homopolymers as the transformation of PB 0300M is slower as compared to DP0401M at temperatures of +5 and +22 °C, where virtually maximum moduli are observed after 4 days of annealing, at temperature of +40 °C after 7 days. However, in PB 0300M the phase transformation is more gradual in whole temperature range with the fastest transformation at +5 °C. The material PB 0300M possesses higher molecular weight compared to DP0401M, which probably may play a role in evolution. Indeed, its molecular weight and consequent number of molecular entanglements is higher as compared do DP 0401M; this limits the system mobility and can results in gradual transformation rate. On the contrary at temperatures of -22 and +60 °C, the phase transformation is notably faster in PB 0300M.

In both homopolymers the tensile modulus slightly increases even after 48 days, which is more pronounced at temperature of -22 and +60 °C. This can be caused by a post-crystallization or by a slow continuous transformation phase II to I.

To obtain detail insight into phase transformation the other tensile properties were also evaluated as yield strength, elongation at break and strength at break.

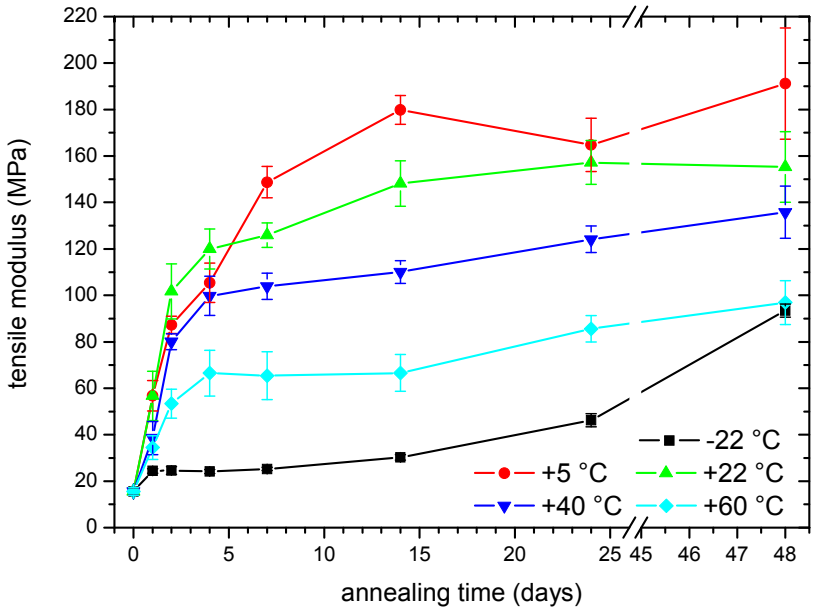

Fig. 14 Evolution of tensile modulus in injection-molded PB 0300M

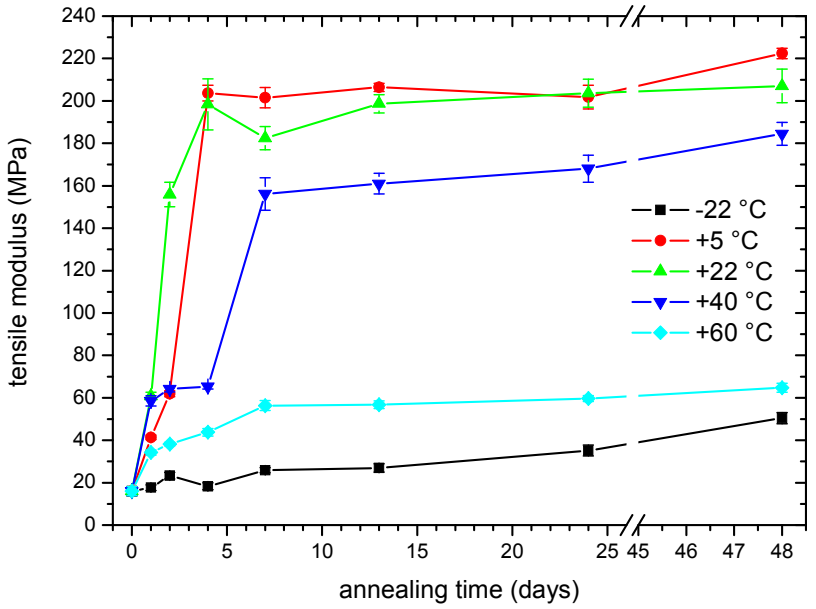

Fig. 15 Evolution of tensile modulus in injection-molded DP 0401M

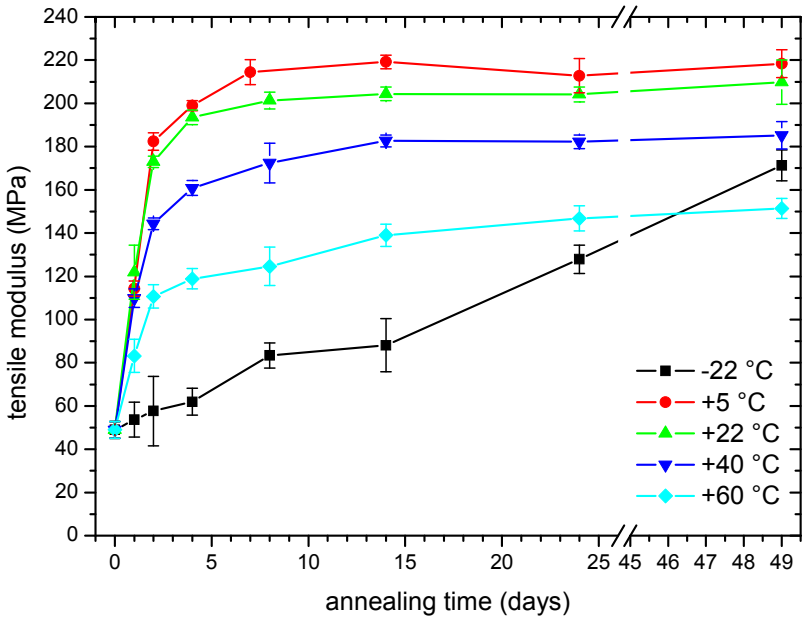

Fig. 16 Evolution of tensile modulus in injection-molded PB 8640M

5.2.2 Tensile yield strength

The tensile yield behavior was evaluated only in DP 0401M (see Fig. 17) for temperatures of +5, +22 and +40 °C since the annealing day 4 resp. 7. It can be seen that yield strength increases with increasing annealing time similarly as the tensile modulus. It can be supposed that observation of yield behavior is affected by a molecular weight; from all three materials DP 0401M possesses the lowest one. In addition, the observation of yield strength can be probably affected by a critical amount of the form I, respectively by a minimal modulus.

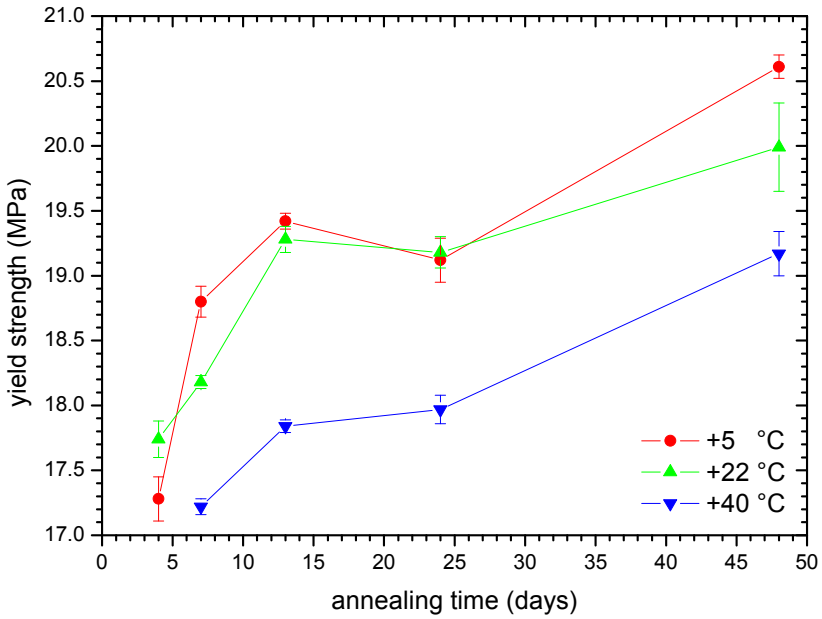

Fig. 17 Evolution of tensile strength at yield in injection-molded DP 0401M

5.2.3 Tensile elongation at break

The tensile elongation at break was observed only in materials PB 0300M and PB 8640M (see Figs 18 and 19), because of the limitation of extension on tensile testing apparatus. It has in the whole temperature range, except the temperature of -22 °C, decreasing trend during annealing. It is opposite effect in respect to the evolution of tensile modulus.

Nevertheless, at annealing temperature of -22 °C a specific behavior is observed in both materials. It can be supposed that evolution in PB 0300M possesses similar behavior as in PB 8640M, where an unexpected increase of elongation at break occurred compared to annealing temperature of +60 °C. Between the days 14 and 24, significant drop to a half value was observed in PB 8640M and further annealing lead to virtually the same value as at temperatures +5, +22 and +40 °C. We suppose that longer annealing of PB 0300M would probably lead to equilibrating of elongation at break for the other annealing temperatures.

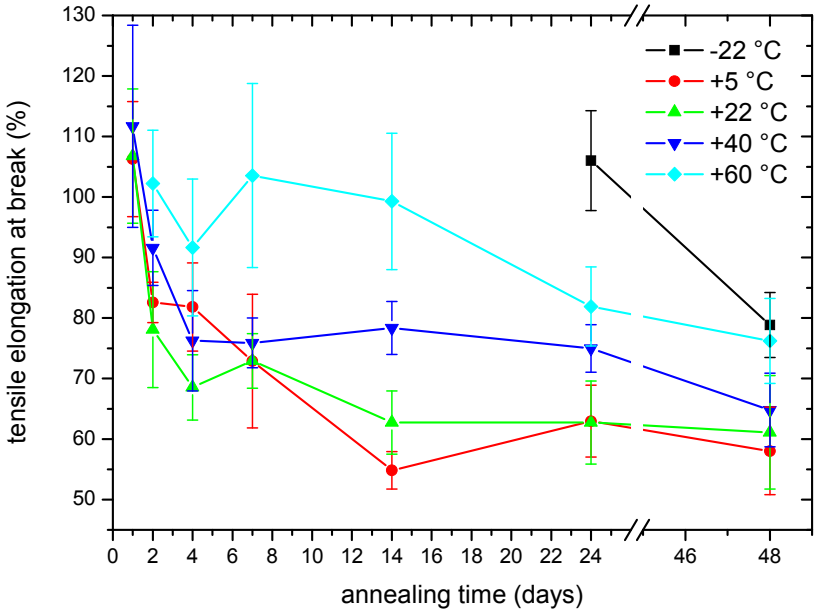

Fig. 18 Evolution of tensile elongation at break in injection-molded PB 0300M

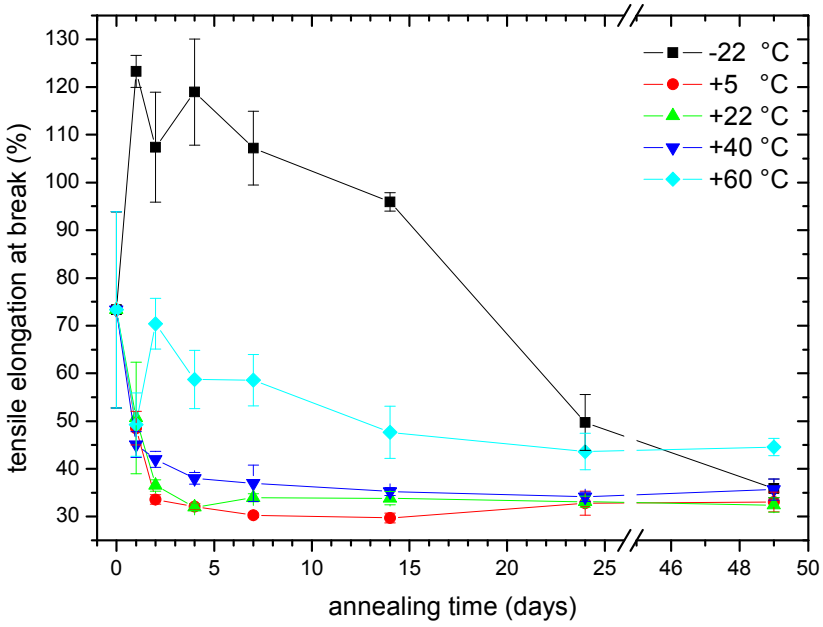

Fig. 19 Evolution of tensile elongation at break in injection-molded PB 8640M

5.2.4 Tensile strength at break

Conversely, the evolution of tensile strength at break gradually rises with increasing annealing time as can be seen in Figs 20 and 21. In both materials, annealing temperature of +5 °C lead to the highest values of strength at break. When both Figs are compared with those of tensile modulus (Figs 14 and 16), similar trend of the evolution can be seen. While in the case of tensile yield strength (in DP 0401M - Fig. 17) the comparing with tensile modulus (Fig. 15) was not possible.

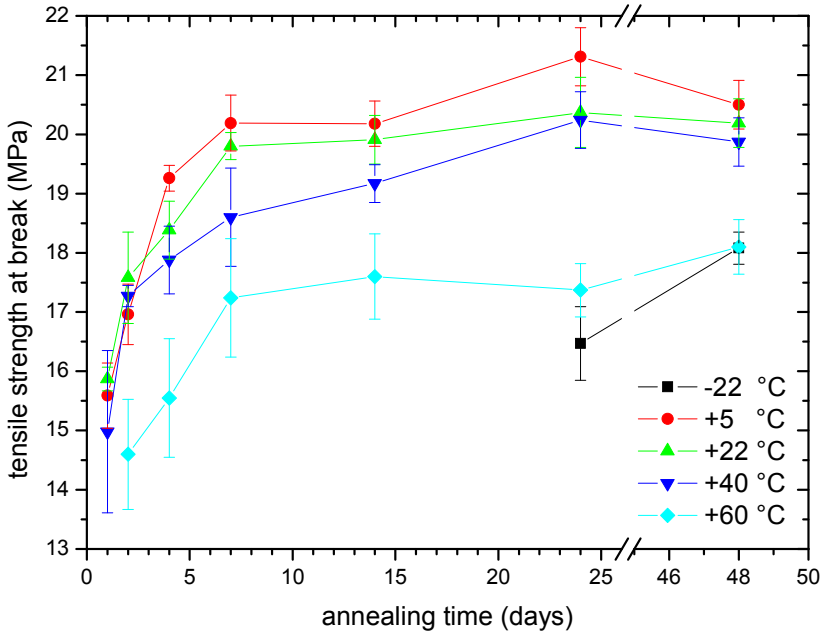

Fig. 20 Evolution of tensile strength at break in injection-molded PB 0300M

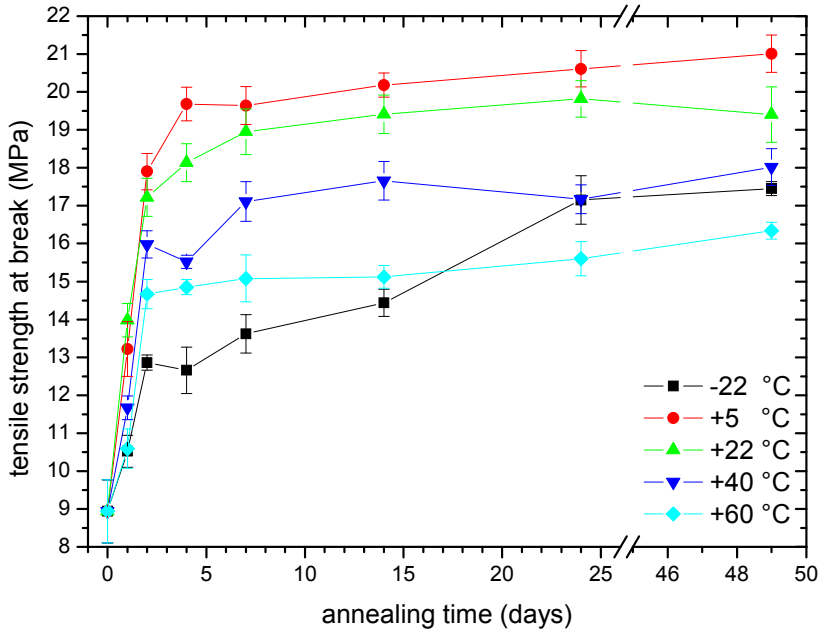

Fig. 21 Evolution of tensile strength at break in injection-molded PB 8640M

5.3 Evolution of structure and properties in PB-1 extrudates

Since PB-1 is also processed by extrusion (mostly for pipe applications), it opens an industrial question whether different processing technology and subsequent morphology can play a role in phase transformation. In comparing with previous Chapter 5.2 with injection-molded specimens, it has been extented by WAXS data.

5.3.1 WAXS evolution

The wide-angle X-ray scattering was performed in transmission mode to observe the evolution of the form I and II in PB 0300M as can be seen in following Fig. 22. It shows a virtually the same evolution of the form I content at five different annealing temperatures. It can be seen that fastest evolution is observed at annealing temperature of +5 °C and from day 14 the form I content becomes constant at approx. 90 %. At temperature of +22 °C the evolution is a rather slower, however during first 3 days its rate is the same as at +5 °C. Gradual evolution occurs at temperature of +40 °C, which is slower compared to +5 and +22 °C but with a similar trend. On the contrary, a peculiar trend of the evolution occurred at annealing temperatures of -22 and +60 °C. Until the day 14, a slow gradual evolution seems to be similar for both temperatures, with respect to peculiar increase and decrease at -22 °C. Nevertheless further observation at time of 22 and 30 days shows unexpected significant increase of the form I content to over 80 %. The confirmation of this behavior was found in subchapter 5.3.3 – Tensile modulus. This can signify that at annealing temperatures of -22 °C an induction time was observed, during which slow transformation occurs until critical amount of the form I is transformed. The reached critical amount can probably accelerate the transformation rate. Nevertheless, this hypothesis cannot be applied for injection-molded specimens, where the phase transformation was faster for +60 °C than for -22 °C. However, this probably signifies that processing technology respectively resulting morphology directly affects the phase transformation during temperature annealing.

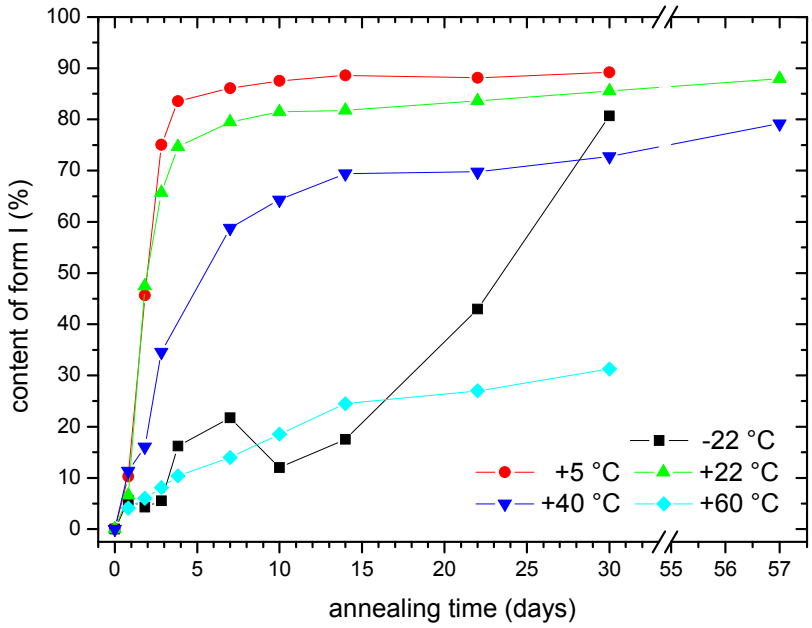

Fig. 22 WAXS evolution of the form I content in extruded PB 0300M for various annealing temperatures upon time

5.3.2 Polarized light microscopy

The morphology of extruded specimens (Fig. 23) shows differences between the materials; isotropic spherulitic structure can be seen. It should be noted that extrusion conditions were the same for all materials. The main difference can be seen in the morphology of homopolymers. Material DP 0401M possesses lower MW and this can probably affects the morphology – remarkably smaller and finer spherulite structure when compared to PB 0300M – the growth rate is apparently higher than the nucleation rate.

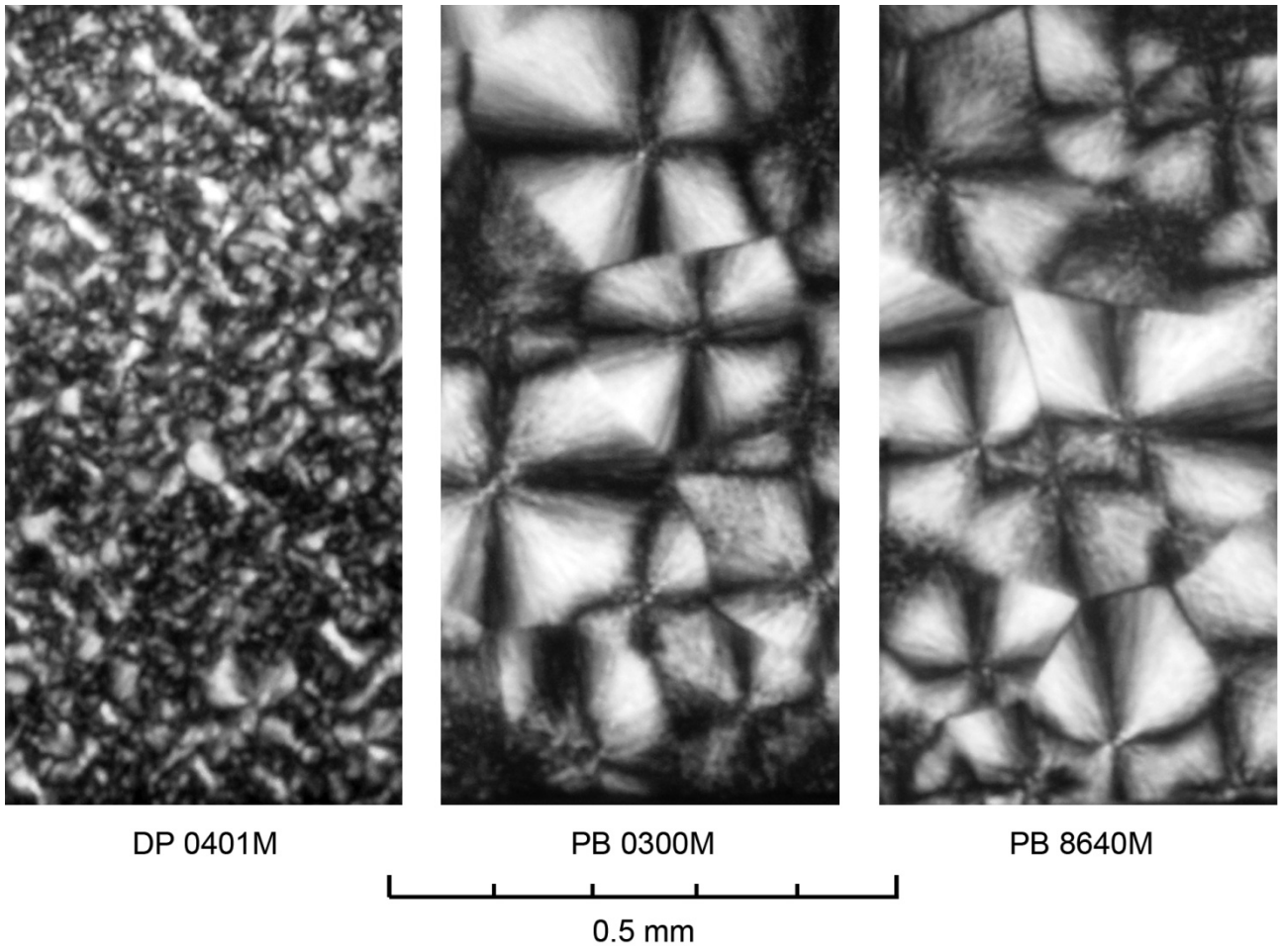

Fig. 23 Images of morphology in extruded PB-1(bottom is border of specimen)

5.3.3 Tensile modulus

The evolution of tensile modulus in all materials is illustrated in following Figs 24-26.

When previous WAXS observation (Fig. 22) and evolution of tensile modulus (Fig. 24) of material PB 0300M are compared, distinct similarities can be seen: (i) a peculiar increase occuring at annealing temperature of -22 °C is observed in both Figs; it crosses at the same time (approx. 28 days) the evolution curve at annealing temperature of +40 °C; (ii) annealing temperature of +40 °C possesses virtually the same trend of gradual evolution; (iii) low content of form I in specimens annealed at +60 °C follows its low tensile modulus; (iiii) rather higher content of the form I in specimens annealed at +5 °C is directly reflected in higher tensile modulus compared to specimens of +22 °C.

As suggested in previous subchapter 5.3.1 WAXS evolution - an induction transformation time during which critical amount of form I is transformed, seems to be relevant. After reaching the critical amount of the form I, a rapid increase is initiated and plato is reached according to annealing temperature.

A comparison of all the materials shows the fastest evolution in PB 8640M as was observed also in injection-molded specimens (Fig. 16). Nevertheless, the peculiar increase at annealing temperature of -22 °C is observed in all the materials; in respect to overall faster evolution in PB 8640M this increase occurs earlier than in homopolymers. This fact evidences that it is not an accidental error as one could suggested. Similarly, at annealing temperature of 60 °C the transformation rate is the slowest with distinct plato.

When evolutions in both injection-molded and extruded specimens (Figs 14-16 and 24-26) are compared distinct similarities and differences resulting from different processing technology can be seen. (Note: different tensile testing apparatus were used and the tensile modulus in injection-molded specimens was calculated using software function without extensometer, while in extrudates an extensometer was used for calculation.) The similarities were found in evolution at annealing temperatures +5, +22 and +40 °C in all materials, nevertheless values of tensile modulus - are remarkably higher for extrudates. Probably differences in injection-molded morphology (skin-core), where typical oriented structure in the skin can be observed (created upon faster cooling), while in extrudates un-oriented structure was observed (Fig. 23), can play an important role in transformation rate and affects final mechanical properties. In all materials at temperature of +60 °C the evolution seems to possess similar trend in the evolution.

On the other hand, the modulus evolution at temperature of -22 is completely different except PB 8640M. A peculiar increase in injection-molded specimens at this temperature can be partially observed remarkably later in time. This observation can confirm significant influence of processing and resulting morphology on phase transformation.

It worth noting that both sets of specimens (injection molded and extruded) were also visually analysed immediately after processing - actually, it was possible to stretch the injection-molded specimens readily by hand. However, even although both sets of specimens possess approx. the same cross-section

areas, it was not possible to stretch the extruded specimens. This confirms the remarkable differences in tensile modulus when comparing both specimens.

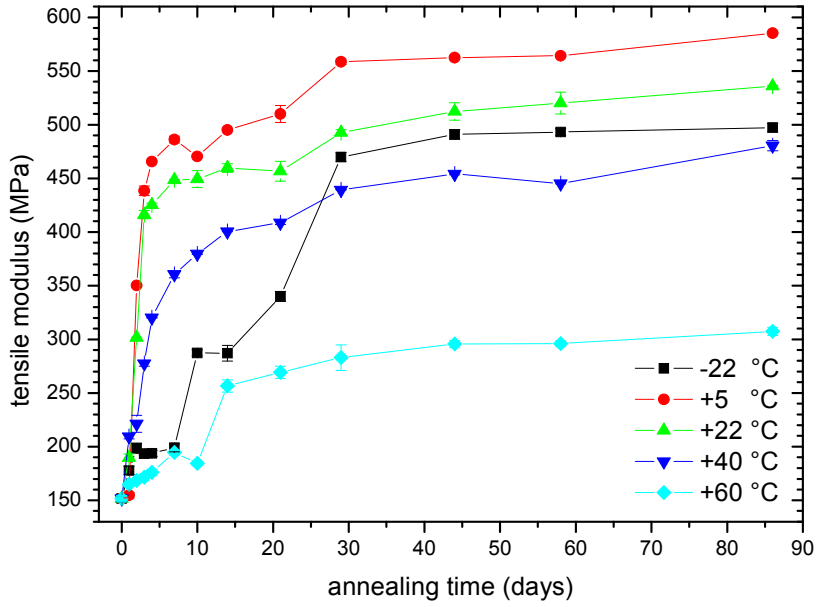

Fig. 24 Evolution of tensile modulus in extruded PB 0300M

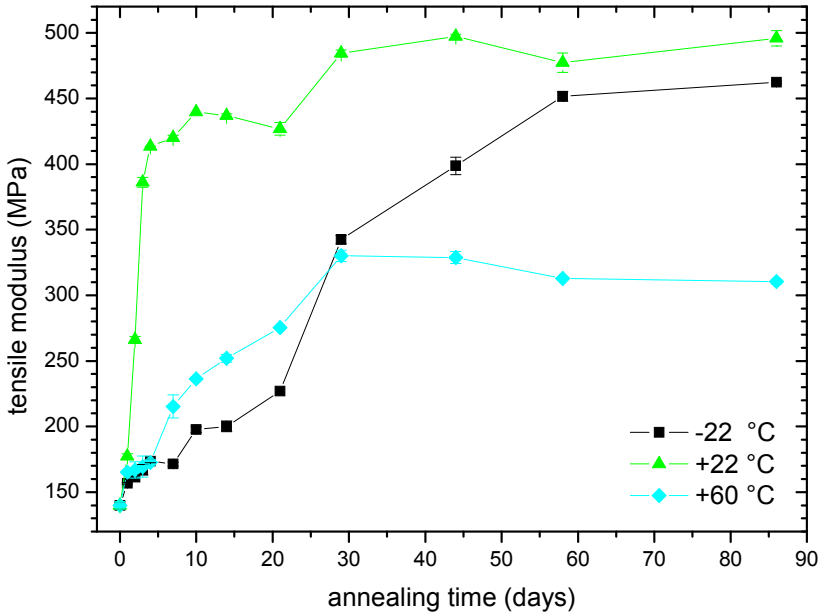

Fig. 25 Evolution of tensile modulus in extruded DP 0401M

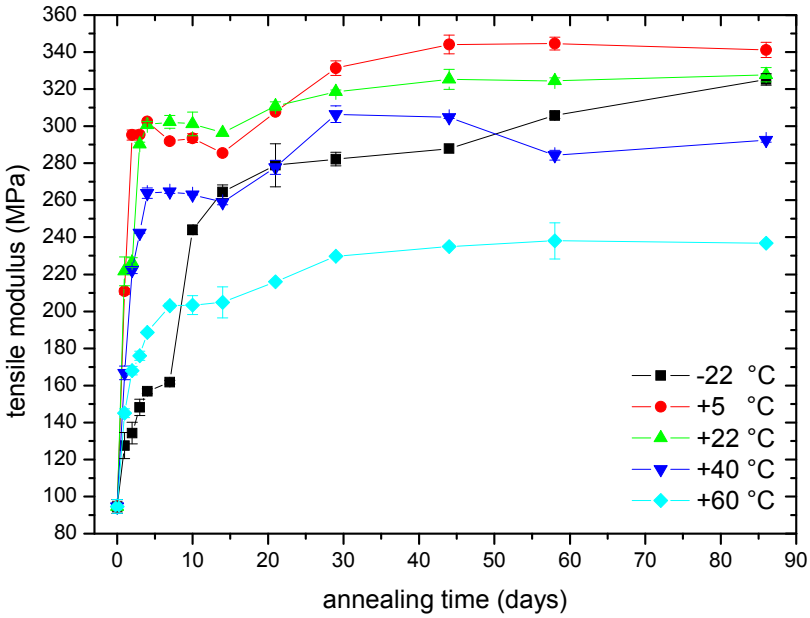

Fig. 26 Evolution of tensile modulus in extruded PB 8640M

5.3.4 Tensile elongation at break

Again, the evolution of tensile elongation at break illustrated in Figs 27-29 shows decreasing trend compared to increasing tensile modulus. What can be seen is remarkably different evolution for each material. In PB 8640M (Fig. 29) no distinct trend can be observed, it can be probably caused by extremely high elongation – 400 ~ 540 %. On the other hand, in homopolymers trends in evolution are obvious and even they differ. In both homopolymers (Figs 27 and 28) at annealing temperature of +60 °C the evolution possesses virtually the same trend as well as at +22 °C. When annealing temperature of -22 °C is compared in both Figs, in case of PB 0300M significant drop is observed between day 14 and 22, and further annealing shows plateau in evolution. While in DP 0401M the elongation at break is gradually decreasing but not fully correlating with tensile modulus (Fig. 25).

When extruded and injection-molded (Figs 18 and 19) results of elongation at break are compared, remarkable differences are clearly seen. In case of extrudates PB 0300M the elongation is 3 ~ 4 times higher than as injection-molded specimens, on the other hand in copolymer PB 8640M the elongation is even 9 ~ 10 times higher; in case of injection-molded DP 0401M the elongations were over 120 % and out of testing possibility on employed testing apparatus. These elongation results certainly confirms the effect of processing on the phase transformation respectively on final mechanical properties.

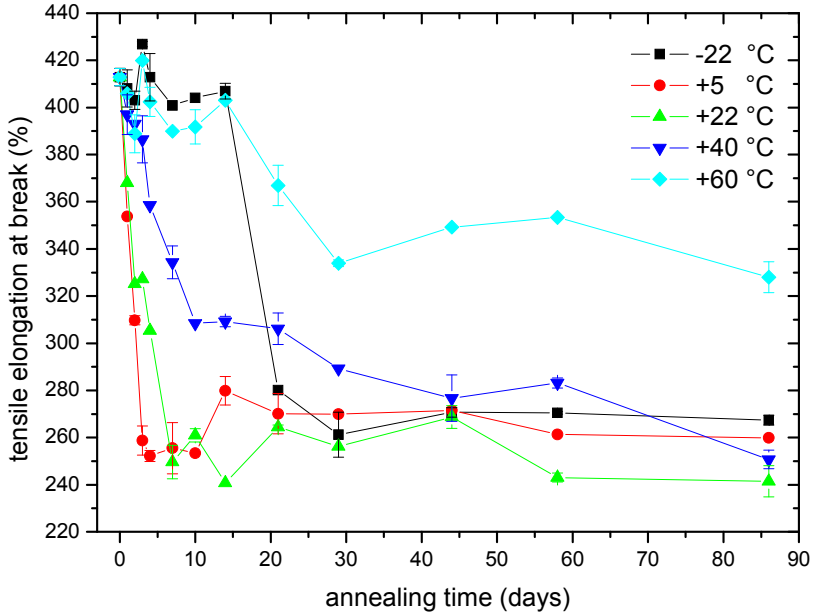

Fig. 27 Evolution of tensile elongation at break in extruded PB 0300M

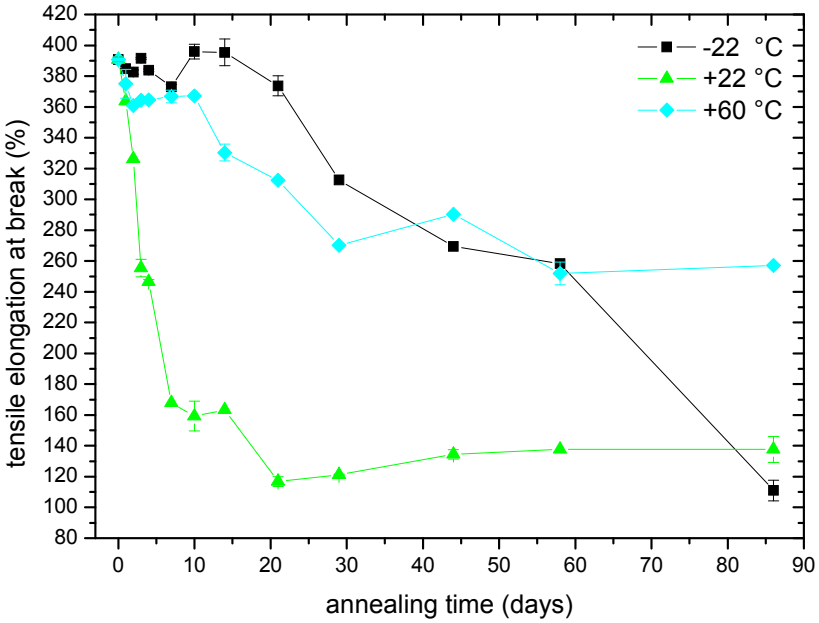

Fig. 28 Evolution of tensile elongation at break in extruded DP 0401M

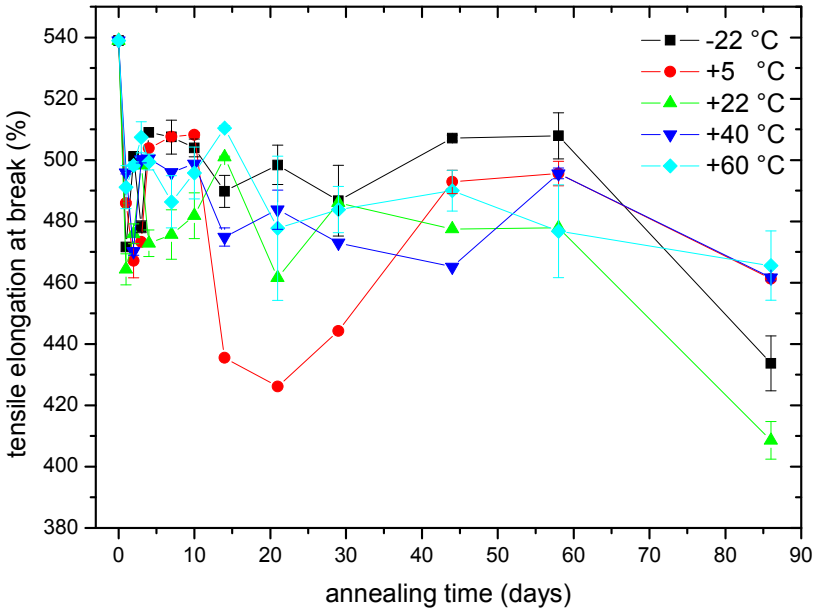

Fig. 29 Evolution of tensile elongation at break in extruded PB 8640M

5.3.5 Tensile strength at break

Following Figs 30-32 illustrate evolution of tensile strength at break, which particularly corresponds to evolution of tensile elongation at break Figs 27-29. Again, no reliable differences of evolution in PB 8640M were observed; on the contrary, in homopolymers significant decrease of strength at break can be seen.

However, these results possess an opposite trend upon annealing time with those observed in injection-molded specimens (Figs 20 and 21). The strengths at break are in case of PB 0300M quite equivalent, except temperatures of -22 and +60 °C; but in PB 8640M the strengths are significantly higher for the extrudates. Generally, one would expect higher drawability and possibly strength at break in injection-molded specimens possessing lower modulus. On the other hand, an enhanced molecular orientation in injection-molded specimens can reduce in general the drawability. However, this rather surprising finding would still require further to be elucidated.

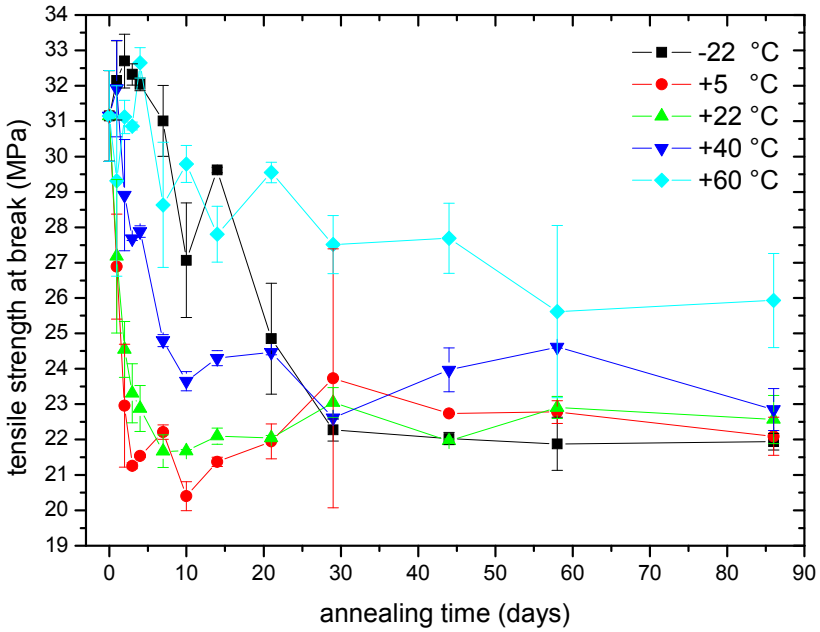

Fig. 30 Evolution of tensile strength at break in extruded PB 0300M

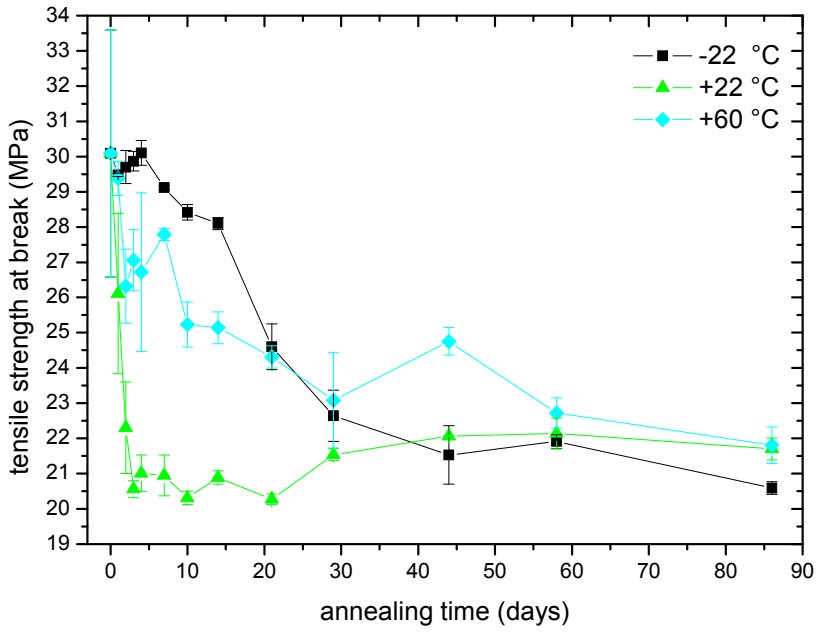

Fig. 31 Evolution of tensile strength at break in extruded DP 0401M

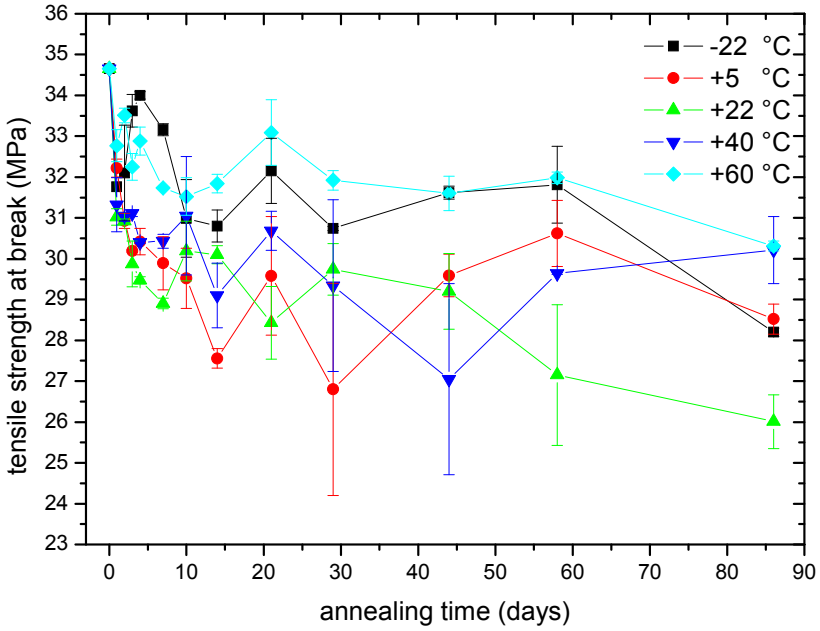

Fig. 32 Evolution of tensile strength at break in extruded PB 8640M

6 MULTISCALE CHARACTERIZATION OF DEGRADATION IN PB-1

The degradation behavior of poly(1-butene) is not still clear yet; it supposed to be similar to isotactic polypropylene due to presence of tertiary carbon on the backbone. The formation of peroxidic species in the polymer backbone is encountered as the primary step of the oxidative degradation. The hydroperoxide groups not only play an important role in inducing both thermal and photo-oxidation of polymers but they are also important intermediates in the overall oxidation reactions. Thus, (hydro)peroxides are the key products in the clear understanding of a mechanism, as well as to gain better insight into correlation between chemical evolution and evolution of the molecular structure (scission/recombination/crosslinking) [5].

Past works related to the phase transformation behavior claims that it is influenced: by physical ageing conditions as temperature, pressure and applied stress; by some additives; by molecular characteristics, addition of ethylene copolymers. However, no papers deal with the influence of degradation on the phase transformation behavior which should subsequently play a role in the possible utilization/recycling of the material at the end of its lifetime.

To follow this idea, a multiscale characterization has been performed on two sorts of specimens. The compression-molded specimens with thickness of 0.3 mm were used for study of degradation during early stages 0 ~ 40 UV irradiation hours or 0 ~ 69 days of artificial weathering. The prolonged times led to disintegration of such specimens. Therefore, the specimens with thickness of 1 mm were used for UV irradiation times 0 ~ 160 hours, respectively 0 ~ 103 days naturally weathered.

6.1 Early stages

6.1.1 DSC study

The melting behavior of degraded specimens of both homopolymers (DP 0401M and PB 0300M) is illustrated in Fig. 33. It can be seen that the melting temperature of the form I, observed by first melting (which corresponds to melting of the form I), vary interval of 122 ~ 127 °C in both materials. No distinct trend is observed compared to the second melting (performed immediately after first melting and controlled crystallization), which corresponds to the melting of the form II. In both materials a decrease of melting temperature with increasing irradiation time is observed with total drop of 10 ~ 12 °C between time 0 and 40 hours. Upon the transformation from form II to I, virtually identical thermal behavior with shifted melting temperature can be seen (melting after transformation is completed corresponds to the melting of the form I after controlled crystallization and annealing during which the transformation II – I occurs), as the slope of m2 and mtr curve in Fig. 33 is similar.

What can be expected in the initial stage of degradation is a prevailing effect of chain scission, which can positively influence the crystallization kinetics. As a consequence, final structure is thermodynamically more stable, and its melting temperature in short-term irradiated specimens can even exceed that of non-irradiated. This is particularly evident in PB 0300M from the melting of phase I upon transformation.

However, chain scission is followed by the introduction of impurities into the molecular structure. This effect leads to the decrease of crystallizability and the crystallization to less stable structure [106]. In thermograms, it is presented by gradual decrease of melting temperatures of both phase II and I with prolonged irradiation time.

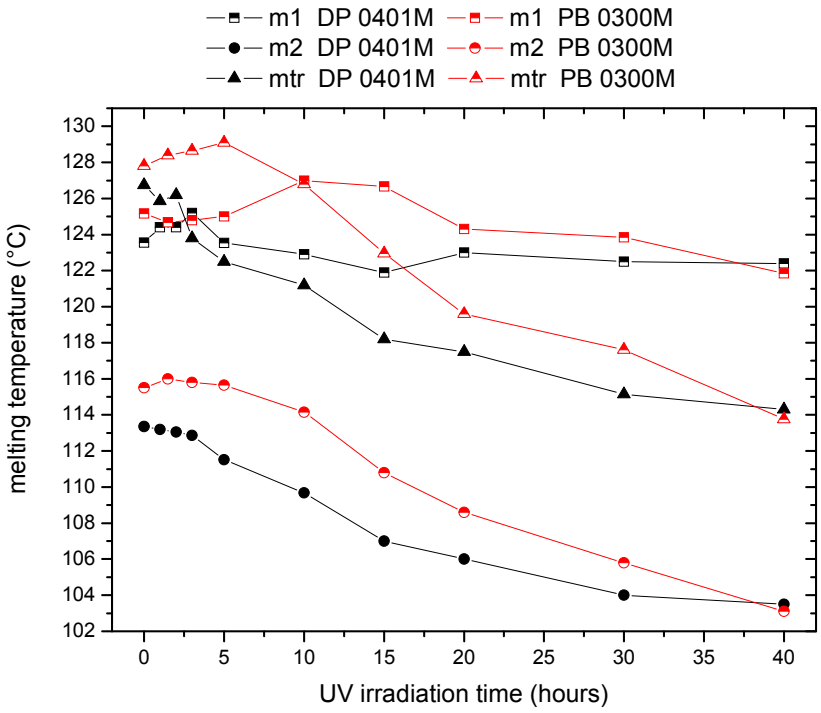

Fig. 33 Melting behavior of PB 0300M and DP 0401M (m1 – first melting, m2 – second melting, mtr – melting after transformation is completed)

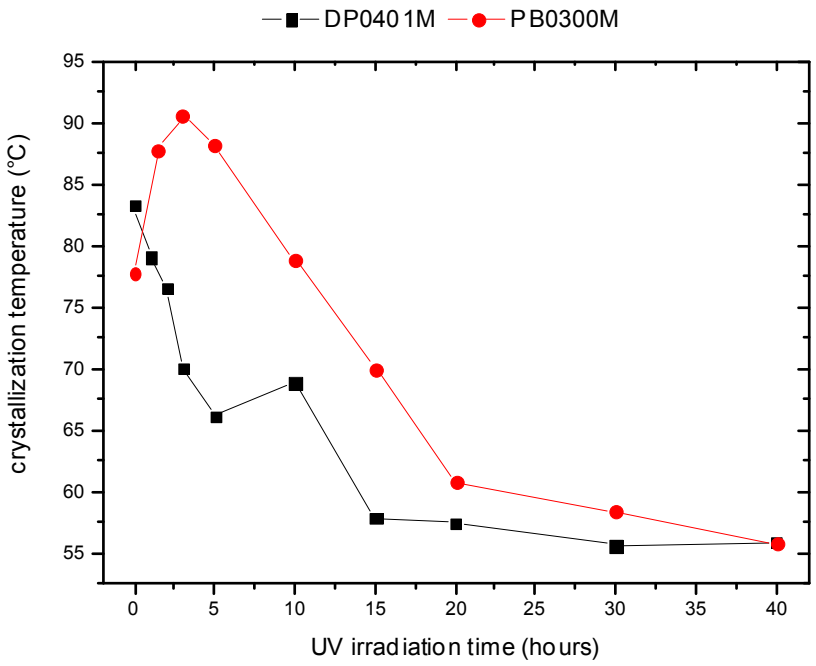

Fig. 34 Crystallization behavior of PB 0300M and DP 0401M

The effect of photo-induced changes on crystallization is even more evident from the crystallization temperature (T_c), as shown in Fig. 34. In the case of PB 0300M, the non-monotonic evolution of T_c can be seen. At the beginning, a significant increase of T_c is observed from 78 to 91 °C and after 10 hours of UV irradiation the initial T_c is reached. This observation confirms that the chains scission positively influences the crystallization rate (molecular mobility increases) and this effect prevails in the initial stage of UV irradiation. However, an increasing number of introduced heterogeneities in polymer chains then causes a linear drop of T_c about 30 °C between 5 and 20 UV irradiation hours. Then in time, a gradual decrease of T_c to 55 °C occurs. The evolution in T_c of DP 0401M upon UV irradiation is slightly different. Crystallization temperature decreases with exposure time. During first 5 hours, degradation leads into a significant drop of T_c, then, from 15 up to 40 hours only a small decrease can be seen up to 55 °C, i.e. the same values as that of PB 0300M. Clearly, the first stage with increasing crystallization rate upon chain scission is missing. It can be supposed that the competition between (i) the increase in crystallization kinetics upon chain scission and (ii) the retardation of crystallization caused by introduction of molecular irregularities is influenced by initial molecular weight. Indeed, the feasible maximum of crystallization rate is faster reached in lower-molecular systems, thus in DP 0401M, in this case its crystallization temperature decreases even upon the initial stage of UV irradiation.

In order to compare a thermal behavior of both specimens artificially and naturally degraded, the material DP 0401 was exposed to natural weathering. Subsequent melting and crystallization temperatures are illustrated in Fig. 35.

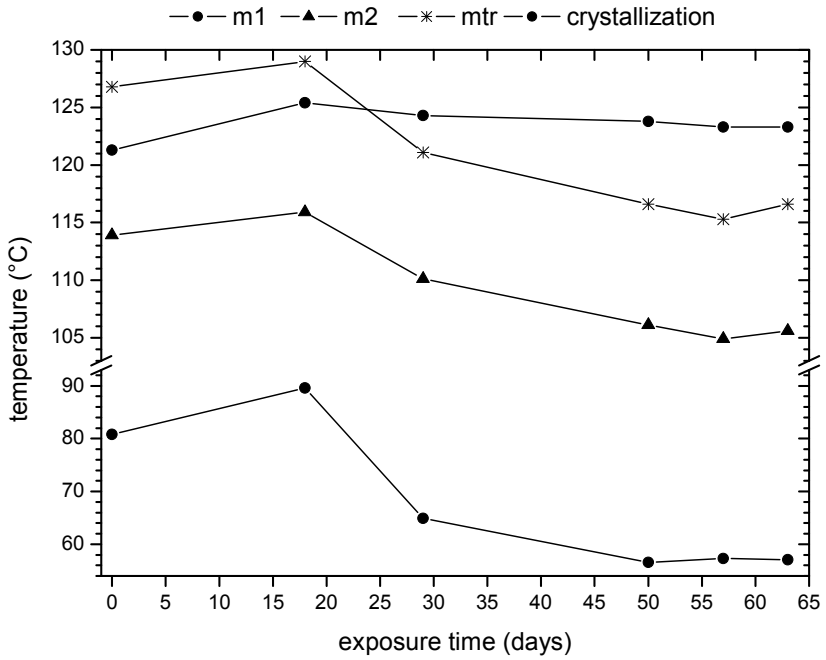

Fig. 35 Melting and crystallization behavior of DP 0401M exposed to natural weathering, (m1 – first melting, m2 – second melting, mtr – melting after transformation is completed)

Similarly to accelerated weathering tests, the melting temperature of form I upon natural test does not significantly changed. Upon the recrystallization, melting temperatures of both form I and II firstly increases and then drops to low values, again similarly to changes arising from accelerated weathering. However, the crystallization temperature shows non-monotonic evolution, which cannot be found within accelerated ageing. Because of weaker intensity and different spectra of UV light are applied during natural weathering, the molecular degradation is slowed down which is reflected by rather similar crystallization behavior as in the case of PB 0300M upon artificial weathering. Upon 18 days of exposition, an increase of T_c is manifested, then, between the days 18 and 28 a significant drop in T_c can be seen. Further, no significant changes occurred from day 50 to 63 in crystallization behavior. It should be noted that during natural weathering and accelerated UV irradiation the final melting and crystallization temperatures are similar.

The evolution of subsequent phase transformation in re-melted UV irradiated specimens is illustrated in following Figs 36-41. The Fig. 36 shows evolution of form I content during phase transformation of degraded DP 0401M. Fig. 37 illustrates the ratios of the melting peaks the forms I and II. From both Figs it is evident that after two hours of UV irradiation no significant change in transformation rate is observed. However, the change of transformation rate is evident between 3 and 10 irradiation hours, when decreasing trend occurs which correlates to decrease of crystallization temperature (Fig. 34). Further minor change in transformation rate between 15 and 40 irradiation hours confirms its dependence on crystallization temperature

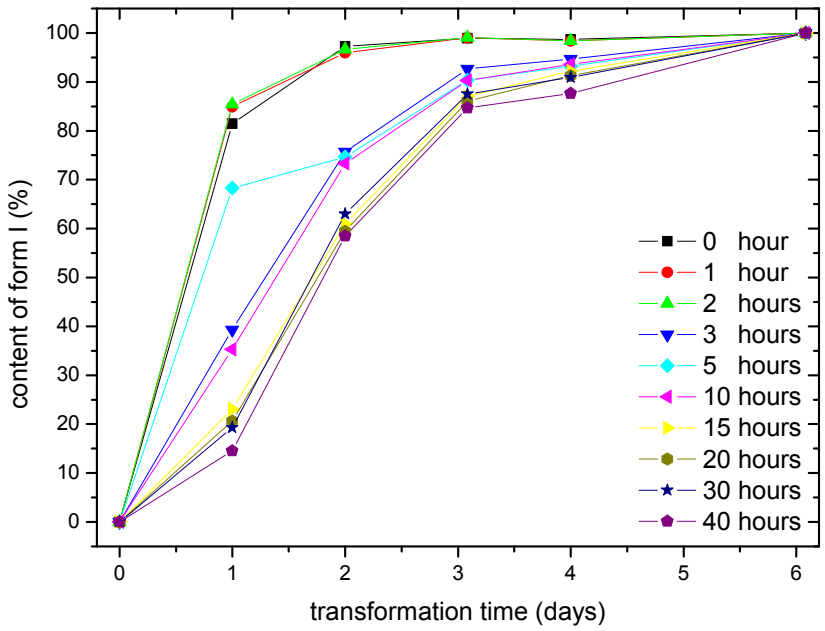

Fig. 36 Evolution of form I content during transformation of degraded specimens for various irradiation times in DP 0401M

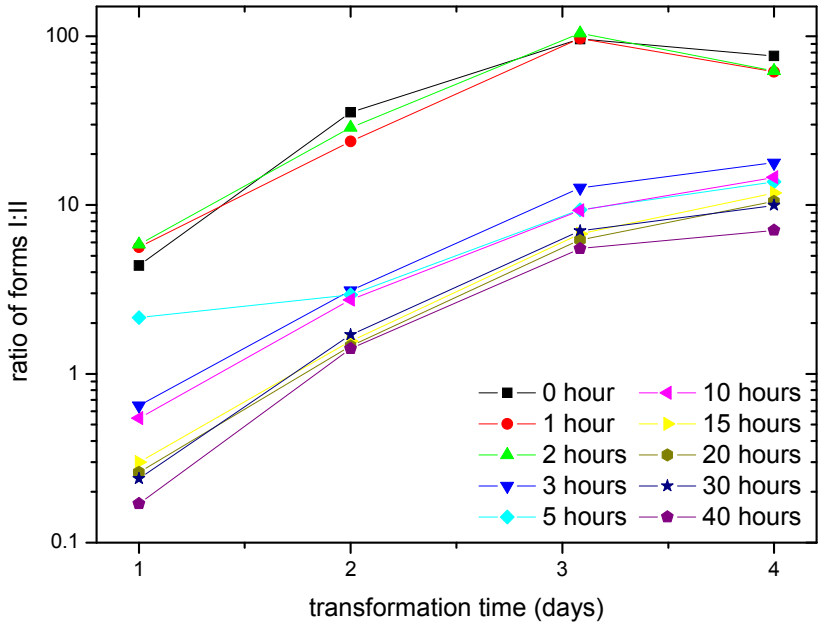

Fig. 37 Evolution of ratio of form I to II during transformation of degraded specimens for various irradiation times in DP 0401M

This fact is supported by Figs 38 and 39 in case of material PB 0300M. The transformation rate of non-irradiated specimen which has a lower T_c compared to UV irradiation time of 1.5, 3 and 5 hours possesses also slower transformation rate. Further irradiation (10 ~ 40 hours) is followed by decreasing trend the same as in Fig. 34. Again, the competition between the molecular mobility and regularity is a key factor influencing the transformation.

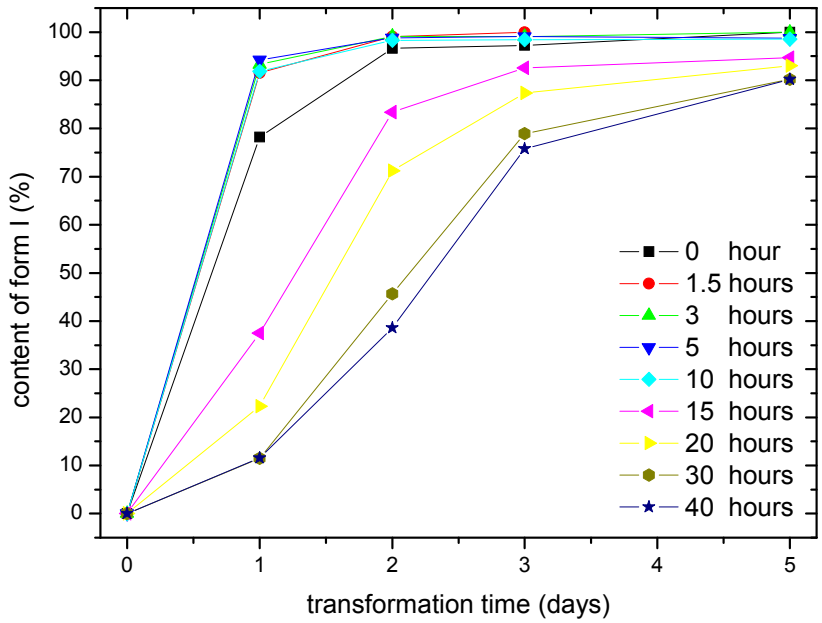

Fig. 38 Evolution of form I content during transformation of degraded specimens for various irradiation times in PB 0300M

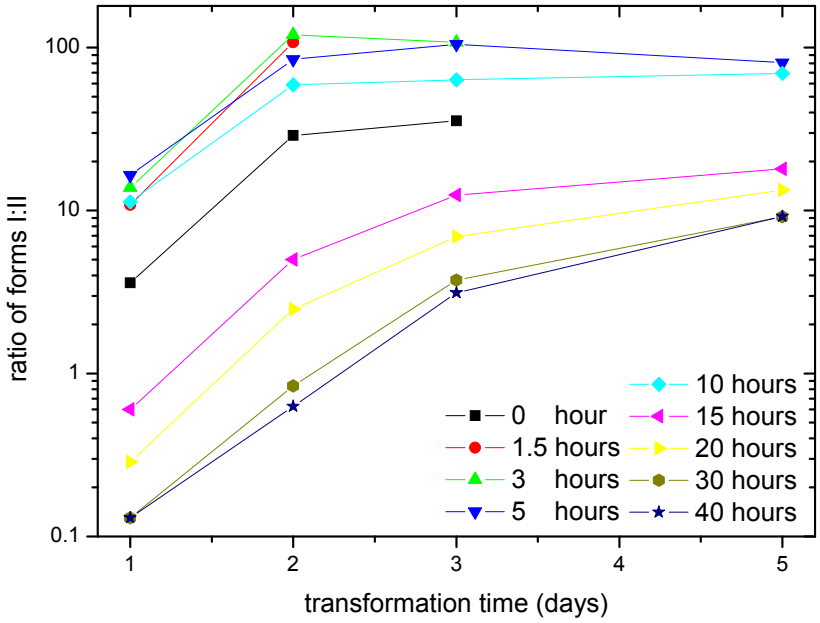

Fig. 39 Evolution of ratio of form I to II during transformation of degraded specimens for various irradiation times in PB 0300M

A virtually the same behavior can be seen in Figs 40 and 41, where the transformation rates also follows the changes of crystallization temperatures in naturally exposed specimens.

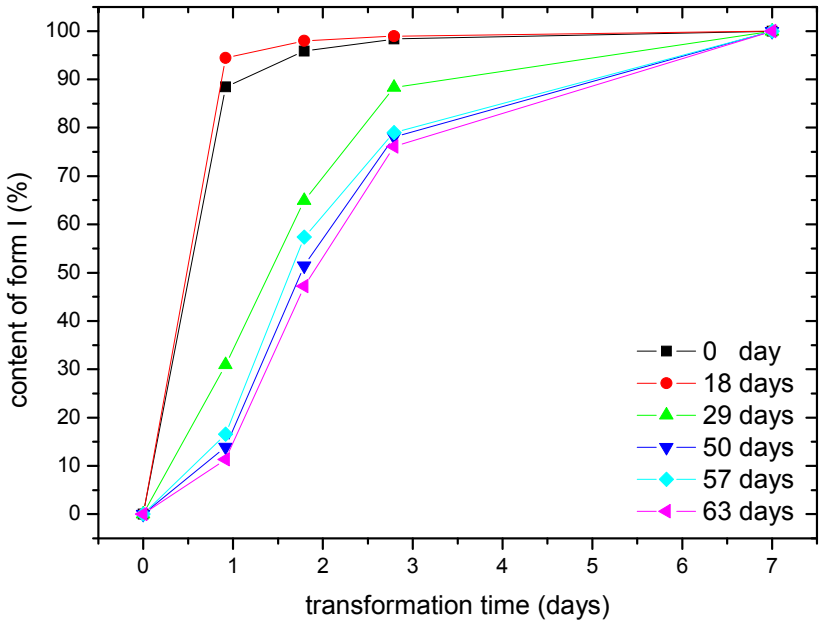

Fig. 40 Evolution of form I content during transformation of degraded specimens for various exposition times in DP 0401M

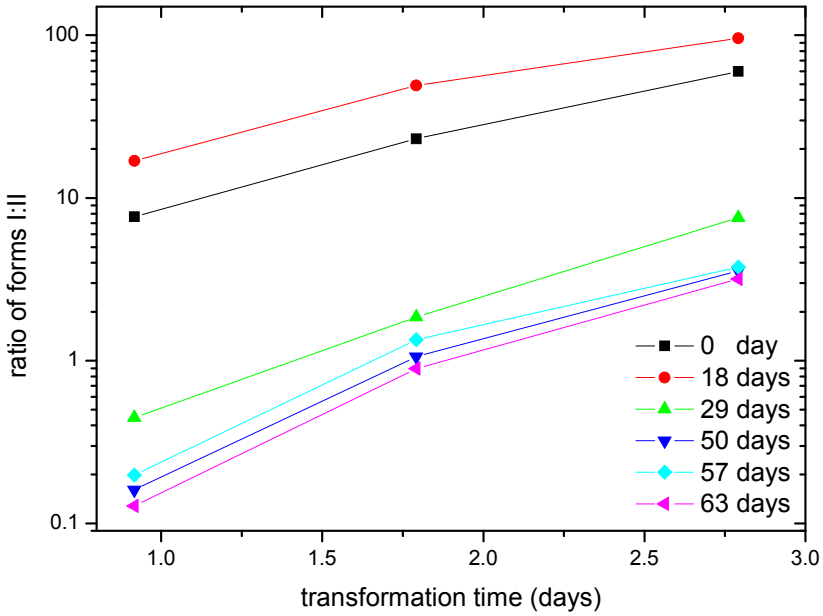

Fig. 41 Evolution of ratio of form I to II during transformation of degraded specimens for various exposition times in DP 0401M specimens

When comparing Figs 37, 39 and 41 it can be seen that curves of the ratios of the forms I and II are particularly superposed to each other. Thus, the transformation rate follows the changes in crystallization temperature; the process is overall slower but with similar mechanism.

6.1.2 FTIR characterization

UV irradiation leads to significant changes in the IR absorption spectra in PB-1. The evolution of chemical species in degraded PB-1 can be seen in following Figs 42-44. The major by-products resulting from presence of atmosphere oxygen are carbonyl products. As the oxidation proceeds, broad absorption bands growth at: 1640, 1712, 1735 and 1780 cm^{-1} are observed. A gradual formation of carboxylic acid (1712 cm^{-1}) can be seen in all cases. With further exposition the formation of esters becomes dominant at 1735 cm^{-1} in case of DP 0401M; the formation at absorption of 1780 cm^{-1} is assigned to peresters or γ-lactones; a weak peak at absorption 1640 cm^{-1} is assigned to vinyl groups [107].

The UV irradiation in DP 0401M and PB 0300M (Figs 42 and 43) shows similar mechanism of degradation, however in DP 0401M the evolution of chemical species is quicker in the initial stage compared to PB 0300M, and as written above the esters (1735 cm^{-1}) become dominant from 60 hours. This behavior follows the DSC observation; the interrelation with the physical effect of transformation is obvious.

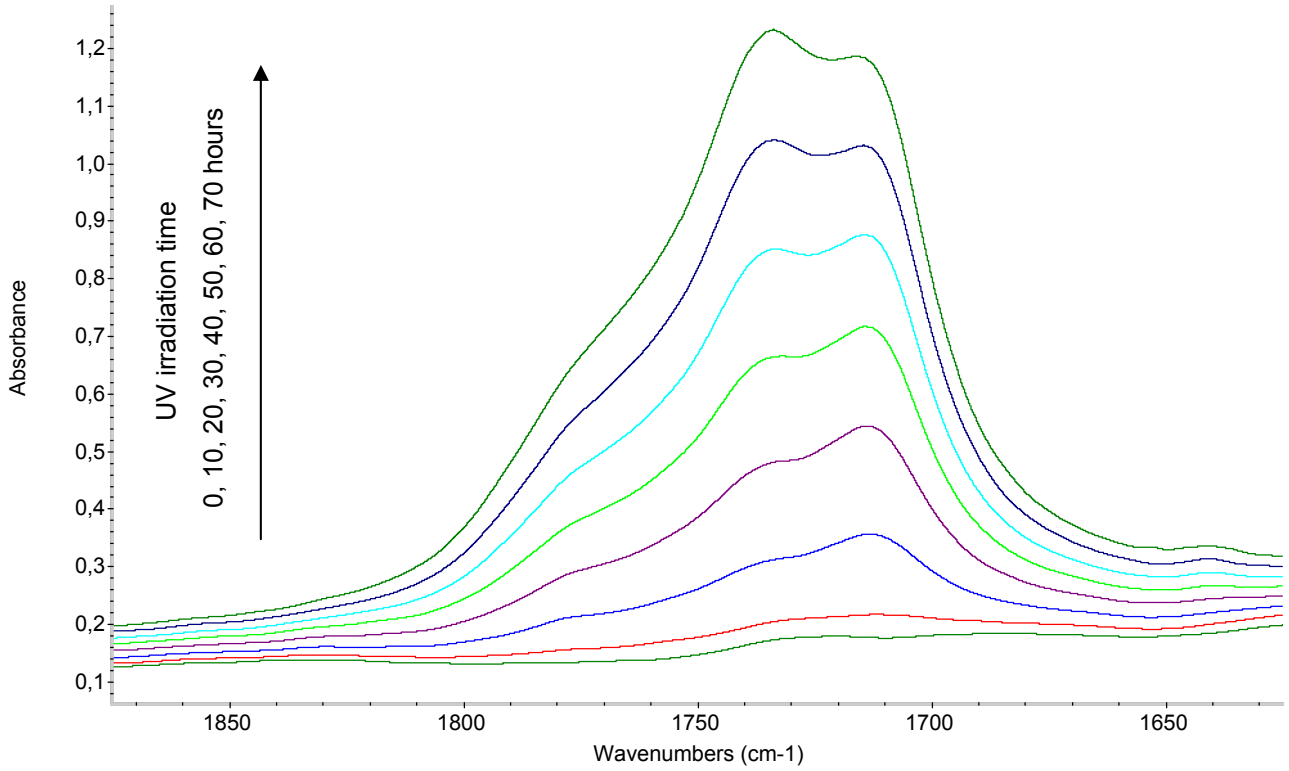

Fig. 42 FTIR spectra of DP 0401M - evolution in carbonyl area during UV irradition

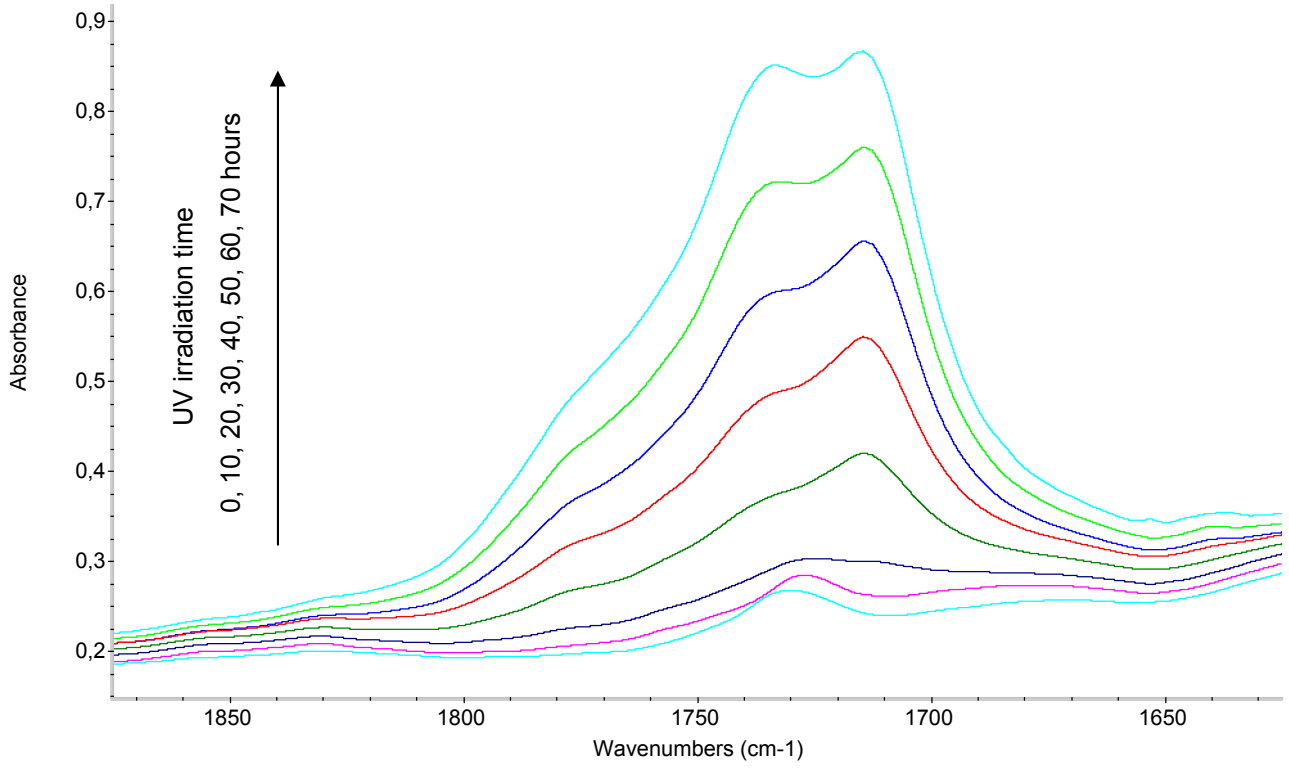

Fig. 43 FTIR spectra of PB 0300M - evolution in carbonyl area during UV irradiation

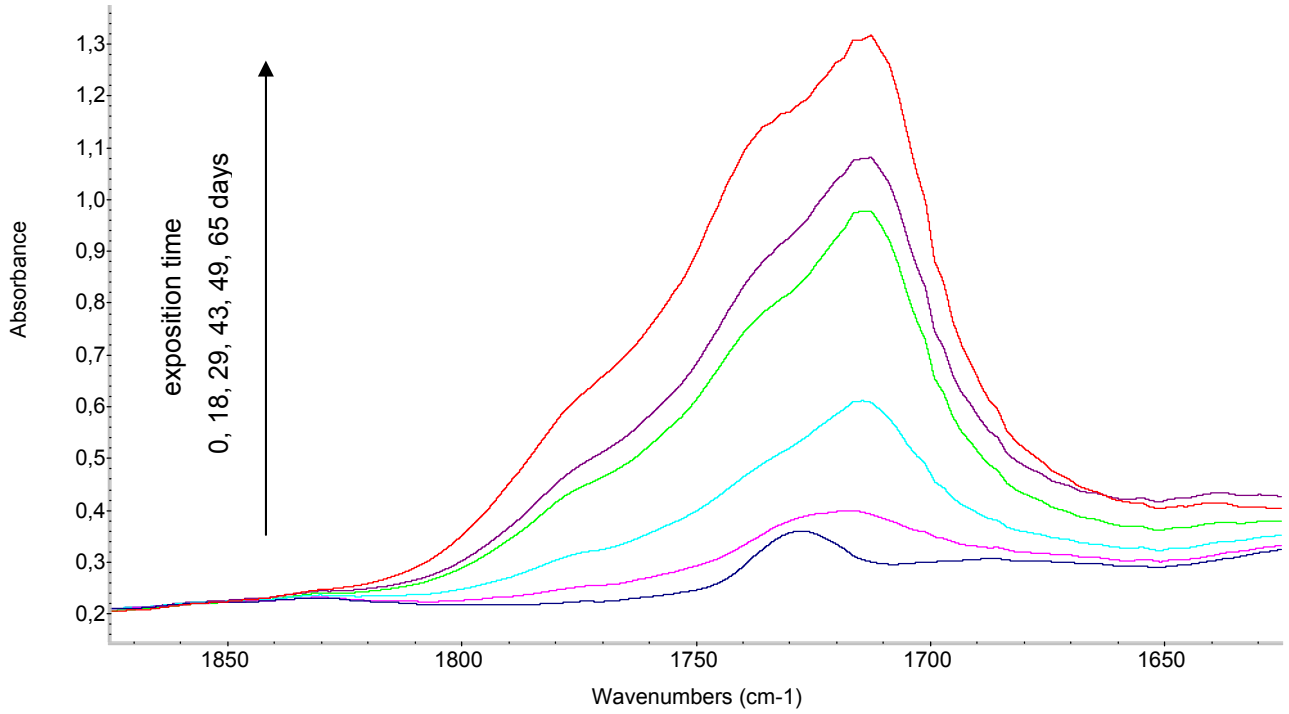

Fig. 44 FTIR spectra of DP 0401M - evolution in carbonyl area during natural exposition

On the other hand comparing UV irradiation and natural exposition in DP 0401M (Figs 42 and 44) shows significantly different behavior where carbonyl groups (1712 cm^{-1}) are predominant.

When absorbancies at 1712 cm^{-1} are plotted versus UV irradiation time or exposition time, as can be seen in Fig. 45, the chemical evolution of PB 0300M is weaker than in DP 0401M. Comparing both degraded DP 0401M it can be seen that natural weathering lead to similar chemical evolution during first 29 days what is in accordance with 30 hours of UV irradiation. Nevertheless, further natural exposition supports formation of carboxylic acids groups (Fig. 42) while in UV irradiated specimens esters groups compete with carboxylic acids.

It should also be noted that FTIR is not able to detect peroxide species, which are during radical reactions transformed to detectable chemical groups. Nevertheless, several reliable methods exist, such as modulated DSC observation, iodometric titration or indirect method based e.g. on rheological behavior.

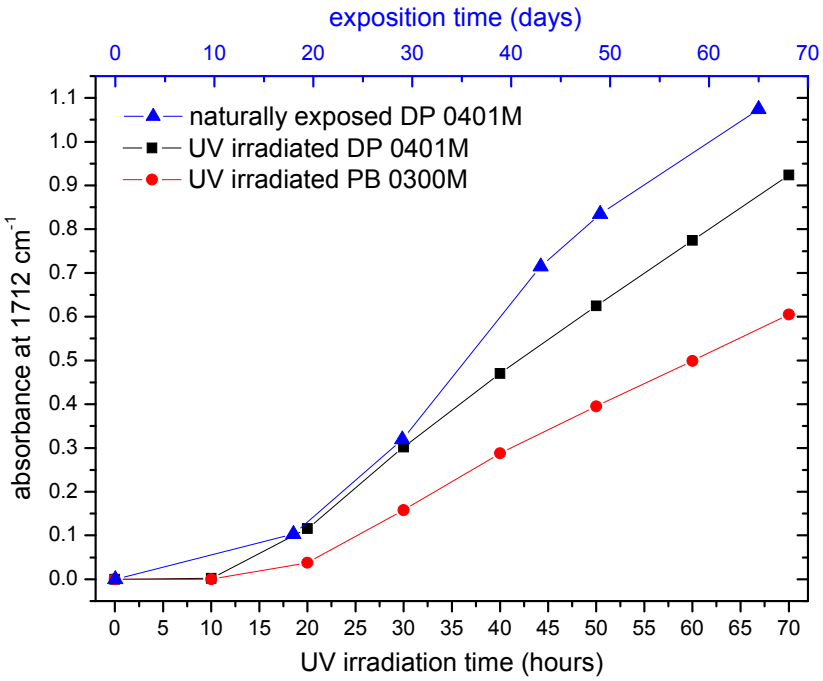

Fig. 45 Comparison of absorbancies at 1712 cm^{-1} in UV irradiated and naturally exposed specimens

6.1.3 Rheology

Figs 46 and 47 show the Cole-Cole plots for the individual times of UV irradiation. In the complex plane this model predicts the variation of the viscosity components (η'' versus η') to be an arc of circle [104]. From this plot it is easy to determine zero shear viscosity η_0 which depends on the molecular weight and follows a power law. It is evident that this is convenient method to determine molecular changes in the short UV irradiation times for PB-1 with respect to MW. In case of DP 0401M (Fig. 46) at the beginning of UV irradiation (1.6 hour) η_0 slightly decreases. During further UV irradiation, 5 hours, η_0 drops and then further significant drop is observed after 10 hours, which shows practically immeasurable low viscosity on employed apparatus, respectively chain scissions occur. Material PB 0300M (Fig. 47) shows at the beginning of UV irradiation virtually the same behavior as DP 0401M. On the other hand during further UV irradiation the decrease of η_0 is progressive which is contributed to approx. 3 times higher η_0 (higher MW) than DP 0401M. It is obvious that chain scission reactions, initiated by hydroperoxides decomposition during melt rheological measurements, are dominant during initial stage of UV irradiation even if recombination reactions occur [75].

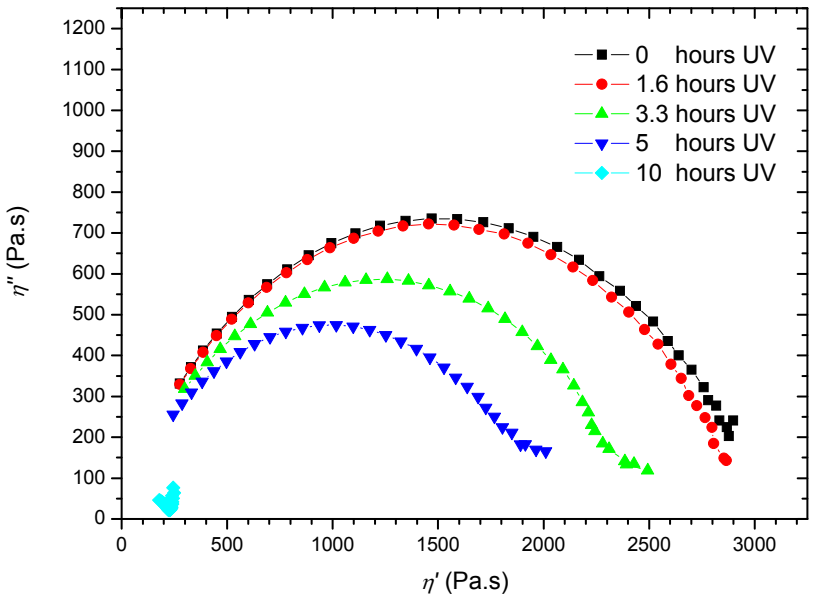

Fig. 46 Cole-Cole plot of DP 0401M up to 10 hours of UV irradiation

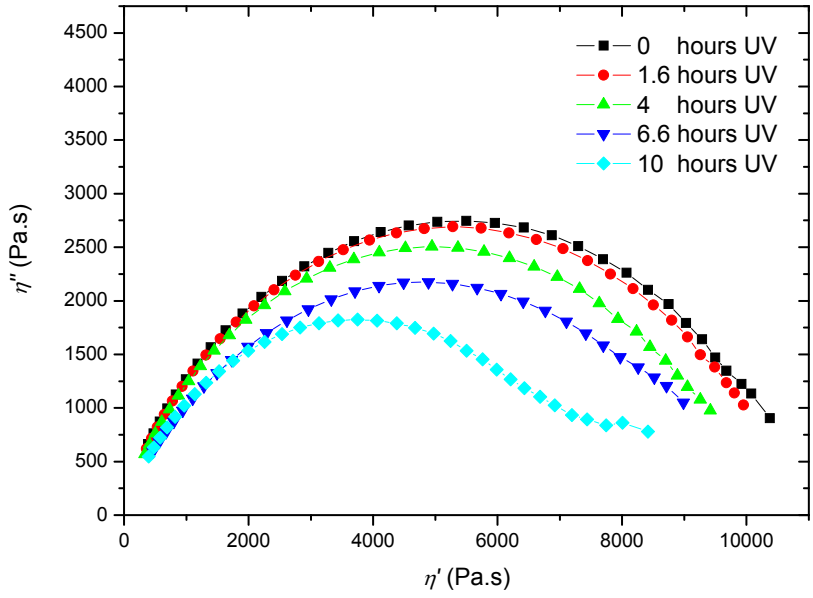

Fig. 47 Cole-Cole plot of PB 0300M up to 10 hours of UV irradiation

The dependences of extrapolated zero shear viscosity η_0 and distribution parameter h on UV irradiation time are illustrated in Fig. 48. The decrease of η_0 directly reflects changes in molecular weight, while parameter h reflects the changes in molecular weight distribution. The drop of h at time of 10 hours signifies double distribution, which can be particularly seen in Fig. 47.

It is evident that DP 0401M degrades more readily because of lower molecular weight compared to PB 0300M which is consistent with observation on the phase transformation.

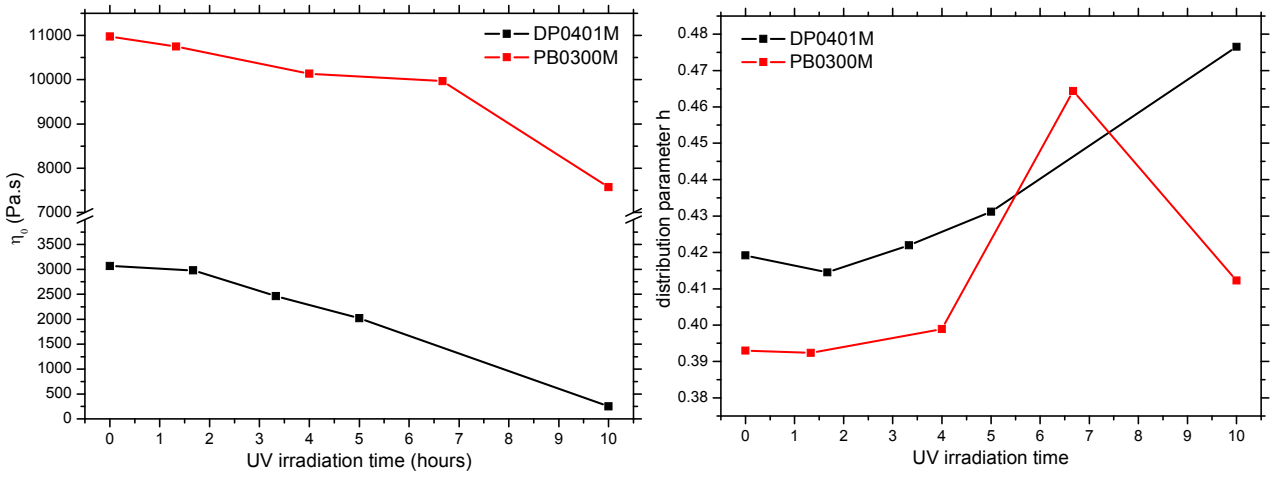

Fig. 48 Evolution of zero shear viscosity and distribution parameter during UV irradiation

6.2 Prolonged stages

6.2.1 DSC study

The melting behavior of UV irradiated 1 mm thick sheets of DP 0401M is illustrated in Fig. 49. The similar trend of decreasing melting and crystallization temperatures were observed in Figs 33 and 34 for the sheet with thickness of 0.3 mm which allowed detail insight to initial stage of degradation in PB-1.

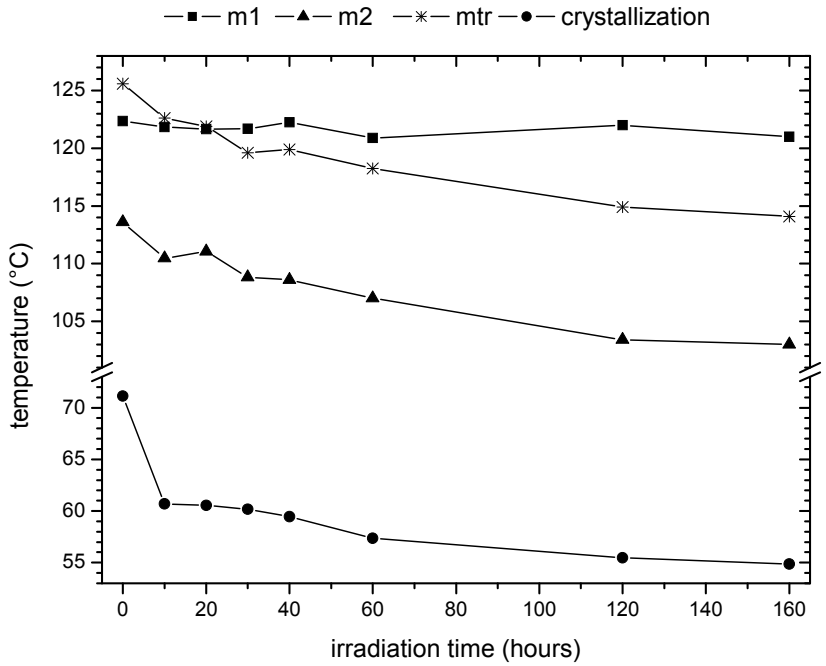

Fig. 49 Melting and crystallization behavior of PB 0401M (m1 – first melting, m2 – second melting, mtr – melting after transformation is completed)

6.2.2 FTIR-ATR characterization

Similarly, the comparing of FTIR and FTIR-ATR spectra of DP 0401M (Figs 42 and 50) shows virtually the same trend in the beginning of UV irradiation. No changes in first 10 hours, then time of 20 hours an increase in carboxylic area (1712 cm^{-1}). Since 60 hours of UV irradiation, a prevailing growth of esters occurs (1735 cm^{-1}).

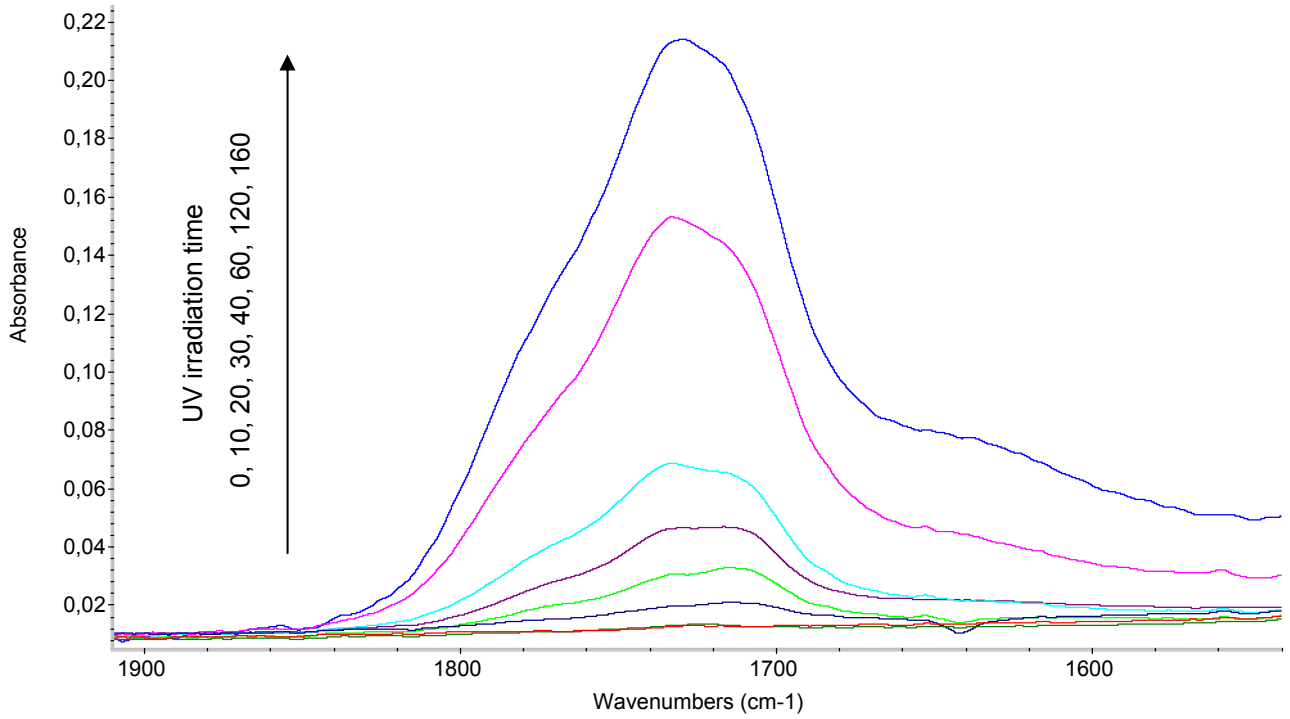

Fig. 50 FTIR-ATR spectra of DP 0401M - evolution of carbonyl area during UV irradiation

6.2.3 Rheology

The thicker sheets also enables to perform rheology experiments in wider time range, because of the penetration of hydroperoxides groups is more gradual in thickness profile of 1.0 mm compared to 0.3 mm.

The rheological measurements of naturally exposed specimens of DP 0401M were practically valueless, because after of only 18 days of exposition, the value of zero shear viscosity η_0 dropped to <100 Pa.s.

The rheological behaviors represented by Cole-Cole plots of both materials are illustrated in Figs 51 and 52. In both materials, UV irradiation lead to virtually the same decrease of zero shear viscosity η_0 after 15 ~ 20 hours. Nevertheless, the development of degradation is completely different during initial 10 hours.

In DP 0401M (Figs 51 and 53) during first 2.5 hours a recombination reactions take place in competition with chain scission reactions or the effect of chemi-crystallization. Thereafter, gradual decrease of η_0 is observed, caused by chain scission reactions and increasing amount of hydroperoxides groups. The changes in parameter h were not observed.

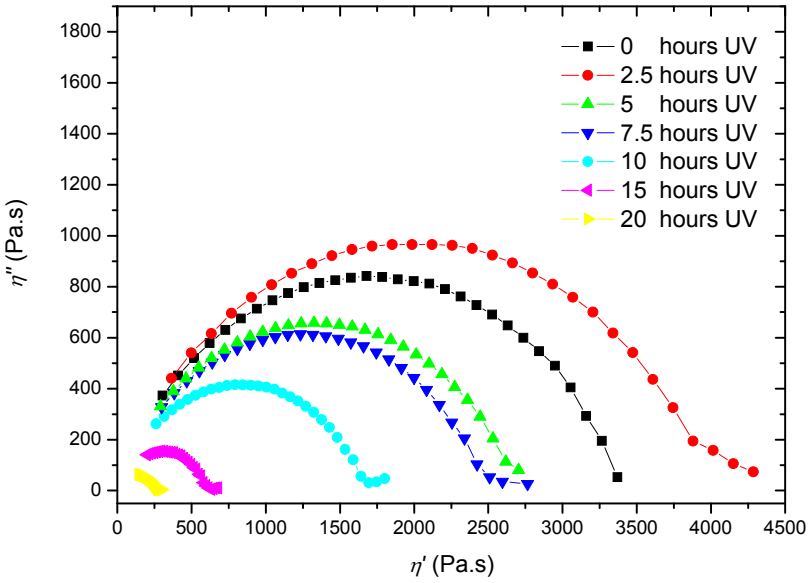

Fig. 51 Cole-Cole plot of DP 0401M up to 20 hours of UV irradiation

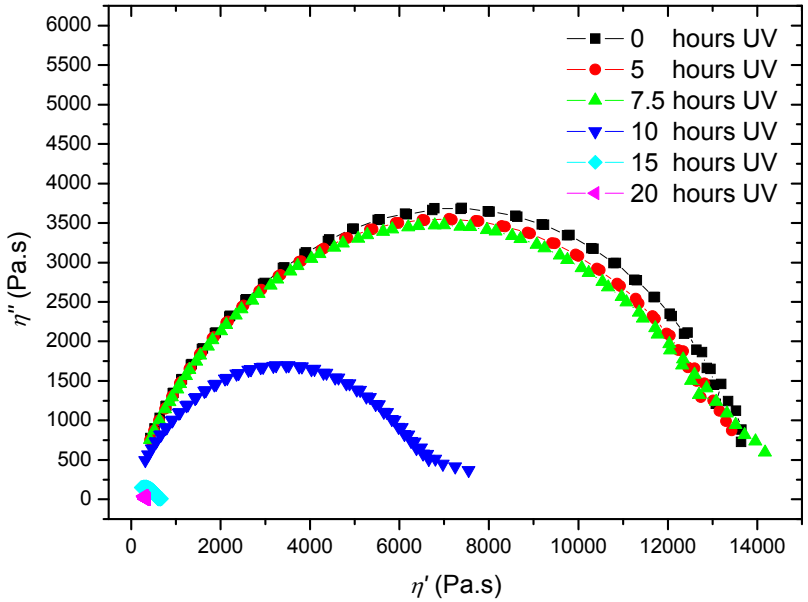

Fig. 52 Cole-Cole plot of PB 0300M up to 20 hours of UV irradiation

The Cole-Cole plot of PB 0300M (Fig. 52) shows a particularly the same behavior as in the Fig. 47 for initial stage. Even if no significant changes in η_0 were observed, the parameter shows its increase as in the Fig. 48. After 10 hours of UV irradiation η_0 remarkably drops to half-value of that at 7.5 hours. Continuous UV irradiation led to further drops in η_0 similarly as in DP 0401M. The changes of parameter h are illustrated in Fig. 54, a similar increasing trend was observed as for sheets with thickness of 0.3 mm (see Fig. 48).

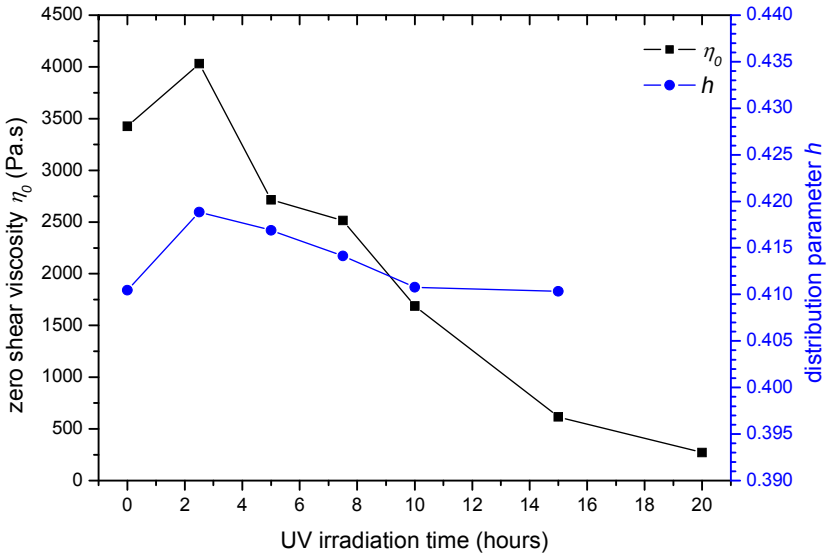

Fig. 53 Evolution of zero shear viscosity and distribution parameter during UV irradiation in DP 0401M

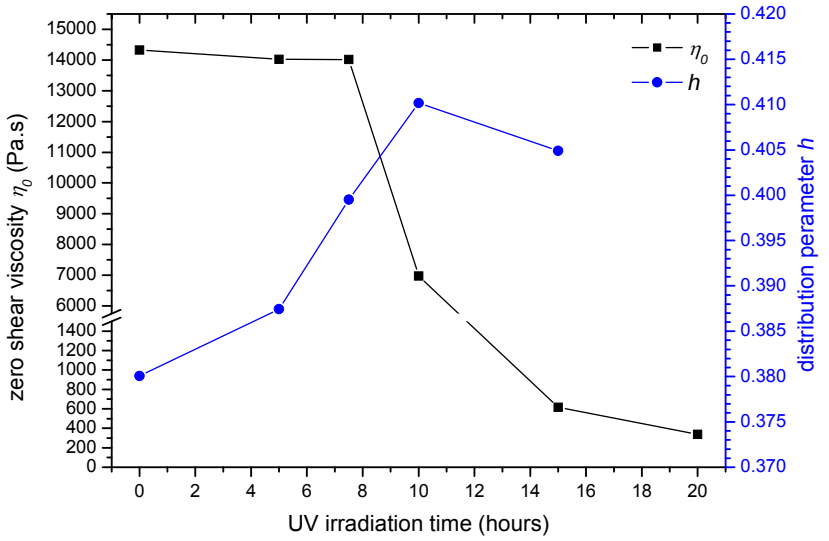

Fig. 54 Evolution of zero shear viscosity and distribution parameter during UV irradiation in PB 0300M

6.2.4 WAXS characterization

In the Figs 55 and 56 X-ray data, namely crystallinity and form II content of both sets of degraded specimens of material DP 0401M can be seen. It is obvious that no distinct trends were observed and both calculated values vary within close interval. This is actually with agreement with previously presented DSC data where the first melting varies within close interval for both types of degradation.

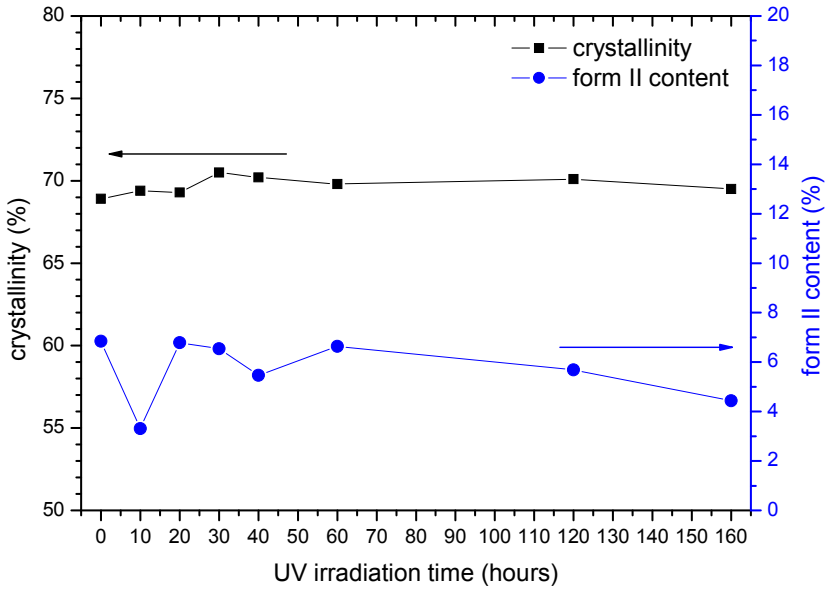

Fig. 55 Evolution of crystallinity and form II content in UV irradiated specimens DP 0401M

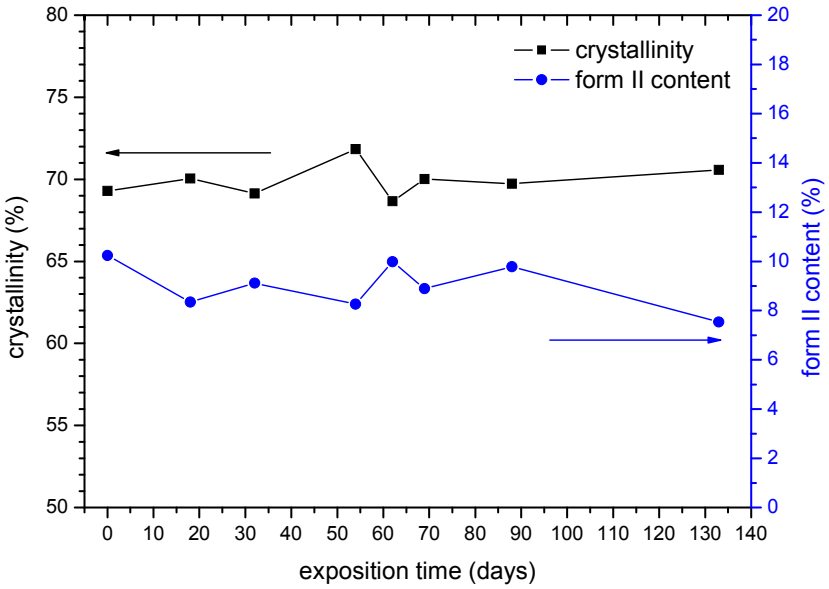

Fig. 56 Evolution of crystallinity and form II content in naturally exposed specimens DP 0401M

6.2.5 Stereomicroscopy

In order to observe the macroscopic effect of UV irradiation on surface changes, a stereomicroscope was used to take images of the degraded specimens (see Fig. 57). What is obvious is the formation of deep surface cracks. Since 40 hours of UV irradiation a tiny crack nucleus are observed, consequently enlarging to deep crack lines after 60 hours. As for 80 hours, it can be seen that crack lines interconnect each other and create a network. Further degradation in time of 120 and 160 hours lead to propagation of such created crack network by widening the crack lines and penetrating into depth.

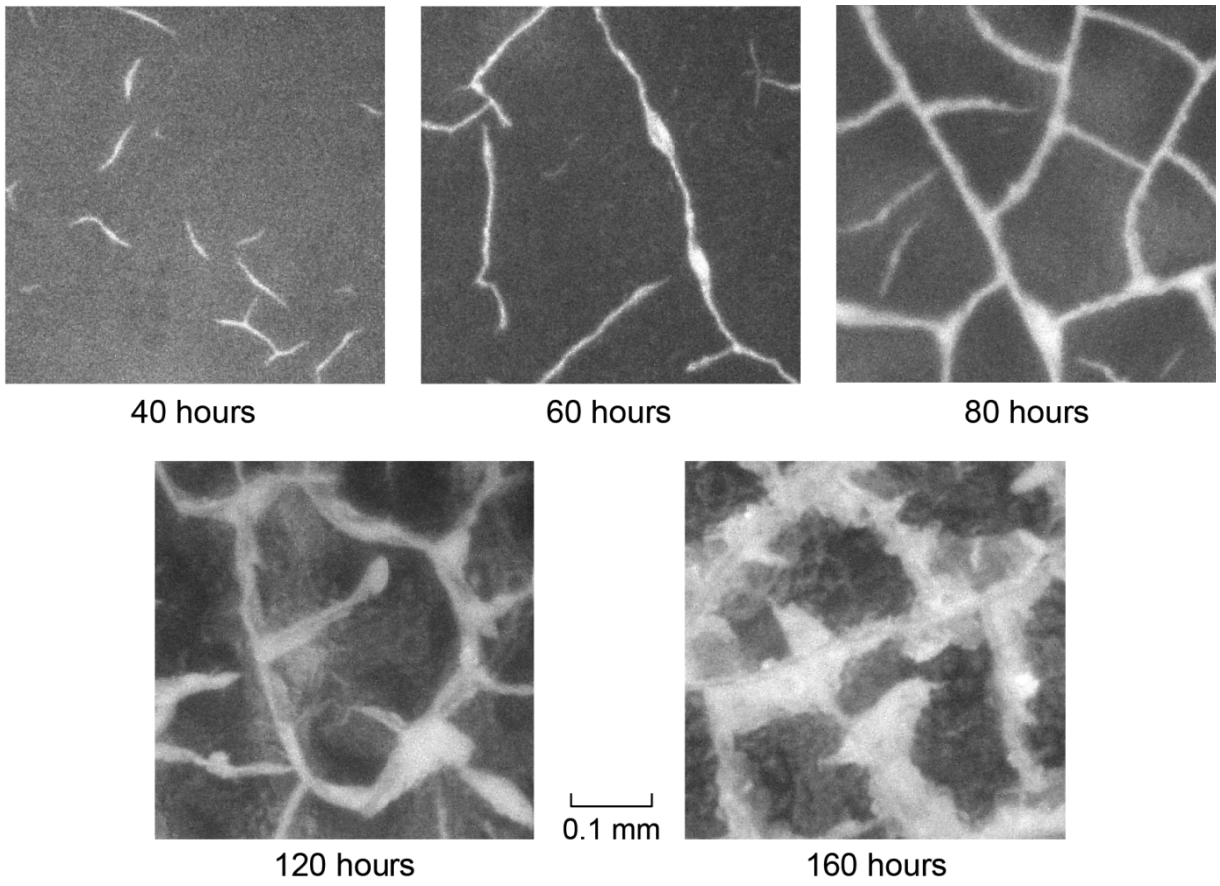

Fig. 57 Images of surface degradation in DP 0401M in various UV irradiation times

6.2.6 Scanning Electron Microscopy

A deeper look inside the structure was performed using scanning electron microscopy (Figs 58 and 59). As can be seen in Fig. 58 the cracks arise on spherulite level following the lamellar growth direction from center of spherulites. For comparison, all three materials were UV irradiated for 160 hours and distinct differences are visible. The similar morphology of PB 0300M does not enable such intensive formation of cracks; this could caused by different MW and probably higher number of tie molecules connecting individual lamellae.

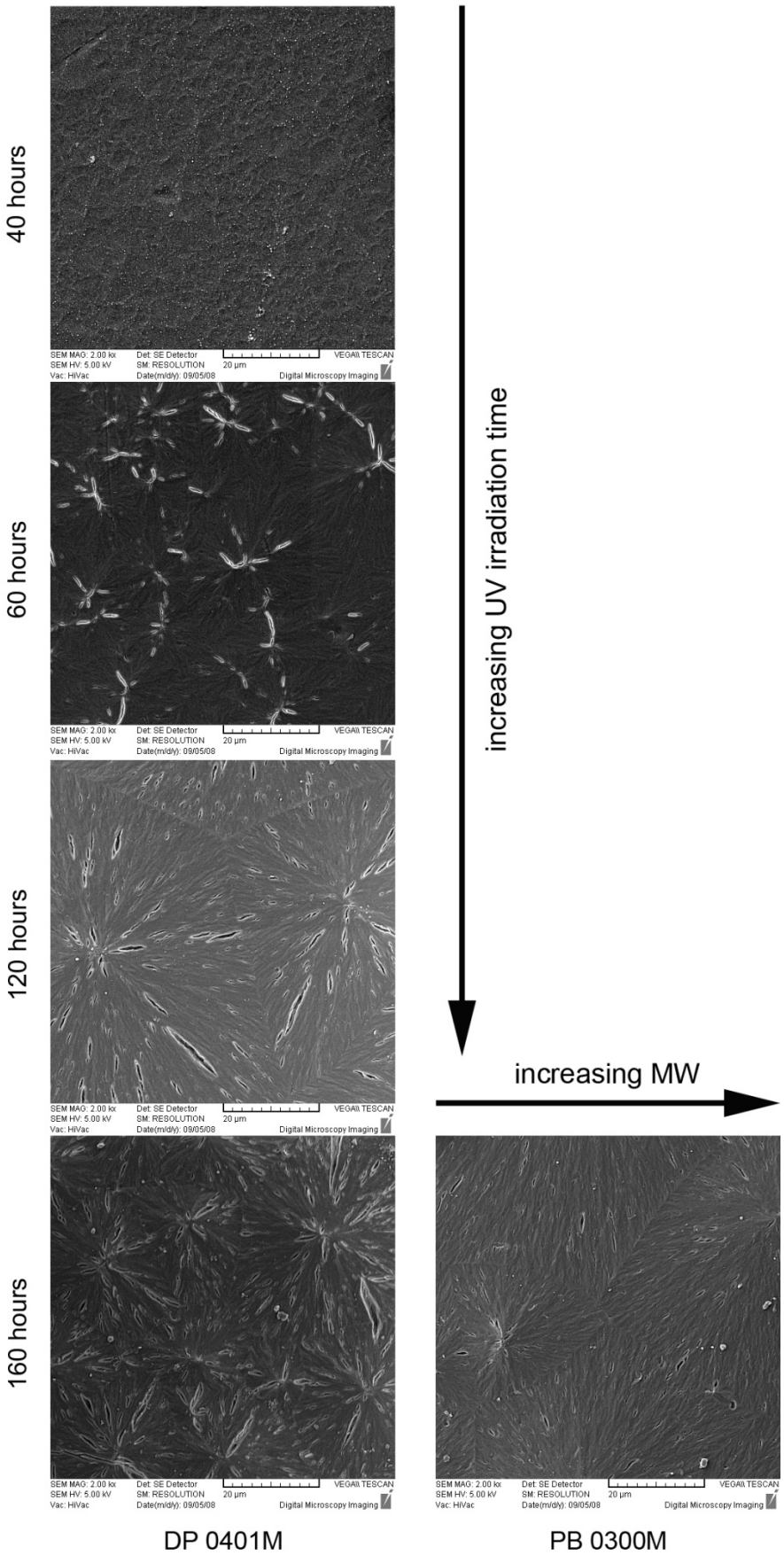

Fig. 58 SEM images of surface degradation in the materials for various UV irradiation times

While Fig. 58 shows surfaces of UV accelerated irradiated specimens, in Fig. 59 the surfaces of naturally degraded specimens can be seen. The formation of cracks is different and especially high amount of smaller cracks without distinct evolution, which is preferentially caused by weathering and erosions.

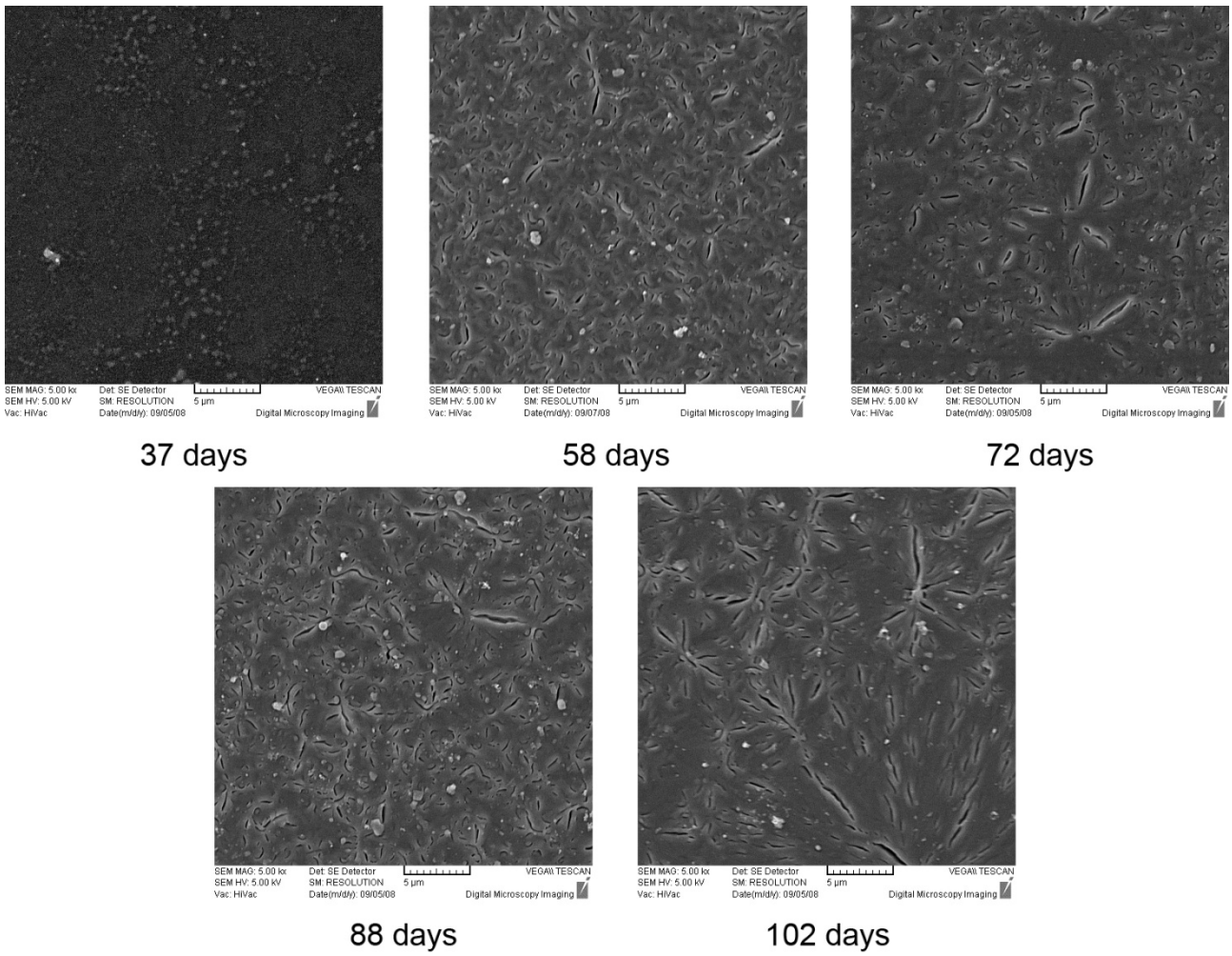

Fig. 59 SEM images of surface degradation in the DP 0401 naturally degraded at various exposition times

6.3 Degradation of extruded PB-1

In previous Chapters 6.1 and 6.2 the compression molded sheets were analyzed using various experimental techniques regarding their degradation and subsequent phase evolution. On the other hand, the following subchapter studies the effect of photodegradation on extruded specimens allowing also the assessment of mechanical properties. Two degradation regimes were used; first set of specimens was UV irradiated from 0 to 300 hours, seconds set of specimens was exposed to natural weathering in period from June 6 to September 17 2008 e.g. 0 ~ 103 days. Then, the degraded sets of specimens were characterized by WAXS, FTIR-ATR, stereo-microscopy and mechanical testing.

6.3.1 Mechanical properties

The evolutions of mechanical properties in DP 0401M during UV irradiation and comparison with natural weathering are illustrated in following Figs 60-62. It is obvious that the natural weathering led to different results in all three measured parameters compared to accelerated UV irradiation. The evolution of tensile modulus (see Fig. 60) is followed in the case of accelerated UV irradiation by a gradual decreased from approx. 500 to 350 MPa, except the variation in the initial time 0 ~ 20 hours. On the contrary, natural weathering lead to a slightly increasing trend of modulus; actually these values partly correspond to the UV irradiation time of 20 hours. This can be related to the chemi-crystallization phenomenon.

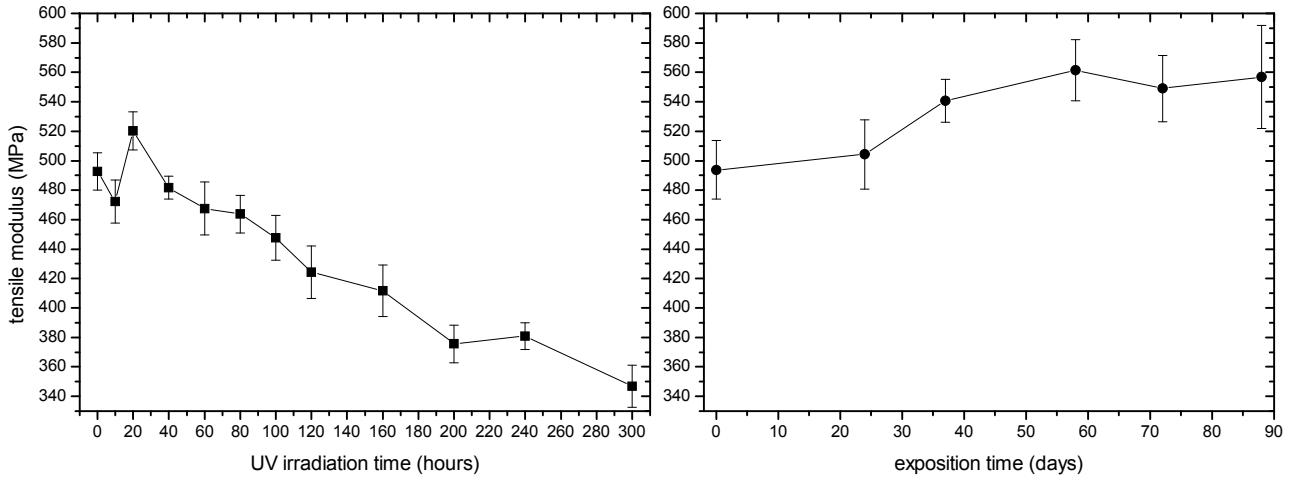

Fig. 60 Evolution of tensile modulus in UV irradiated and naturally exposed specimens

The Fig. 61 illustrates the tensile strength at break behavior of degraded specimens. Similarly as in the tensile modulus the UV irradiation time between 0 ~ 20 hours shows a specific behavior with a slight increase (or no change) in 10 hours being probably caused by mentioned chemi-crystallization, but the further irradiation lead to drop from 21 to 15 MPa . From 40 hours, the further UV irradiation causes gradual decrease to 11.5 MPa. On the other hand, the behavior of natural weathered specimens leads to

an insignificant decrease of strength at break after 24 days of exposition. Nevertheless, after 35 days a drop to a half of initial value occurred, followed by a decrease to the values between 8 ~ 9 MPa. Thus the determination of degradation factor between both, accelerated UV irradiation and natural weathering is practically restricted to the short exposition times to 35 days, and 40 hours respectively.

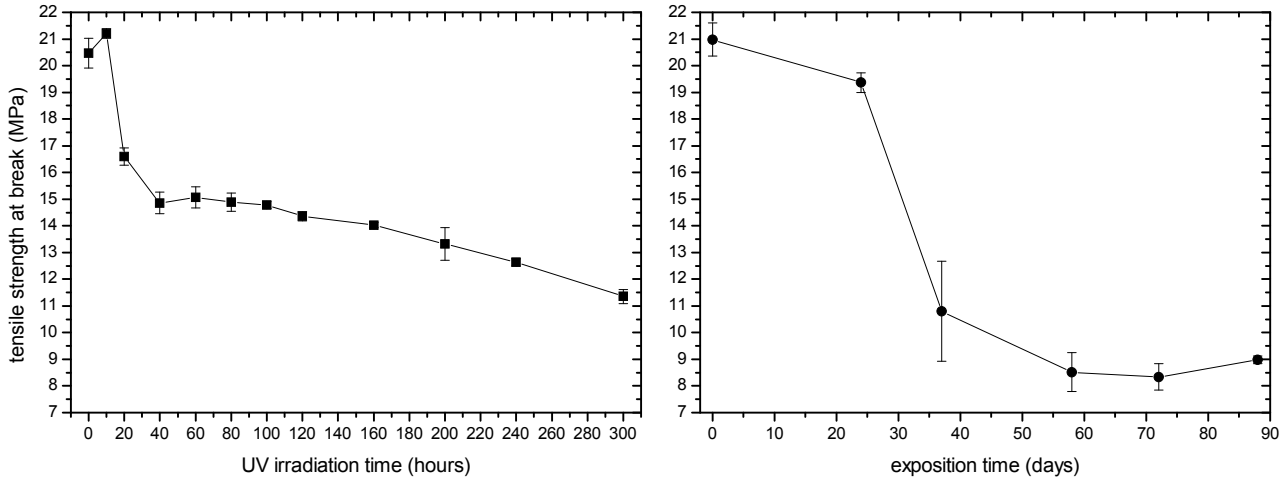

Fig. 61 Evolution of tensile stress at break in UV irradiated and naturally exposed specimens

Again, the specific evolution in the initial UV irradiation time of 0 ~ 40 hours can be seen in Fig. 62. The elongation at break significantly drops from approx. 38 % to a few percent after 20 hours. Further irradiation does not influences elongation at break and the value vary between 9 ~ 11 %; it is worth noting that such values are already rather low, probably on their minima. Similar behavior is observed in naturally exposed specimens, after the initial drop to 10 %, the elongation vary in interval 3 ~ 5 %. It can be suggested that 20 ~ 40 hours of UV irradiation corresponds to 24 days of natural weathering, nevertheless this factor cannot be applied for longer exposition time. It should be mentioned that the both effect the chemi-crystallization and chain scission will in general lead to a decrease of the material drawability.

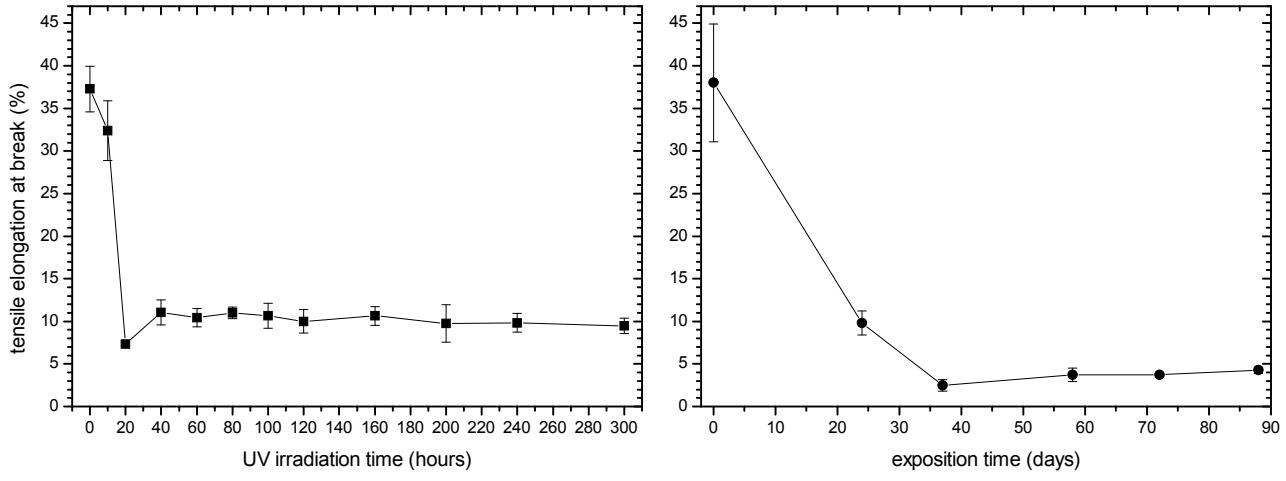

Fig. 62 Evolution of tensile elongation at break in UV irradiated and naturally exposed specimens

The testing of mechanical properties offers a suggestion that natural exposition with lower UV intensity leads to the chemi-crystallization, which slightly increases tensile modulus. Therefore, naturally exposed specimens become more brittle as has been observed in its tensile elongation at break and strength at break. On the contrary, in the UV irradiated specimens the chemi-crystallization process and modulus increase is overshadowed by the erosion of crystallites themselves upon strong accelerated UV irraditation.

6.3.2 FTIR-ATR characterization

FTIR-ATR characterization of degraded specimens was performed to understand the evolution of mechanical properties. From comparison of Figs 63 and 64 it is obvious that different chemical evolution occurred. In UV irradiated specimens (Fig. 63), a unvalued difference between time 0 and 10 hours can be seen within region 1700 ~ 1750 cm^{-1}, and with rising time 20 and 40 hours gradual increase is observed. Further irradiation lead to gradual increase in this region. The increase of peak in region 1645 cm^{-1} which belongs to vinyl groups is observed in both sets of degraded specimens. On the contrary, in the naturally exposed specimens (Fig. 64) within region 1700 ~ 1750 cm^{-1} the significant step is observed after 24 days and the formation of carboxylic acids (1712 cm^{-1}) is pronounced as well in all naturally exposed specimens.

When absorbance values are compared (see Fig. 65), UV irradiation time of 20 hours corresponds to the exposition times 24 ~ 37 days and further exposition days lies between 20 ~ 40 hours.

From Fig. 65 the chemi-crystallization influencing mechanical properties can be clarified. In naturally exposed specimens positive effect of chemi-crystallization has lead to increase of modulus which is correlates to moderate increase of carboxylic acids with partial plato in the surface layer. On the other hand, in UV irradiated specimens the content of chemical groups sharply increase resulting probably also in crystallite erosion and material disintegration.

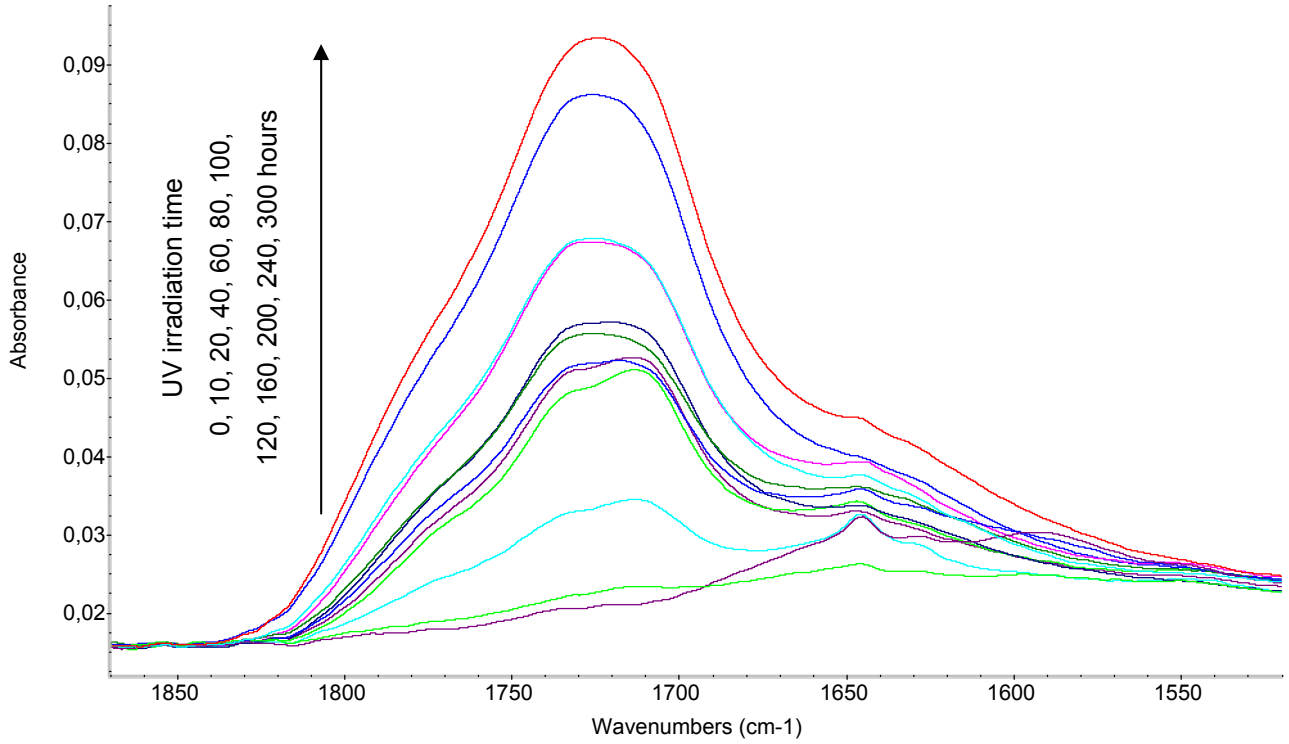

Fig. 63 FTIR-ATR spectra of UV irradiated specimens

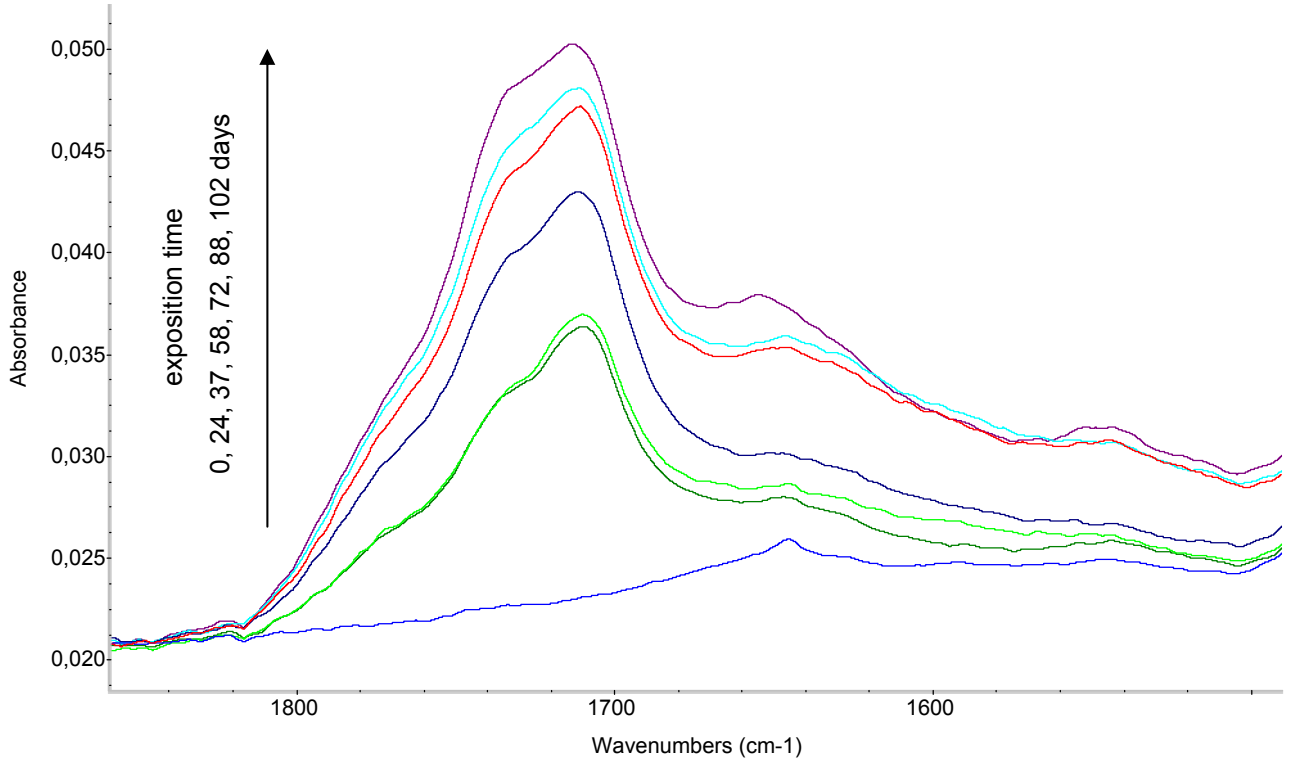

Fig. 64 FTIR-ATR spectra of naturally exposed specimens

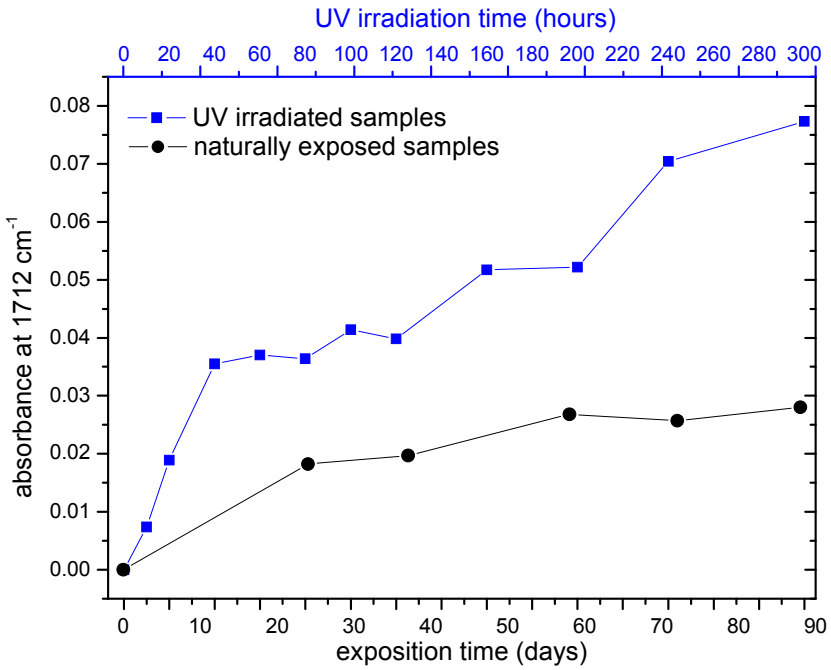

Fig. 65 Comparison of absorbancies at 1712 cm^{-1} in UV irradiated and naturally exposed specimens

6.3.3 WAXS characterization

X-ray scattering data with crystallinity and form II content of both sets of degraded specimens are illustrated in Figs 66 and 67. It should be noted that both sets were prepared from the same extruded tape however the WAXS was performed in reflection mode and improvement of crystallinity in the core may not be observed, although the most obvious effect of photodegradation can be anyhow expected in the skin-layer. It can be seen in both Figs that crystallinity vary within interval of approx. 2 % as has been observed in previous chapters and first melting in DSC study. What is important is the fact that crystallinity of naturally exposed specimens is slightly higher than in UV irradiated specimens, and do not virtually decrease during degradation. In both Figs, distinct changes in the evolution of form II content can be seen. Upon UV irradiation form II content of UV irradiated specimens quite fluently decreases from approx. 6 to 3 %. On the contrary, in naturally exposed specimens different variation of form II content can be seen. The slight increase can be probably caused by chemi-crystallization, however, further exposition lead to the decrease to the virtually the same from II content as in the UV irradiated specimens.

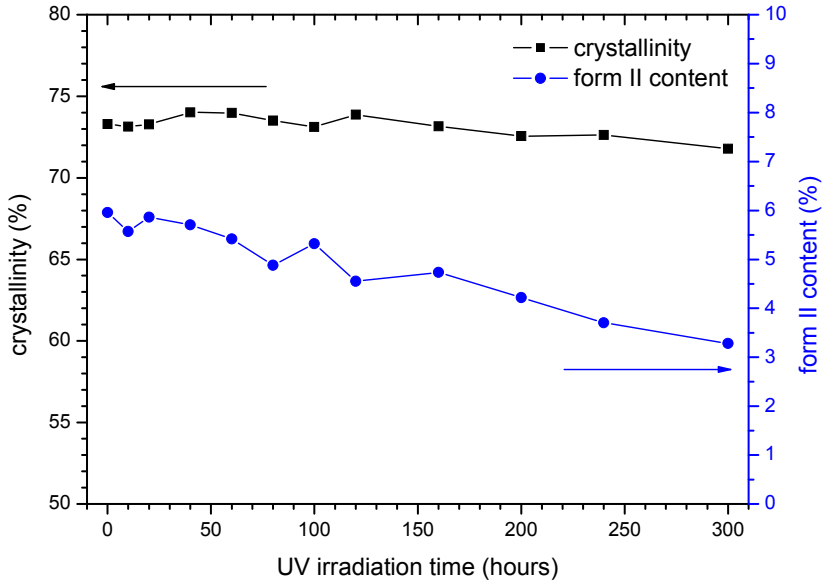

Fig. 66 Evolution of crystallinity and form II content in UV irradiated specimens

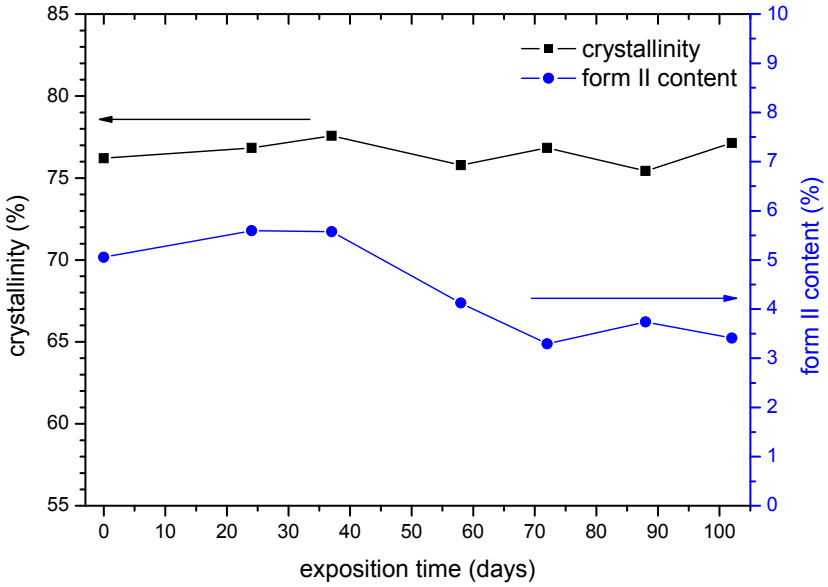

Fig. 67 Evolution of crystallinity and form II content in naturally exposed specimens

6.3.4 Stereomicroscopy

The observation of the degraded surfaces of the UV irradiated specimens is shown in Fig. 68. Similarly as in the Fig. 57, initial visible cracks appear after 40 hours of UV irradiation. While in the compression molded specimens the initial cracks possess random direction of growth, in extruded specimens the crack lines are in parallel direction as extrusion direction. With increasing UV irradiation time, parallel cracks are perpendicularly interconnects to a crack network after 120 hours; further UV irradiation lead again to widening the crack lines.

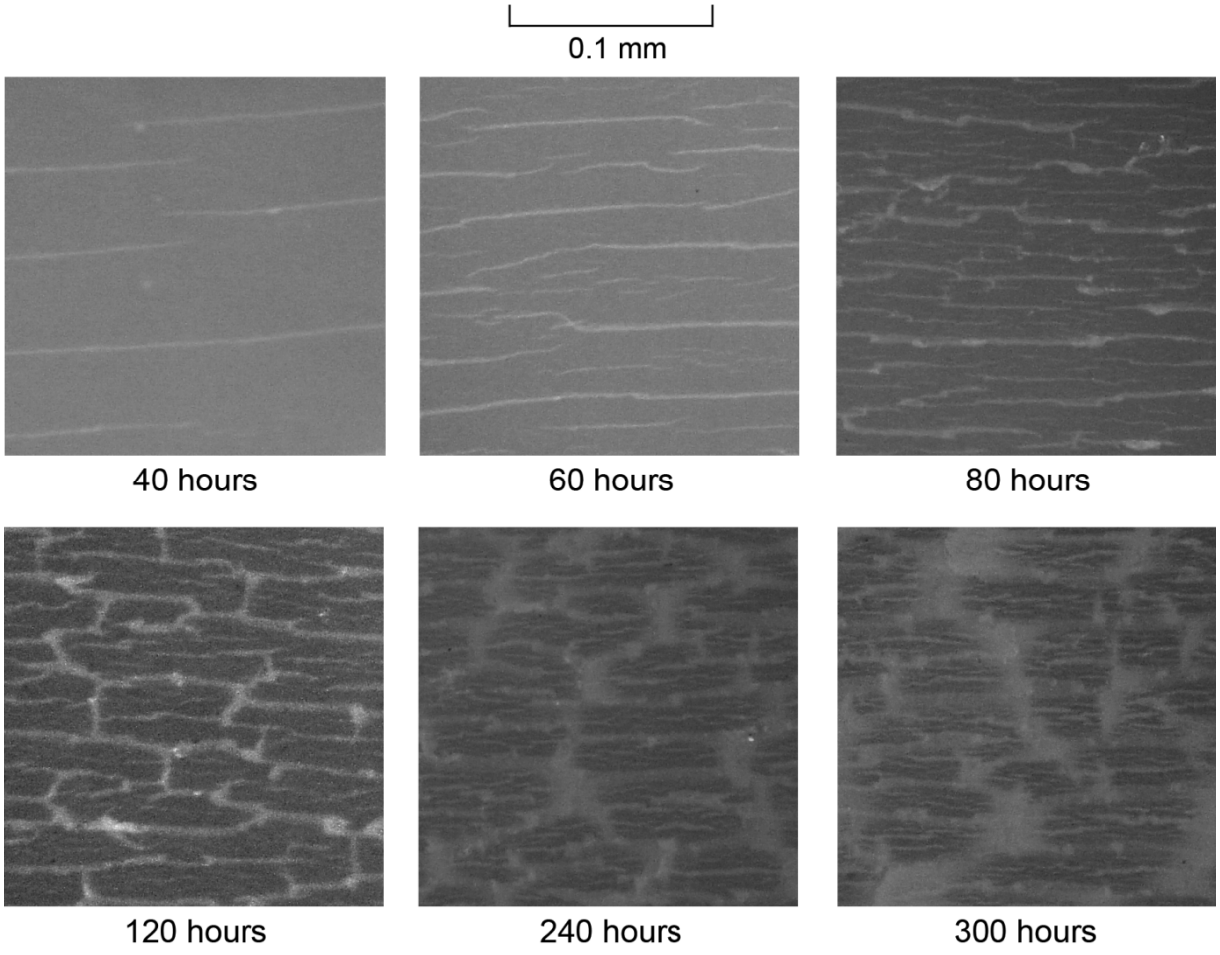

Fig. 68 Images of extruded tapes DP 0401M in various UV irradiation times

6.3.5 Effect of temperature on crystallinity and form II content

The effect of synergy of the temperature during UV irradiation was shortly studied using WAXS. Thus, two series of specimens, which were stored at room conditions for 6 months, were used. First series of them was UV irradiated at temperature of 60 °C and the other was annealed in oven with constant temperature of 60 °C. Crystallinity and content of form II were calculated from WAXS data and plotted in Figs 69 and 70.

It can be seen in Fig. 69 that crystallinity in both types of DP 0401M slightly increases in dependence of time. This increase is more significant for annealing in oven at 60 °C, while during a synergy of UV irradiation the crystallinity increase is lower indicating that the simultaneous processes of morphology perfection are slow down, however just after long-time exposure. The difference however is rather small (statistically insignificant) to openly talk about any real effects. Interestingly, further research of such interrelations would be relevant (note in Fig. 55 the crystallinity of the UV degraded tapes of DP 0401M varied and decreases with UV irradiation time).

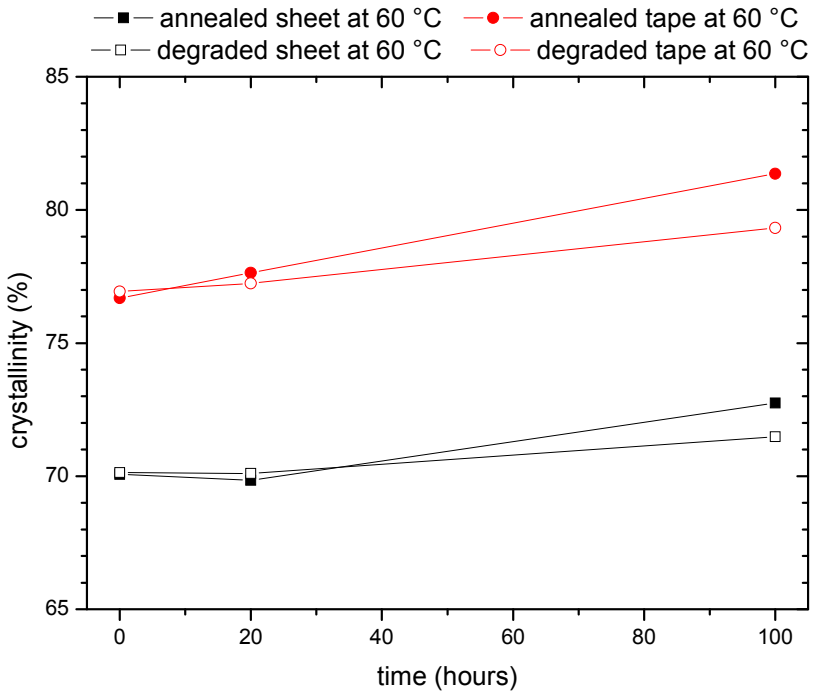

Fig. 69 Evolution of crystallinity in annealed and degraded specimens

Similarly, in Fig. 70 the evolution of the form II content shows virtually no significant differences which could however changed upon long-term exposure. However, the decrease of crystallinity and form II content reported in Fig. 66 can be then related mainly the effect of degradation.

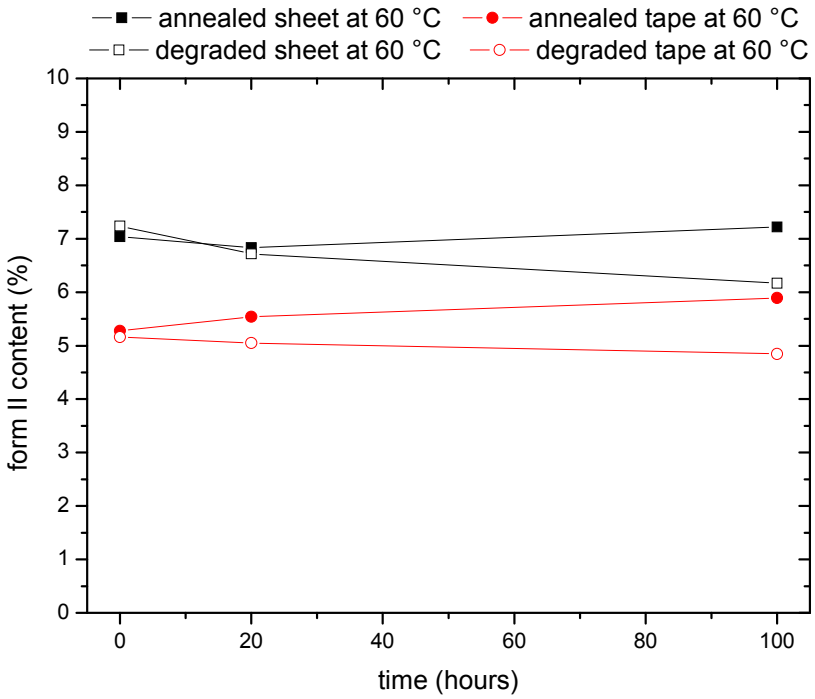

Fig. 70 Evolution of form II content in annealed and degraded specimens

7 CONCLUSION AND PERSPECTIVES

In the bibliographic study, the present state of knowledge concerning the phase transformation and degradation of PB-1 are introduced and discussed. The experimental part of this thesis has been then divided into the two main parts: 1. a study of the phase transformation PB-1 and subsequent property evolution and 2. the role of UV light in such transformation.

The first part studies the influence of the temperature on the phase transformation from several sides on various three PB-1 materials. Firstly, the DSC experiments were performed to observe thermal behavior during annealing under five various temperatures. It was confirmed that addition of ethylene comonomer positively increases molecular mobility and consequently the phase transformation. The fastest rate was observed at annealing temperatures of +5 and +22 °C, while with increasing temperature up to 60 °C the transformation slows down and the slowest rate occurred at -22 °C.

Then, the materials were processed by both injection-molding and extrusion technology to answer the question whether processing with subsequent variation in morphology gradients can affect the phase transformation being characterized by the evolution of tensile properties in the same materials and annealing temperatures as was performed in DSC study. The DSC results were confirmed; however the evolution of tensile properties on injection-molded or extrudates take remarkably longer time than in DSC specimens. Probably thickness of the specimens can play a role in the rate of the phase transformation; further research would be desirable. It was observed that the processing significantly influences elongation break and tensile strength at break, which was higher in extrudates than in oriented injection-molded specimens.

The second part characterizing the degradation behavior of the material is actually the first study in this area screening such effects for PB-1. Thermal analysis determined significant changes in crystallization behavior influencing morphology arrangement and resulting thermal properties. Also, the effect of degradation on the phase transformation has been proven; the degradation significantly slows down the phase transformation. The significant differences were found between the accelerated UV irradiation and natural weathering. Rheological behavior was suitable method for determination of early stages in photodegradation of PB-1 using Cole-Cole plot, where other techniques do not properly record any relevant changes. Microscopic methods showed the evolution on the surface of degraded specimens.

Further step was to study the effect of degradation on mechanical properties of the extrudates and subsequent analysis to understanding. The effect of different design of the degradation procedure lead to different evolution of tensile modulus. In naturally exposed specimens, the chemi-crystallization phenomenon was observed resulting in increase of tensile modulus while in accelerated UV irradiated specimens decrease of modulus was observed caused by erosion of crystallites in the surface layers. In both sets, elongation at break and tensile strength decreases upon photodegradation. The photodegradation also lead to a slight decrease of form II content in both sets.

Further promising research could be concerned on high-pressure behavior of PB-1, because as written in bibliographic part, pressure increases the rate of the phase transformation however interrelations with morphology has not been offered yet. Partial research on self-reinforcemement of PP and PB-1 blend has already been done at the Department of Polymer Engineer. Another option based on a high PB-1 sensitivity to photodegradation could be an use of PB-1 as a suitable basic material for bio- (or oxo-) degradable materials, even if the price is nowadays higher than for common polyolefins; on the other hand, a proper stabilization could bring further applicability of PB-1 favorable based on its phase transformation.

8 REFERENCES

1. **Brydson, J.A.** *Plastic materials.* 7th. Oxford : Butterworth-Heineman Linacre House, 1999.

2. **Federation, British Plastic.** Polybutene-1 (PB-1). *British Plastic Federation.* [Online] British Plastic Federation. [Cited: 11 23, 2008.] http://www.bpf.co.uk/Plastipedia/Polymers/Polybutene1.aspx.

3a. Polybutene-1: Versatility, value and opportunity. *www.industriepark-hoeachst.com.* [Online] [Cited: 12 17, 2005.] http://www.industriepark-hoechst.com/broschuere-iphunternehmen_en.pdf.

3b. **Chvátalová, L., et al.** *Plasty a Kaučuk, 2007,* Vol. 44, p. 202 (in czech).

4. **Kalay, G. and Kalay, C.R.** *J. Polym. Sci.: Part B: Polym. Phys.* 2002, Vol. 40, p. 1828.

5. **Huang, Q., et al.** *Polym. Int.* 2001, Vol. 50, p. 45.

6. **Maring, D., et al.** *J. Polym. Sci.* 2000, Vol. 38, p. 2611.

7. **Luciani, L., Seppalle, J. and Lofgren, B.** *Prog. Polym. Sci.* 13, 1988, p. 37.

8. **Natta, G., Corradini, P. and Bassi, I.** *Nuovo Cimento Suppl.* 1960, Vol. 15, p. 52.

9. **Natta, G., et al.** *Rend. Accad. Naz. Lincei.* 1955, Vol. 19, p. 397.

10. **Winkel, A.K. and Miles, M.J.** *Polymer* 2000, Vol. 41, p. 2312.

11. **Turner-Jones, A.J.** *J. Polym. Sci.* 1963, Vol. B 18, p. 455.

12. **Kopp, S., Wittmann, J.C., Lotz, B.** *Polymer* 1994, Vol. 35, p. 908.

13. **Yamashita, M.** *Jounal of Crystal Growth* 2008, Vol. 310, p. 1739.

14. **Armeniades, C.D. and Baer, E.** *J. Macromol. Sci. - Phys.* 1967, Vol. B1, p. 309.

15. **G., Goldbach and Peitscher, G.** *J. Polym. Sci.* 1968, Vol. B6, p. 783.

16. **Holland, V.F. and Miller, R.L.** *J. Appl. Phys.* 1964, Vol. 35, p. 3241.

17. **Boor, J. and Mitchell, J.** *J. Polym. Sci.* 1963, Vol. A1, p. 59.

18. **Cooke, J., Ryan, A.J. and Bras, W.** *Nucl. Instr. Meth. Phys. Res.* 1995, Vol. B 97, p. 269.

19. **Baert, J. and Puyvelde, P.V.`.** *Polymer* 2006, Vol. 47, p. 5871.

20. **Lauritzen, J. I., Jr. and Hoffman, J. D.** *J. Appl. Phys.* 1973, Vol. 44, p. 4340.

21. **Acierno, S., Gruzzuti, N. and Winter, H.H.** *Macromolecules.* 2002, Vol. 35, p. 5043.

22. **Monasse, B. and Haudin, J.M.** *Macromol. Symp.* 1988, Vol. 20/21, p. 295.

23. **Fu, Q., et al.** *Macromolecules* 2001, Vol. 34, p. 2502.

24. Site plan. *Site plan.* [Online] 03 15, 2006. [Cited: 03 15, 2006.] http://www.pbpsa.com/eng/siteplan.asp.

25. **Hadinata, C., et al.** *Rheol. Acta* 2006, Vol. 45, p. 631.

26. **Marigo, A., Marega, C., Cecchin, G., Collina, G., Ferrara, G.** *Europ. Pol. J.* 2000, Vol. 36, 1, p. 131.

27. **Oda, T., et al.** *Polymer* 1994, Vol. 35, p. 908.

28. **Goldbach, G.A.** *Macromol. Chem.* 1974, Vol. 39, p. 175.

29. **Nakafuku, C. and Miyaki, T.** *Polymer* 1983, Vol. 39, p. 175.

30. **Maring, D., Meuer, B. and Weill, G.** *J. Polym. Sci. Part B: Polym. Phys.* 1995, Vol. 33, p. 1235.

31. **Miyoshi, T, et al.** *Macromolecules* 2002, Vol. 35, p. 6060.

32. **Tosaka, M., et al.** *Macromolecules* 2000, Vol. 33, p. 9666.

33. **Lotz, B. and Thierry, A.** *Macromolecules* 2003, Vol. 36, p. 286.

34. *Polybutene-1: pipe extrusion guide.* s.l. : Basell Polyolefine, 2005.

35. **Miller, R.L. and Holland, V.F.** *Polym. Lett.* 1964, Vol. 2, p. 519.

36. **Fujiwara, Y.** *Polym. Bull.* 1985, Vol. 13, p. 253.

37. **Kaszonyiová, M., Rybnikář, F. and Geil, P.H.** *J. Macromol. Sci. Phys.* 2004, Vol. 43, p. 1095.

38. **Rubin, I.D.** *J. Polym. Sci.* 1964, Vol. B2, p. 747.

39. **Hsu, T.C. and Geil, P.H.** *J. Macromol. Sci.* 1989, Vol. B28, p. 69.

40. **Zhang, B., Yang, S. and Yan, J.** *J. Polym. Sci. Part B: Polym. Phys.* 2002, Vol. 40, p. 2641.

41. **Yamashita, M., Hoshino, A. and Kato, J.** *J. Polym. Sci. Part B: Polym. Phys.* 2007, Vol. 45, p. 684.

42. **Yamashito, M. and Ueno, S.** *Cryst. Res. Technol.* 2007, Vol. 42, p. 1222.

43. **Azzurri, F., et al.** *Macromolecules* 2002, Vol. 35, p. 9069.

44. **Azzurri, F., et al.** *Polymer* 2003, Vol. 44, p. 1641.

45. **Gohil, R.M., Miles, M.J. and Petermann, J.** *J. Macromol. Sci. - Phys.* 1982, Vol. B21, p. 43.

46. **Chau, K.W., Yang, Y.C. and Geil, P.H.** *J. Mater. Sci.* 1986, Vol. 21, p. 3002.

47. **Luongo, J.P. and Salovey, R.** *J. Polym. Sci.* 1966, Vol. A2, p. 997.

48. **Choi, C.H. and White, J.L.** *Polym. Eng. Sci.* 2001, Vol. 41, p. 6.

49. **Foglia, A.J.** *J. Appl. Polym.Sci., Appl. Polym. Symp.* 1969, Vol. 11, p. 1.

50. **Turner-Jones, A.J.** *Polymer* 1966, Vol. 7, p. 23.

51. **Azzurri, F., et al.** *Macromolecules* 2004, Vol. 37, p. 3755.

52. **Wanjale, S.D. and Jog, J.P.** *Polymer* 2006, Vol. 47, p. 6414.

53. **Wanjale, S.D. and Jog, J.P.** *J. Macromol. Sci. Phys.* 2003, Vol. 42B, p. 1141.

54. **Wanjale, S.D. and Jog, J.P.** *J. Polym. Sci. Polym. Phys.* 2003, Vol. 41, p. 1014.

55. **Krikorian, V. and Pochan, D.** *Macromolecules* 2004, Vol. 37, p. 6480.

56. **Wiemann, K., et al.** *Macromol. Chem. Phys.* 2005, Vol. 206, p. 1472.

57. **Causin, V., et al.** *Polymer* 2006, Vol. 47, p. 4773.

58. **Aronne, A., Napolitano, R. and Pirozzi, B.** *Eur. Polym. J.* 1986, Vol. 9, p. 703.

59. **Brandrup, J., Immergut, E.H. and Grullke, E.A.** *Polymer handbook.* 4th. 1999. 0-471-16628-6.

60. **Sasaki, D., et al.** *Polym. Degr. Stab.* 2007, Vol. 92, p. 271.

61. **Mleziva, J. and Šňupárek, J.** *Polymery: výroba, struktura, vlastnosti a použití.* 2nd. Praha : Sobotáles, 2000. 80-58920-72-7 (in czech).

62. **Rabek, J.F.** *Polymer Photodegradation: Mechanisms and Experimental Methods*: Kluwer Academic Publishers, 1995. 0412584808.

63. **Audouin, L., et al.** *J. Mater. Sci.* 1994, Vol. 29, p. 569.

64. **Rabello, M.S. and White, J.R.** *Polym. Degrad. Stab.* 1997, Vol. 56, p. 55.

65. **Rabello, M.S. and White, J.R.** *Polymer* 1997, Vol. 38, p. 6389.

66. **Commereuc, S., et al.** *Polym. Degrad. Stab.* 1997, Vol. 57, p. 175.

67. **Lacoste, J., Vaillant, D. and Carlsson, D.J.** *J. Polym. Sci. part A: Polym. Chem.* 1993, Vol. 31, p. 715.

68. **Lacoste, J., et al.** *Polym. Degrad. Stab.* 1991, Vol. 34, p. 309.

69. **Verney, V. and Michel, A.** *Polym. Proc. Eng.* 1986, Vol. 4, p. 321.

70. **Ouldmetidji, Y., et al.** *Polymer Testing* 2001, Vol. 20, p. 765.

71. **Kockott, D.** Weathering. [ed.] R. Brown. *Handbook of polymer testing. Physical methods.* Shawbury : Rapra Technology, 1999, pp. 697-734.

72. **Sampers, J.** *Polym. Degrad. Stab.* 2002, Vol. 76, p. 455.

73. **Pospíšil, J., et al.** *Polym. Degrad. Stab.* 2006, Vol. 91, p. 417.

74. **Pospíšil, J. and Nešpůrek, S.** *Prog. Polym. Sci.* 2000, Vol. 25, p. 1261.

75. **Kumar, A., Commereuc, S. and Verney, V.** *Polym. Degrad. Stab.* 2004, Vol. 85, p. 751.

76. **Kumar, A., Commereuc, S. and Verney, V.** *Polym. Degrad. Stab.* 2003, Vol. 81, p. 333.

77. **Pospíšil, J. and Nešpůrek, S.** Highlights in the inherent chemical activity of polymer stabilizers. [ed.] S.H. Hamid. *Handbook of polymer degradation.* 2nd. New York : Marcel Dekker, 2000, pp. 191-276.

78. **Lundback, M., et al.** *Polym. Degrad. Stab.* 2006, Vol. 91, p. 842.

79. **Craig, I.H., White, J.R. and Kin, P.C.** *Polymer* 2005, Vol. 46, p. 505.

80. **Papet, G., L.J., Audouin and Verdu, J.** *Radiat. Phys. Chem.* 1987, Vol. 26, p. 65.

81. **Wunderlich, B.** *Macromolecular physics. Crystal nucleation, growth, annealing.* New York : Academic Press, 1976. Vol. 2.

82. **Ballara, A. and Verdu, J.** *Polym. Degrad. Stab.* 1989, Vol. 26, p. 361.

83. **Albertsson, A.C., et al.** *Polymer* 1995, Vol. 36, p. 3075.

84. **Mani, R., et al.** *Polym. J.* 1994, Vol. 26, p. 185.

85. **Ogier, L., Rabello, M.S. and White, J.R.** *J. Mater. Sci.* 1995, Vol. 30, p. 2364.

86. **Rabello, M.S. and White, J.R.** *Polym. Compos.* 1996, Vol. 17, p. 691.

87. **Shyichuk, A.V., Stavychna, D.Y. and White, J.R.** *Polym. Degrad. Stab.* 2001, Vol. 72, p. 279.

88. **Shyichuk, A.V., et al.** *Polym. Degrad. Stab.* 2004, Vol. 86, p. 377.

89. **Li, T. and White, J.R.** *Plast., Rubber Compos. Process. Appl.* 1996, p. 226.

90. **Li, T. and White, J.R.** *Polym. Eng. Sci.* 1997, Vol. 37, p. 321.

91. **Obadal, M., et al.** *Polym. Degrad. Stabil.* 2006, Vol. 91, p. 459.

92. **LyondellBasell.** Polybutene-1. [Online] Basell Service Company, 1 20, 2008. http://polymers.lyondellbasell.com/portal/site/basell/polybutene-1?filterType=resin&resin=2.

93. **Nivnice, Municipal authority.** Pocasi u nas. *Nivnicke noviny.* 3, 4, 5, 2008, Vol. 18 (in czech).

94. **Samon, J.M., et al.** *J. Polym. Sci., Part B: Polym. Phys.* 2000, Vol. 38, p. 1872.

95. **Obadal, M., Čermák, R. and Stoklasa, K.** *Macromol. Rapid. Commun.* 2005, Vol. 26, p. 1253.

96. **Turner-Jones, A., Aizlewood, J.M., Beckett, D.R.** *Macromol. Chem.* 1964, Vol. 74, p. 134.

97. **Commereuc, S.** *J. Chem. Ed.* 11, 1999, Vol. 76, p. 1528.

98. **Bernard, D.A. and Noolandi, J.** *Macromolecules* 1982, Vol. 15, p. 1553.

99. **Winter, H.H.** Gel point. *Encyclopedia of polymer science and engineering.* New York : John Wiley & Sons, 1989, p. 343.

100. **Verney, V. and Mitchel, M.** *Rheol. Acta* 1989, Vol. 28, p. 54.

101. **Montfort, J.P., Marin, G. and Monge, P.** *Macromolecules* 1996, Vol. 17, p. 1551.

102. **Commereuc, S., et al.** *Polymer* 2000, Vol. 41, p. 917.

103. **Vega, J.F., et al.** *Macromolecules* 1996, Vol. 29, p. 960.

104. **Garcia-Franco, C.A., Mead, D.W.** *Rheol. Acta* 1999, Vol. 38, p. 34.

105 **Alfonso, G.C., Azzurri, F. and Castellano, M.** *J. Therm. Anal. Calorim.* 2001.

106. **Obadal, M., et al.** *Polym. Degrad. Stab.* 2005, Vol. 88, p. 532.

107. **Delprat, P., Duteurtre, X. and Gardette, J.-L.** *Polym. Degrad. Stab.* 1995, Vol. 50, p. 1.

AUTHOR'S PUBLICATIONS

Conference contributions

1. **Beníček, L., Čermák, R., Verney, V., Commereuc, S., Obadal, M**.; The effect of UV irradiation on melting and crystallization behaviour of poly(1-butene). *Submitted for ANTEC 2009 - Society of Plastic Engineers,* Chicago, IL, USA, June 22-24 2009
2. **Hnidáková D., Čermák, R., Beníček, L. Navrátilová J., Vaysse, M.**; The development of microfibrillar-phase morphology in PB-1/PP blends. *Submitted for ANTEC 2009 - Society of Plastic Engineers,* Chicago, IL, USA, June 22-24 2009
3. **Beníček, L., Verney, V., Čermák, R., Commereuc, S**.; Multiscale characterization of photodegradation in polybutene-1. *Biannual Conference on Modification, Degradation and Stabilisation of Polymers, MoDeSt2008*, Liege, Belgium, 2008
4. **Beníček, L., Chvátalová, L., Čermák, R., Verney, V.**; Evolution of mechanical properties during polymorphic transformation in polybutene-1. *Biannual Conference on Modification, Degradation and Stabilisation of Polymers, MoDeSt2008*, Liege, Belgium, 2008
5. **Beníček, L., Verney, V., Čermák, R., Commereuc, S.**; Characterization of photodegradation in polybutene-1: from early to prolonged stages. *IUPAC 42th World Polymer Congress, MACRO 2008,* Taipei, 2008
6. **Beníček, L., Verney, V., Commereuc, S., Čermák, R., Mošnovská, R., Navrátilová, J.**; Early stages of photodegradation in polybutene-1. *Polymer Processing Society 24th Annual Meeting ~ PPS-24 ~ ,* Salerno, Italy, 2008
7. **Beníček, L., Chvátalová, L., Čermák, R., Verney, V.**; Polymorphic transformation in polybutene-1: temperature influence. *Polymer Processing Society 24th Annual Meeting ~ PPS-24 ~ ,* Salerno, Italy, 2008
8. **Beníček, L., Chvátalová, L., Čermák, R., Verney, V.**; Thermal-induced transformation of structure and properties of polybutene-1. *ANTEC 2008 - Society of Plastic Engineers,* Milwaukee, WI, USA, 2008
9. **Beníček, L., Verney, V., Commereuc, S., Čermák, R.**; Characterization of photodegradation in polybutene-1 via rheological measurements. *Journées des jeunes rhéologues 2008 (Groupe Français de Rhéologie)*, Erdeven, France, 2008
10. **Beníček, L., Verney, V., Commereuc, S., Čermák, R.**; Rheology upon photodegradation of polybutene-1. *42éme Colloque du Groupe Francais de Rhélogie*, Clermont-Ferrand, France, 2007
11. **Beníček, L., Verney, V., Commereuc, S., Obadal, M., Čermák, R.**; Rheology evolution of polybutene-1 upon photodegradation; *European Polymer Congress 2007,* Portorož, Slovenia, 2007
12. **Beníček, L., Obadal, M., Čermák, R.**; Non-isothermal high-pressure crystallization of β-polypropylenes; *European Polymer Congress 2007,* Portorož, Slovenia, 2007
13. **Beníček, L., Obadal, M.**; High-pressure crystallization of polypropylenes; *10th International Research/Expert Conference „Trends in The Development of Machinery and Associated Technology" TMT 2006,* Lloret de Mar, Spain, 2006
14. **Polášková, M., Čermák, R., Beníček, L., Obadal, M.**; Polymer blends with microfibrillar-phase morphology; *10th International Research/Expert Conference „Trends in The Development of Machinery and Associated Technology" TMT 2006,* Lloret de Mar, Spain, 2006

15. **Obadal, M., Čermák, R., Beníček, L., Hnidáková, D.**; Structure and properties of cast films produced from β-nucleated polypropylenes; *10th International Research/Expert Conference „Trends in The Development of Machinery and Associated Technology" TMT 2006,* Lloret de Mar, Spain, 2006
16. **Čermák, R., Obadal, M., Habrová, V., Beníček, L.***;* Alpha and beta polypropylenes: The effects of processing on final properties; *ANTEC 2006 - Society of Plastic Engineers,* Charlotte NC, USA, 2006
17. **Obadal, M., Čermák, R., Beníček, L.,Stoklasa, K.**; Tailoring of multicomponent crystalline systems in isotactic polypropylene; *23rd discussion conference – Current and future trends in polymeric materials, 2005 Prague meetings on macromolecules,* Prague, CZ, 2005

CURRICULUM VITAE

Personal data:

Name:	Lubomír Beníček
Date of Birth:	1981, July 16
Present Address:	Sadová 942, 687 51 Nivnice, Czech Republic
E-mail:	Benicek@ft.utb.cz

Education:

2006 - 2009	Joint Ph.D. degree programme: - Laboratoire de Photochimie Moleculaire et macromoleculaire, Blaise Pascal Université in Clermont-Ferrand, France - Department of Polymer Engineering, Faculty of technology, Tomas Bata University in Zlín
2005 – 2006	Department of Polymer Engineering, Faculty of technology, Tomas Bata University in Zlín Ph.D. degree programme: *Chemistry and Technology of Materials – Technology of Macromolecular Substances*
1999 – 2005	Faculty of technology, Tomas Bata University in Zlín Master degree programme: *Chemistry and Technology of Materials - Rubber and Plastic Technology* Master Thesis: *High-pressure crystallization of polypropylene* (in English) appreciated by Dean Award for the best Master Thesis.
1995 – 1999	Technical College in Uherský Brod

Employment:

From 2009	Assistant - Department of Polymer Engineering, Faculty of technology, Tomas Bata University in Zlín
8 – 9 / 2005	Aliachem a.s., Fatra Napajedla – consultant to injection molding processing and technology
1999 - 2004	KASTEK komponenty s.r.o., – production of shoes components, technical and automotive parts

Others:

2 – 10 / 2006	Member of student chamber at Academic Senate of the Faculty of Technology; Student representative at Dean's Council of the Faculty of technology
From 2005	Society of Plastics Engineers – member

RÉSUMÉ

Cette thèse porte sur l'inter relation entre la superstructure moléculaire, les propriétés et la dégradabilité du poly butène isotactique. L'évolution la plus importante est une transformation de phase particulière de la forme cristalline II à la forme cristalline I après cristallisation du polymère à partir de l'état fondu. Cette transformation a été caractérisée par calorimétrie, par diffraction des rayons X aux grands angles et par l'analyse des propriétés mécaniques en fonction des conditions de thermique de recuit. L'effet de la mise en forme sur la superstructure résultante a été mis en évidence sur des échantillons obtenus par injection ou par extrusion en utilisation les propriétés mécaniques en traction. Du fait de la très grande sensibilité du PB-1 vis-à-vis de la photodégradation des effets significatifs sur les propriétés thermiques et sur la transformation de phase ont été observés. Une caractérisation multi-échelle en photodégradation a été réalisée à partir d'analyses calorimétriques, d'analyse en spectroscopie infrarouge, de la diffraction des rayons X et des propriétés mécaniques en traction et ceci tant en photovieillissement en conditions accélérées qu'en conditions d'exposition naturelle.

ABSTRACT

This dissertation work is focused on the interrelations between supermolecular structure, properties and degradability of isotactic poly(1-butene) (PB-1). The most important evolution in PB-1 is a peculiar phase transformation from form II to form I after crystallization from melt. This phase transformation is characterized using calorimetry, wide-angle X-ray scattering and mechanical testing where changes in dependence on annealing conditions in time are observed. The effect of processing on resulting supermolecular structure is proven on injection-molded and extruded specimens using tensile testing. Because of high sensitivity of PB-1 to photodegradation, significant effects on thermal properties and the phase transformation is observed. Multiscale characterization is performed using calorimetric measurements, infra-red spectroscopy, rheology, X-ray scattering, microscopic techniques and tensile testing to describe consequences of photodegradation. As well, the effect of various degradation processes – natural weathering and accelerated UV irradiation lead to different results affecting resulting macroscopic properties.

ABSTRAKT

Tato dizertační práce je zaměřena na studium vzájemných vztahů mezi nadmolekulární strukturou, vlastnostmi a degradabilitou izotaktického poly(1-butenu) (PB-1). Nejvýznamnější vývoj v PB-1 je jeho zvláštní fázová transformace z formy II do formy I, jenž nastává po krystalizaci z taveniny. Tato fázová transformace je charakterizována pomocí kalorimetrického měření, široko-úhlé rentgenografie a mechanickými zkouškami, kde byly pozorovány změny v závislosti na podmínkách stárnutí. Vliv zpracovatelské technologie – vstřikování a vytlačování - na výslednou nadmolekulární strukturu byl prokázán na základě mechanických zkoušek. Jelikož je PB-1 velmi náchylný k fotodegradaci, významné změny byly zaznamenány v termálních vlastnostech a fázové transformaci. Široce zaměřená charakterizace důsledků fotodegradace byla provedena pomocí kalorimetrických měření, infračervené spektroskopie, reologie, rentgenografie, mikroskopických technik a tahových zkoušek. Rovněž byl posouzen vliv rozdílných degradačních procesů – venkovní stárnutí a zrychlené UV ozařování – které vedly k odlišným výsledkům ovlivňující výsledné makroskopické vlastnosti.